Understanding cardiac metabolism through elucidation of mitochondrial protein-protein interactions

Arianne Caudal

A dissertation

submitted in partial fulfillment of the

requirements for the degree of

Doctor of Philosophy

University of Washington

2021

Reading Committee:

Rong Tian, Chair

James B. Hurley

Young Kwon

Program Authorized to Offer Degree:

Biochemistry

University of Washington

Abstract

Understanding cardiac metabolism through elucidation
of mitochondrial protein-protein interactions

Arianne Caudal

Chair of the Supervisory Committee:

Rong Tian

Anesthesiology and Bioengineering

Cardiovascular disease is the leading cause of death worldwide, yet developments of new treatment has been stalled for nearly three decades and novel concepts and strategies are urgently needed. Mitochondria play a central role in cardiac physiology due to the extraordinary energy demands of the heart. It is well recognized that mitochondrial and metabolic remodeling can be maladaptive in the cardiac response to acute and chronic stress, therefore, treatments that specifically target mitochondrial metabolism would be highly desirable. Our limited understanding of mechanisms that connect mitochondrial dysfunction to cellular responses to stress has hindered progress of therapeutic innovation. In order to gain a more comprehensive understanding of the mitochondrial compartment, we used cross-linking mass spectrometry to determine the protein interaction landscape in respiring isolated mitochondria, intact cardiac tissue, and from animal models of heart failure. These efforts uncovered structural insight into how proteins behave in their native environments and in the presence of pathological stress. Comprehensive visualization of the diverse mitochondrial protein landscape is expected to pave for new therapies and novel drug candidates for heart failure. Furthermore, advancement of a technological strategy for system-wide study of proteins is applicable across a wide range of both physiological and pathological systems and models.

Table of Contents

List of abbreviations

ACE – angiotensin converting enzyme

ADP – adenosine diphosphate

ANT/ADT – adenosine nucleotide translocase

ATP – adenosine triphosphate

BDP-NHP – biotin-aspartate proline-PIR n-hydroxyphthalimide

BDH – D-beta-hydroxybutyrate dehydrogenase

CypD – cyclophilin D

CytC – cytochrome C

DE – dead-end cross-link

ETC – electron transport chain

FAO – fatty acid oxidation

FDR – false discovery rate

$FADH_2$ – flavin adenine dinucleotide

GLUT1 – glucose transporter 1

HIF1 – hypoxia inducible factor 1

HF – heart failure

HFrEF – heart failure with reduced ejection fraction

IMS – intermembrane space

iqPIR – isobaric quantitative protein interaction reporter

MICOS – mitochondrial contact site and cristae organizing system

mPTP – mitochondrial permeability transition pore

mtDNA – mitochondrial DNA

NAD^+/NADH – nicotinamide adenine dinucleotide (reduced)

OCR – oxygen consumption rate

OXPHOS – oxidative phosphorylation

PGC1α – peroxisomal proliferator-activated receptor gamma coactivator 1-alpha

PIR – protein interaction reporter

PPARα – peroxisome proliferator-activated receptor

PPIs – protein-protein interactions

PRM – parallel reaction monitoring

PTMs – post translational modifications

RCR – respiratory capacity ratio

RH – reporter heavy

ROS – reactive oxygen species

SCOT1 – succinyl-CoA: 3-oxoacid-CoA transferase

SH – stump heavy

TAC – transverse aortic constriction

TAGs - triacylglycerides

THIL/ACAT – Acetyl-CoA acetyltransferase

VDAC – voltage dependent anion channel

XL-MS – cross-linking mass spectrometry

List of Figures and Tables

Acknowledgement

I am extremely grateful to my thesis advisor, Dr. Rong Tian, for her guidance, support, and the unbelievable opportunities she provided for the duration of my graduate study. I would like to thank past and present members of the Tian Laboratory, for their encouragement and engagement. Specifically Drs. Chi Fung Lee, Julia Ritterhoff, and Frauke Drees for always taking the time to teach. I would also like to thank Drs. James Bruce, Juan Chavez, Xiaoting Tang and members of the Bruce Laboratory for providing an incredible opportunity to learn and collaborate. I am grateful to my thesis committee members Drs. James Bruce and Richard Palmiter, and especially Drs Rong Tian, Young Kwon, and James Hurley for reading my dissertation. I am extremely fortunate to have the support of Dr. Trisha Davis and Erin Kirschner, and cannot thank them enough for their unwavering encouragement. Finally, I am forever grateful to my wonderful family and support system. Mom, Dad, Aessa, Leon, Jeff, and Adalyn, I could not have done this without you – thank you for everything.

Chapter 1: Introduction

1.1 Mitochondrial function

The mitochondrion is an ancient organelle derived from the endosymbiotic relationship of proteobacteria with its host (1). Mitochondria still maintain characteristics of their bacterial ancestry, such as the double membrane architecture, circular genome (mtDNA), and fluid movements that allow integration into dynamic networks. During the course of evolution, mitochondria forfeited autonomy and surrendered most of their genes to the nuclear genome of eukaryotic cells (2, 3). In this process, many genes were lost and the chromosomal DNA of mitochondria was drastically reduced. The remaining human mtDNA encodes only thirteen proteins, including the translation machinery needed to encode them (3). The behavior of mitochondria dramatically changed and even acquired a myriad of new functions (2). Now essential for physiological cell functions, mitochondria provide a diverse subset of cellular roles with over 1,100 different proteins (3, 4). Still, many functions of mitochondria, especially those in specialized cell types or in conditions of disease, remain unknown. Here, I summarize the core components of known mitochondrial pathways.

Mitochondria are colloquial “powerhouses” given their inherited ability to supply adenosine triphosphate (ATP), the energetic currency of the cell, by oxidative phosphorylation (OXPHOS). The process of OXPHOS occurs when electrons are transferred from carriers (reducing equivalents e.g, NADH and $FADH_2$) to the electron transport chain (ETC). The transfer of electrons is coupled to the pumping of protons into the inter-membrane space (IMS), which generates an electrochemical gradient. The flow of electrons down this gradient is harnessed to regenerate ATP from ADP via ATP Synthase (5, 6). Oxygen, the final electron acceptor, is ultimately reduced to water and the process is referred to as mitochondrial respiration.

A variety of carbon sources such as glucose, fatty acids, and amino acids are metabolized by specific pathways that eventually converge on the TCA cycle to regenerate reducing equivalents through iterative oxidations (6). Mitochondria encounter both classical and unconventional fuels and must therefore balance the generation of ATP with biosynthesis and waste removal (5). Fuel preference appears to be cell- and condition-specific, and it remains a poorly understood phenomenon in metabolic research.

Mitochondria possess elaborate machinery to shuttle and maintain compartmentalized pools of cofactors, reducing equivalents, substrates, and ions, all of which partake in cell signaling. The cytosol maintains an oxidizing environment while the mitochondria maintain a reducing environment with more NADH than NAD^+ (7). Beyond its importance to OXPHOS, NAD^+/NADH ratio is crucial for maintaining the acetylation status of proteins, which can alter enzymatic activities, substrate-binding, and protein stability (8-10). Similarly, calcium is an activator of many metabolic enzymes (6, 11, 12) and the role of calcium homeostasis is an important toggle between mitochondrial health and cell death.

Crucial for sustaining life, mitochondria also paradoxically play an essential role in cell death. The prolonged opening of the mitochondrial transition permeability pore (mPTP) is the cellular point of no return. Opening of mPTP allows for non-selective passage of molecules < 1.5kDa, including protons, into and out of the mitochondria. This dissipates the electrochemical gradient and inhibits ATP synthesis and other voltage gated dependent processes (13). More troublesome is the release of IMS proteins such as cytochrome C (CytC), which activates and promotes release of various caspases in the cytosol (14). To date, the protein identity of the non-specific mPTP remains controversial in mitochondrial research (15-18). Voltage dependent anion channel (VDAC) and adenosine nucleotide translocase (ANT/ADT) were once considered candidates for

mPTP, but animal knock-out studies suggested otherwise. Complex V/ATP Synthase of OXPHOS has also been nominated as a candidate for the identity of mPTP (15, 17, 19). While its identity remains a topic of debate, the regulatory role of cyclophilin C (CypD) on mPTP is well-accepted (13, 20). Beyond metabolism, mitochondria maintain many independent processes such as transcription, translation, maintenance of membrane architecture, and dynamics (2). How these processes converge and coordinate with the thousands of metabolic processes remains unknown.

1.2 Physiological role of mitochondria in the heart

The heart starts contracting in the third week of human embryogenesis and starts pumping blood in the fourth week. The fetal heart has a hypoxic environment rich in glucose and lactate that promotes biosynthesis of lipids, nucleotides, and other biosynthetic molecules needed for rapid growth (21). The progression into neonatal development coincides with increased hemodynamic workload and oxygen tension, which decreases HIF-1 glycolytic signaling (22). Shortly after birth, cardiomyocytes become post-mitotic and undergo hypertrophy, an enlargement of cell size and mass that promotes contraction force. In parallel, a burst in mitochondrial biogenesis greatly increases the oxidative capacity of the neonatal heart through increased PGC1-α /PPARα and the insulin-sensitive GLUT4 transporter (23). Maternal breast milk supplies increased levels of circulating free fatty acids and triacylglycerides (TAGs) (24-26) and fatty acid oxidation (FAO) becomes the most prominent energy source for ATP in the post-natal heart (27).

The adult human heart consumes and produces nearly six kg of ATP per day, nearly 15 times its own weight, in order to sustain the incessant beating necessary to pump blood throughout the body (21, 28). Approximately 80% of the ATP supply supports the binding and release of actin

and myosin during contraction (systole), as well as the sequestration of calcium ions back into the sarcoplasmic reticulum during relaxation (diastole). Therefore, cardiac function heavily relies on impeccable matching of metabolic supply and demand (29-32).

Due to their extraordinary energy demands, cardiomyocytes are the most mitochondria-rich cells in the body (29, 33). The OXPHOS machinery and glycolysis generate approximately 95% and 5% of the ATP in the adult heart, respectively. Fatty acids are the primary fuel in the adult heart. Contributions from lactate, ketones, and amino acids are considered minor due to the low circulating levels under normoxia (21). Under physiological stressors such as fasting or exercise, the healthy heart relies on metabolic plasticity to switch carbon sources in order to maintain ATP supply (28, 34, 35).

1.3 Mitochondrial metabolism in heart failure

Heart failure (HF) is the leading cause of death worldwide. In the United States alone there are approximately one million hospitalizations, generating over $30 billion dollars in treatment costs annually (36, 37). Etiologies of heart failure are vast but approximately 50% of cases are HF with reduced ejection fraction (HFrEF). HFrEF is defined by at least 40% decrease in the ability of the left ventricle to pump blood due to cardiac remodeling that leads to thinning of the heart wall (37). In 1939, the concept that the failing heart is an engine out of fuel was proposed (38), and for decades after the energy-starvation hypothesis was pursued by many groups (39-41). Today, myocardial energetics, or energy metabolism in the heart, remains a topic of interest because current energy-sparing drugs, such as angiotensin-converting enzyme (ACE) inhibitors, and beta-receptor blockers (42-44), improve patient outcomes. Conversely, approaches that

increase energy demand, such as inotropes, result in worsening of clinical outcomes (45). Targeting mitochondrial pathways directly may be a viable strategy for new cardiac therapies. Altered mitochondrial functions are prevalent across a wide variety of diseases (20, 46-48). Biosynthetic pathways are extensively upregulated in highly proliferative tissues, such as cancers and activated T cells (49). Mitochondria in Alzheimer's disease have increased reactive oxygen species (ROS), ETC dysfunction, and depletion of mtDNA (50). Similarly, mitochondrial dysfunction is a well-accepted maladaptive mechanism in the progression of heart failure (6, 29, 51). During the initial phase of compensation, cardiomyocytes undergo rapid growth in cell size and mass resulting in thickening of the ventricle walls, referred to as hypertrophy. Pathological cardiac hypertrophy temporarily supports contraction during increased workload. The decompensated state leads to thinning of the ventricle wall and poor cardiac function, as observed in end-stage HF (52). During this progression, cardiac remodeling includes an energetically unfavorable metabolic shift away from fatty acid oxidation toward glucose and ketone body utilization, which consequently reduces the overall oxidative capacity and reserve in the heart (53-55). The reactivation of the fetal, metabolic-gene profile (21) that leads to decreased energetic supply has been the longstanding link between mitochondrial dysfunction and the inability of the heart to contract (6). Forcing the pathological heart to consume either fatty acids (56, 57) or ketones improves myocardial function, but it remains unclear whether the benefit goes beyond ATP supply.

Alterations in fuel metabolism directly alters the accumulation of acyl-CoAs in the mitochondria (58). Acyl-CoAs, combined with redox imbalance (NAD^+/NADH ratio) due to insufficient OXPHOS, greatly increases acylation of mitochondrial enzymes, which further dysregulates metabolic pathways (20, 59, 60). Impairments in OXPHOS also increase generation of ROS that

causes oxidative damage to mtDNA and protein machinery, impairments in redox, and leads to a vicious cycle of ROS-induced ROS release in the cell (61, 62). ROS and calcium overload both sensitize opening of mPTP, which is disastrous as it dissipates the membrane potential and releases mitochondrial content into the cell to initiate a cell death and inflammatory response (63, 64).

1.4 Application of cross-linking mass spectrometry to mitochondria

Cross-linking mass spectrometry (XL-MS) utilizes the covalent binding of a reactive cross-linker with proximal residues. Chemical cross-linkers are composed of a reactive group and a spacer. The reactive group dictates the specific targetable residue of which spatial proximity will be determined. The spacer is what remains of the cross-linker after the covalent reaction, which affects downstream processing and workflow including MS acquisition and analysis. The length of the most extended conformation of the soluble cross-linking reagent determines the upper-bound distance constraint. Depending on the experimental procedure, cleavable, labelled, and enriched moieties can be integrated into the cross-linker backbone (65).

After the cross-linking reaction, samples are digested, enriched, and tandem MS-based data are acquired and peptides are identified by searching against a database. Improvements in reagents, instrumentation, cross-link detection, identification, and overall sensitivity have allowed XL-MS to be utilized in ambitious structural studies of large complexes such as the mitochondrial ribosome (66), membrane-bound nuclear pore complex (67), and RNA polymerase II complex (68).

Proteins and protein complexes are dynamic molecules. Unlike most other structural techniques, cross-linking mass spectrometry (XL-MS) does not require sample homogeneity. Its unique

advantage is the ability to capture an ensemble of protein conformational states (65). Cryo-EM, crystallography, and NMR have greatly advanced to resolve mitochondrial protein complexes of sizes unimaginable only a few years ago (69-72). Still, how protein complexes behave in the native environment, in the presence of cofactors, metabolites, molecular crowding, and cellular stressors are poorly understood and cannot be addressed by conventional techniques. XL-MS is a high-throughput extension of proteomics that allows for unbiased determination of protein interactions in physiological conditions, without the need for affinity purification or overexpression of a bait protein.

In the following chapters, work from our group employs XL-MS to define the intact mitochondrial interactome landscape (73), intact cardiac tissue interactome (74), and quantitative interactome of mitochondria from healthy and failing mouse hearts (unpublished).

1.5 Animal models for heart failure

Use of small animal models have greatly increased our understanding of diseased pathologies and paved the way for the development of viable therapeutics. The mouse model has rapidly moved to the forefront of cardiac biology as characteristics that define human cardiac mechanics, performance, rhythm, and structural integrity can all be miniaturized and modeled in this system (75). Since its validation in 1991, transverse aortic constriction (TAC) has become a commonly used method for induction of pressure-overload induced hypertrophy and heart failure (76). TAC is conducted by performing chest thoracotomy on anesthetized mice. The transverse aorta is identified and ligated with a suture in between the innominate and left carotid arteries. The chest cavity is closed, and mice are closely monitored and treated with analgesia post-surgery. Sham surgery mimics the surgical protocol without banding of the aorta (76). The pressure gradient

across the aortic arch can be measured using a high frequency Doppler probe that measures the ratio between the left and right arteries.

Pathological hypertrophy can be observed as early as seven days post-surgery in TAC model, with transition to decompensated hypertrophy occurring at approximately four weeks. The remodeling of cardiac geometry and function can be monitored by serial echocardiography of anesthetized mice. Molecular hallmarks include increased expression of β-myosin heavy chain, atrial natriuretic peptide, interleukin-1, interleukin-6, and TNF-α (76). An advantage of TAC is disease progression that includes the initial compensatory phase with concentric hypertrophy, followed by decompensation deterioration of left ventricular contraction, chamber dilation and pulmonary congestion (76).

Age, gender, body weight, and genetic strain of the mice used for TAC should be considered during study design (76, 77). Aside from the labor-intensive learning curve required of murine microsurgeries, there are major caveats to using TAC to study cardiovascular diseases. TAC induces a sudden onset of pressure overload where this may take decades to develop in humans, and it does not include co-morbidities such as atherosclerosis and diabetes, which is common in human end-stage heart failure (76, 78).

1.6 Dissertation and significance

The goal of this thesis project was to dissect the pathogenic role of mitochondrial remodeling in the progression of heart failure. We used cross-linking technology to conduct systems-level screens for novel mitochondrial PPIs, and greatly expanded applications for XL-MS technology throughout the scope of this dissertation. Chapters 2-4 describe novel approaches of XL-MS in isolated mitochondria, in-tact cardiac tissue, and in a failing heart comparison.

First, to improve understanding of mitochondrial function we used XL-MS to identify 2,427 cross-linked peptide pairs across 327 proteins from isolated respiring murine mitochondria. In situ interactions were observed in proteins throughout the ETC membrane complexes, ATP synthase, and the mitochondrial contact site and cristae organizing system (MICOS) complex. Second, while conventional structural technologies have greatly improved the size, type, and resolution of proteins, the ability to derive large-scale information on proteins as they exist in their native state was virtually nonexistent. Therefore, we ventured to apply XL-MS to identify protein structural features and interactions in intact tissue samples, providing systems-biology insight into protein complexes as they exist in the mouse heart. Findings from the tissue-interactome include resolution of the sarcomere protein contraction apparatus and higher order assemblies of OXPHOS machinery.

Finally, application of isobaric quantitative protein interaction reporter technology (iqPIR) to whole heart tissue led to the first comparative and quantitative study between mitochondria proteins from healthy and failing mouse hearts. Our largest mitochondrial dataset to date, it features a total of ~4000 cross-linked peptide pairs. Furthermore, 544 statistically significant cross-linked peptide pairs were altered in heart failure. Structural insight into ketone oxidation metabolons, OXPHOS machinery, and nucleotide transporter conformations, explain disease phenotypes while bringing forth new hypotheses for pathological mechanisms.

Taken together, these studies expand the depth of knowledge for mitochondrial function, and highlight dynamic and complex mechanisms for regulating protein function in a disease relevant system.

1.7 References

1. A. J. Roger, S. A. Muñoz-Gómez, R. Kamikawa, The Origin and Diversification of Mitochondria. *Current Biology* **27**, R1177-R1192 (2017).
2. J. R. Friedman, J. Nunnari, Mitochondrial form and function. *Nature* **505**, 335-343 (2014).
3. S. B. Vafai, V. K. Mootha, Mitochondrial disorders as windows into an ancient organelle. *Nature* **491**, 374-383 (2012).
4. D. J. Pagliarini *et al.*, A Mitochondrial Protein Compendium Elucidates Complex I Disease Biology. *Cell* **134**, 112-123 (2008).
5. J. B. Spinelli, M. C. Haigis, The multifaceted contributions of mitochondria to cellular metabolism. *Nature Cell Biology* **20**, 745-754 (2018).
6. B. Zhou, R. Tian, Mitochondrial dysfunction in pathophysiology of heart failure. *The Journal of Clinical Investigation* **128**, 3716-3726 (2018).
7. L. R. Stein, S.-i. Imai, The dynamic regulation of NAD metabolism in mitochondria. *Trends in Endocrinology & Metabolism* **23**, 420-428 (2012).
8. K. N. Papanicolaou, B. O'Rourke, D. B. Foster, Metabolism leaves its mark on the powerhouse: recent progress in post-translational modifications of lysine in mitochondria. *Frontiers in Physiology* **5**, 301 (2014).
9. R. M. Parodi-Rullán, X. R. Chapa-Dubocq, S. Javadov, Acetylation of Mitochondrial Proteins in the Heart: The Role of SIRT3. *Frontiers in Physiology* **9** (2018).
10. Gregory R. Wagner, Matthew D. Hirschey, Nonenzymatic Protein Acylation as a Carbon Stress Regulated by Sirtuin Deacylases. *Molecular Cell* **54**, 5-16 (2014).

11. R. M. Denton, D. A. Richards, J. G. Chin, Calcium ions and the regulation of NAD+-linked isocitrate dehydrogenase from the mitochondria of rat heart and other tissues. *Biochemical Journal* **176**, 899-906 (1978).

12. B. Glancy, W. T. Willis, D. J. Chess, R. S. Balaban, Effect of Calcium on the Oxidative Phosphorylation Cascade in Skeletal Muscle Mitochondria. *Biochemistry* **52**, 2793-2809 (2013).

13. A. P. Halestrap, What is the mitochondrial permeability transition pore? *Journal of Molecular and Cellular Cardiology* **46**, 821-831 (2009).

14. S. W. G. Tait, D. R. Green, Mitochondrial regulation of cell death. *Cold Spring Harbor perspectives in biology* **5**, a008706 (2013).

15. J. E. Walker, J. Carroll, J. He, Reply to Bernardi: The mitochondrial permeability transition pore and the ATP synthase. *Proceedings of the National Academy of Sciences* **117**, 2745 (2020).

16. P. Bernardi, The mitochondrial permeability transition pore: a mystery solved? *Frontiers in Physiology* **4** (2013).

17. P. Bernardi, A. Rasola, M. Forte, G. Lippe, The Mitochondrial Permeability Transition Pore: Channel Formation by F-ATP Synthase, Integration in Signal Transduction, and Role in Pathophysiology. *Physiological Reviews* **95**, 1111-1155 (2015).

18. K. N. Alavian *et al.*, An uncoupling channel within the c-subunit ring of the F1FO ATP synthase is the mitochondrial permeability transition pore. *Proceedings of the National Academy of Sciences* **111**, 10580-10585 (2014).

19. V. Giorgio *et al.*, Dimers of mitochondrial ATP synthase form the permeability transition pore. *Proceedings of the National Academy of Sciences* **110**, 5887-5892 (2013).

20. C. F. Lee *et al.*, Normalization of NAD+ Redox Balance as a Therapy for Heart Failure. *Circulation* (2016).

21. J. Ritterhoff, R. Tian, Metabolism in cardiomyopathy: every substrate matters. *Cardiovascular Research* **113**, 411-421 (2017).

22. G. D. Lopaschuk, M. A. Spafford, Energy substrate utilization by isolated working hearts from newborn rabbits. *American Journal of Physiology-Heart and Circulatory Physiology* **258**, H1274-H1280 (1990).

23. G. W. Dorn, R. B. Vega, D. P. Kelly, Mitochondrial biogenesis and dynamics in the developing and diseased heart. *Genes & Development* **29**, 1981-1991 (2015).

24. M. Hamosh, M. R. Simon, H. Canter, P. Hamosh, Lipoprotein lipase activity and blood triglyceride levels in fetal and newborn rats. *Pediatric research* **12**, 1132-1136 (1978).

25. O. Portman, R. Behrman, P. Soltys, Transfer of free fatty acids across the primate placenta. *American Journal of Physiology-Legacy Content* **216**, 143-147 (1969).

26. J. Girard, P. Ferre, J. Pegorier, P. Duee, Adaptations of glucose and fatty acid metabolism during perinatal period and suckling-weaning transition. *Physiological reviews* **72**, 507-562 (1992).

27. G. D. Lopaschuk, J. S. Jaswal, Energy metabolic phenotype of the cardiomyocyte during development, differentiation, and postnatal maturation. *Journal of cardiovascular pharmacology* **56**, 130-140 (2010).

28. J. S. Ingwall, *ATP and the Heart* (Springer Science & Business Media, 2002), vol. 11.

29. D. A. Brown *et al.*, Mitochondrial function as a therapeutic target in heart failure. *Nature Reviews Cardiology* **14**, 238-250 (2017).

30. R. S. Balaban, Domestication of the cardiac mitochondrion for energy conversion. *Journal of Molecular and Cellular Cardiology* **46**, 832-841 (2009).

31. R. S. Balaban, The role of Ca^{2+} signaling in the coordination of mitochondrial ATP production with cardiac work. *Biochimica et Biophysica Acta (BBA) - Bioenergetics* **1787**, 1334-1341 (2009).

32. F. Brunner, L. H. Opie, Role of Endothelin-A Receptors in Ischemic Contracture and Reperfusion Injury. *Circulation* **97**, 391-398 (1998).

33. E. Barth, G. Stämmler, B. Speiser, J. Schaper, Ultrastructural quantitation of mitochondria and myofilaments in cardiac muscle from 10 different animal species including man. *Journal of Molecular and Cellular Cardiology* **24**, 669-681 (1992).

34. S. C. Kolwicz Jr, S. Purohit, R. Tian, Cardiac metabolism and its interactions with contraction, growth, and survival of cardiomyocytes. *Circulation research* **113**, 603-616 (2013).

35. T. Doenst, T. D. Nguyen, E. D. Abel, Cardiac metabolism in heart failure: implications beyond ATP production. *Circulation research* **113**, 709-724 (2013).

36. S. Neubauer, The Failing Heart — An Engine Out of Fuel. *New England Journal of Medicine* **356**, 1140-1151 (2007).

37. S. P. Murphy, N. E. Ibrahim, J. L. Januzzi, Jr, Heart Failure With Reduced Ejection Fraction: A Review. *JAMA* **324**, 488-504 (2020).

38. G. Herrmann, G. M. Decherd Jr, The chemical nature of heart failure. *Annals of Internal Medicine* **12**, 1233-1244 (1939).

39. J. S. Ingwall, R. G. Weiss, Is the failing heart energy starved? On using chemical energy to support cardiac function. *Circulation research* **95**, 135-145 (2004).

40. H. Taegtmeyer, Metabolism—the lost child of cardiology. *Journal of the American College of Cardiology* **36**, 1386-1388 (2000).

41. G. D. Lopaschuk, I. M. Rebeyka, M. F. Allard (2002) Metabolic modulation: a means to mend a broken heart. (Am Heart Assoc).

42. M. A. Pfeffer *et al.*, Effect of Captopril on Mortality and Morbidity in Patients with Left Ventricular Dysfunction after Myocardial Infarction. *New England Journal of Medicine* **327**, 669-677 (1992).

43. M. Packer *et al.*, The Effect of Carvedilol on Morbidity and Mortality in Patients with Chronic Heart Failure. *New England Journal of Medicine* **334**, 1349-1355 (1996).

44. B. Pitt *et al.*, The Effect of Spironolactone on Morbidity and Mortality in Patients with Severe Heart Failure. *New England Journal of Medicine* **341**, 709-717 (1999).

45. S. Tariq, W. S. Aronow, Use of Inotropic Agents in Treatment of Systolic Heart Failure. *International Journal of Molecular Sciences* **16**, 29060-29068 (2015).

46. P. H. Reddy, Mitochondrial medicine for aging and neurodegenerative diseases. *Neuromolecular medicine* **10**, 291-315 (2008).

47. G. Antoun *et al.*, Impaired mitochondrial oxidative phosphorylation and supercomplex assembly in rectus abdominis muscle of diabetic obese individuals. *Diabetologia* **58**, 2861-2866 (2015).

48. L. A. Gómez, T. M. Hagen, Age-related decline in mitochondrial bioenergetics: Does supercomplex destabilization determine lower oxidative capacity and higher superoxide production? *Seminars in cell & developmental biology* **23**, 758-767 (2012).

49. S. Vyas, E. Zaganjor, M. C. Haigis, Mitochondria and cancer. *Cell* **166**, 555-566 (2016).

50. J. M. Perez Ortiz, R. H. Swerdlow, Mitochondrial dysfunction in Alzheimer's disease: Role in pathogenesis and novel therapeutic opportunities. *British Journal of Pharmacology* **176**, 3489-3507 (2019).

51. M. G. Rosca, C. L. Hoppel, Mitochondria in heart failure. *Cardiovascular Research* **88**, 40-50 (2010).

52. K. A. Ammar *et al.*, Prevalence and Prognostic Significance of Heart Failure Stages. *Circulation* **115**, 1563-1570 (2007).

53. M. Allard, B. Schonekess, S. Henning, D. English, G. D. Lopaschuk, Contribution of oxidative metabolism and glycolysis to ATP production in hypertrophied hearts. *American Journal of Physiology-Heart and Circulatory Physiology* **267**, H742-H750 (1994).

54. A. Akki, K. Smith, A.-M. L. Seymour, Compensated cardiac hypertrophy is characterised by a decline in palmitate oxidation. *Molecular and cellular biochemistry* **311**, 215-224 (2008).

55. G. Aubert *et al.*, The Failing Heart Relies on Ketone Bodies as a Fuel. *Circulation* **133**, 698-705 (2016).

56. S. C. Kolwicz *et al.*, Cardiac-Specific Deletion of Acetyl CoA Carboxylase 2 Prevents Metabolic Remodeling During Pressure-Overload Hypertrophy. *Circulation Research* **111**, 728-738 (2012).

57. I. C. Okere *et al.*, High-Fat Diet Prevents Cardiac Hypertrophy And Improves Contractile Function In The Hypertensive Dahl Salt-Sensitive Rat. *Clinical and Experimental Pharmacology and Physiology* **32**, 825-831 (2005).

58. L. Lai *et al.*, Energy Metabolic Reprogramming in the Hypertrophied and Early Stage Failing Heart. *Circulation: Heart Failure* **7**, 1022-1031 (2014).

59. M. A. Walker *et al.*, Acetylation of muscle creatine kinase negatively impacts high-energy phosphotransfer in heart failure. *JCI Insight* **6** (2021).

60. F. L. Sheeran, S. Pepe, Posttranslational modifications and dysfunction of mitochondrial enzymes in human heart failure. *American Journal of Physiology - Endocrinology And Metabolism* **311**, E449 (2016).

61. D. B. Zorov, M. Juhaszova, S. J. Sollott, Mitochondrial Reactive Oxygen Species (ROS) and ROS-Induced ROS Release. *Physiological Reviews* **94**, 909-950 (2014).

62. D. B. Zorov, C. R. Filburn, L.-O. Klotz, J. L. Zweier, S. J. Sollott, Reactive Oxygen Species (Ros-Induced) Ros Release: A New Phenomenon Accompanying Induction of the Mitochondrial Permeability Transition in Cardiac Myocytes. *Journal of Experimental Medicine* **192**, 1001-1014 (2000).

63. H. Nakayama *et al.*, Ca2+- and mitochondrial-dependent cardiomyocyte necrosis as a primary mediator of heart failure. *The Journal of Clinical Investigation* **117**, 2431-2444 (2007).

64. T. Oka *et al.*, Mitochondrial DNA that escapes from autophagy causes inflammation and heart failure. *Nature* **485**, 251-255 (2012).

65. F. J. O'Reilly, J. Rappsilber, Cross-linking mass spectrometry: methods and applications in structural, molecular and systems biology. *Nature Structural & Molecular Biology* **25**, 1000-1008 (2018).

66. B. J. Greber *et al.*, The complete structure of the 55S mammalian mitochondrial ribosome. *Science* **348**, 303-308 (2015).

67. K. H. Bui *et al.*, Integrated structural analysis of the human nuclear pore complex scaffold. *Cell* **155**, 1233-1243 (2013).

68. Z. A. Chen *et al.*, Architecture of the RNA polymerase II–TFIIF complex revealed by cross-linking and mass spectrometry. *The EMBO journal* **29**, 717-726 (2010).

69. A.-N. A. Agip *et al.*, Cryo-EM structures of complex I from mouse heart mitochondria in two biochemically defined states. *Nature Structural & Molecular Biology* **25**, 548-556 (2018).

70. H. R. Bridges *et al.*, Structure of inhibitor-bound mammalian complex I. *Nature Communications* **11**, 5261 (2020).

71. J. A. Letts, L. A. Sazanov, Clarifying the supercomplex: the higher-order organization of the mitochondrial electron transport chain. *Nat Struct Mol Biol* **24**, 800-808 (2017).

72. C. Xia, Z. Fu, K. P. Battaile, J.-J. P. Kim, Crystal structure of human mitochondrial trifunctional protein, a fatty acid β-oxidation metabolon. *Proceedings of the National Academy of Sciences* **116**, 6069 (2019).

73. D. K. Schweppe *et al.*, Mitochondrial protein interactome elucidated by chemical cross-linking mass spectrometry. *Proceedings of the National Academy of Sciences* **114**, 1732-1737 (2017).

74. J. D. Chavez *et al.*, Chemical Cross-linking Mass Spectrometry Analysis of Protein Conformations and Supercomplexes in Heart Tissue. *Cell Systems* **6**, 136-141.e135 (2018).

75. J. D. Molkentin, J. Robbins, With great power comes great responsibility: Using mouse genetics to study cardiac hypertrophy and failure. *Journal of Molecular and Cellular Cardiology* **46**, 130-136 (2009).

76. A. C. Gomes, I. Falcão-Pires, A. L. Pires, C. Brás-Silva, A. F. Leite-Moreira, Rodent models of heart failure: an updated review. *Heart Failure Reviews* **18**, 219-249 (2013).

77. L. Garcia-Menendez, G. Karamanlidis, S. Kolwicz, R. Tian, Substrain specific response to cardiac pressure overload in C57BL/6 mice. *American Journal of Physiology-Heart and Circulatory Physiology* **305**, H397-H402 (2013).

78. C. Riehle, J. Bauersachs, Small animal models of heart failure. *Cardiovascular Research* **115**, 1838-1849 (2019).

Chapter 2: Mitochondrial protein interactome elucidated by chemical cross-linking mass spectrometry

2.1 Abstract

Mitochondrial protein interactions and complexes facilitate mitochondrial function. These complexes range from simple dimers to the respirasome supercomplex consisting of oxidative phosphorylation Complexes I, III, and IV. To improve understanding of mitochondrial function, we used chemical cross-linking mass spectrometry (XL-MS) to identify 2,427 cross-linked peptide pairs from 327 mitochondrial proteins in whole, respiring murine mitochondria. *In situ* interactions were observed in proteins throughout the electron transport chain (ETC) membrane complexes, ATP synthase, and the mitochondrial contact site and cristae organizing system (MICOS) complex. Cross-linked sites showed excellent agreement with empirical protein structures and delivered complementary constraints for *in silico* protein docking. These data established direct physical evidence of the assembly of the Complex I–III respirasome and enabled prediction of *in situ* interfacial regions of the complexes. Finally, we established a database and tools to harness the cross-linked interactions we observed as molecular probes, allowing quantification of conformation-dependent protein interfaces and dynamic protein complex assembly.

2.2 Rationale

Mitochondrial proteins play a diverse role in cellular biology and disease. Mitochondrial dysfunction directly causes multiple inherited diseases (1) and is implicated in common diseases, including neurological developmental disorders (2, 3), neurodegenerative and cardiovascular

diseases (4-6), diabetes (7), asthma (8), cancer (9), and age-related disease (10). In mammals, these organelles have evolved to retain more than 1,000 proteins that interact within a complex, i.e., dual membrane architecture (11, 12). Within the mitochondrial proteome, the "powerhouse" functions are carried out by the core constituents of the oxidative phosphorylation (OXPHOS) system [Complexes I–IV of the electron transport chain (ETC) and ATP synthase (Complex V)]. These proteins are necessary for creation of the mitochondrial electrochemical gradient that powers synthesis of ATP. This system includes critical protein–protein interactions within individual OXPHOS complexes as well as "supercomplex" interactions between ETC complexes I, III, and IV in the respirasome (13). Deficient supercomplex formation has been proposed as a critical mitochondrial defect in failing heart (5, 6, 14, 15), and dynamic rearrangement of supercomplexes has been implicated in noncanonical mitochondrial functions such as antibacterial innate immune responses (16). Assessing these interactions is further complicated by regulatory posttranslational modification and conformational changes of mitochondrial proteins (17-20). Advances in this area have been impeded, in part, by the lack of large-scale detection of dynamic, sometimes transient, interactions between membrane proteins. Thus, large-scale determination of the protein interactome within mitochondria would provide a valuable tool to advance understanding of mitochondrial function and dysfunction and would provide a strong complement to new cryo-EM–derived structures of mitochondrial complexes (21).

Chemical cross-linking mass spectrometry (XL-MS) capabilities now have developed to enable high-throughput identification of protein interactions in complex mixtures and living cells (22, 23). Work by many groups has led to improvements in instrumentation (24), cross-linker chemistry (25, 26), database searching (23, 24, 27, 28), spectral match filtering (29), and structural analysis based on sites of cross-linking (30-32). Large-scale XL-MS offers two key

benefits. First, in conjunction with *in silico* modeling of structures, the identification of cross-linked interactions enables the observation of the physical features of proteins, including membrane proteins (33, 34). These capabilities can uncover novel functions derived from protein–protein interactions, and cross-links have provided data complementary to cryo-EM and crystallography to enhance the understanding of the structure and function of complex systems (27). Second, large-scale chemical cross-linking analyses applied to living systems can enable the determination of protein interactions and conformational changes in complex, dynamic native environments, including the quantification of changes in response to pharmacological intervention (35). In the present study, protein interaction reporter (PIR)-based XL-MS was performed using a peptide-based chemical cross-linking molecule for unambiguous identification of cross-linked peptides (33, 34, 36-38). PIR workflows leverage tandem mass spectrometry (MS^n, where n = stages of MS) methods based on the expected PIR mass relationships observed between MS and MS^2 spectra to enable spectral identification of peptides and protein–protein interactions (24).

We applied PIR technologies to determine protein interactions in functional mitochondria and identified 2,427 nonredundant cross-linked peptide pairs from 327 mitochondrial proteins across 459 protein–protein interactions. These data provide insight into the structures of many mitochondrial proteins, including the five OXPHOS complexes. Importantly, intercomplex cross-linked peptides were identified, supporting the existence of respirasomes in whole, respiring mitochondria. These data enable structural modeling of large protein assemblies *in situ*, in excellent agreement with cryo-EM models. In the future, identified *in situ* cross-linked sites can be used as molecular probes for the study of condition-specific protein complex formation

and conformations and the roles of these complexes in mitochondrial function, dysfunction, and disease.

2.3 Results and Discussion

Chemical cross-linking provides evidence of proximal solvent accessible sites on proteins *in vivo* and is a means to predict and assemble models of protein structures (34, 35, 39). It is important to note that the chemical cross-linking workflow in this study was performed on whole, functional mitochondria. The resulting cross-links provide evidence for protein interactions in their native environment because respiring mitochondria were harvested and cross-linked to ensure the capture of physiologically relevant *in situ* interactions (Fig. 2.1A) (17, 40). The activity of isolated cardiac mitochondria was examined by substrate-driven respiration (Fig 2.1B). Mitochondria were loaded with pyruvate and malate as substrates, and oxygen consumption rates (OCR) were measured after the addition of ADP and then oligomycin A. The addition of ADP induced robust oxygen consumption (State 3 respiration), whereas the addition of the ATP synthase/Complex V inhibitor, oligomycin A, lowered the OCR (State 4 respiration). Isolated cardiac mitochondria from the same protocol showed efficient calcium uptake (41). The high respiratory control ratio (RCR =11.7, the ratio of state 3/state 4 OCR) indicates that the isolated mitochondria were highly coupled (42). Therefore these mitochondria contained functional OXPHOS complexes and intact inner mitochondrial membranes.

Functional, respiring mitochondria were cross-linked *in situ* using a PIR cross-linker, biotin-aspartate proline-PIR n-hydroxyphthalimide (BDP-NHP) (33-35, 39), and were assembled into an interactome consisting of 2,427 nonredundant cross-linked peptide pairs across 11 individual murine samples (Dataset S1). We identified 327 unique mitochondrial proteins, 31.3% of the

murine mitochondrial proteome (327 of 1,042 proteins; MitoCarta 2.0) (Fig. 2.1C) (43), a greater than fourfold increase over recent studies identifying protein interactions in the mitochondrial interactome (44).

We note that acetylation previously has been shown to be an important modification in functional mitochondria (17). Therefore, we included the modification while searching our LC-MS^n data. We were able to identify many peptides that were both cross-linked and acetylated (Dataset S1). An example was an acetylated lysine residue within the ATP/ADP translocase protein ADT1 at K52. This acetylation event was coidentified within a cross-linked peptide pair linking ADT1 K49 to K147. Homologous sites from a bovine empirical structure of ADT1 [Protein Data Bank (PDB) ID code 2C3E] are depicted in Fig. S1A (45). This link highlighted the potential of identifying posttranslational modifications within large-scale cross-linking datasets and points to the future use of XL-MS to dissect the roles of posttranslational modifications and their effects on protein interactions.

A total of 571 non-redundant cross-linked interactions were mapped to the large, multi-subunit mitochondrial contact site and cristae organizing system (MICOS) and OXPHOS complexes. The MICOS/mitochondrial intermembrane space-bridging (MIB) proteins are critical for normal inner membrane morphology and cristae formation. However, little information was available for the MICOS complex, a subcomplex of the MIB complex. We identified eight cross-linked MICOS/MIB complex proteins that demonstrate site-specific interactions in the MICOS/MIB complex (Fig. S1B) (46), including MIC19 and MIC60 homo-multimerization (in which the same lysine site is linked to itself) (Fig. S1B and C), as well as cross-links between MIC60's C-terminus and three MICOS proteins (MIC10, MIC13, and MIC19) (Fig. S1C and D).

Six cross-linked sites in MIC60 (K281 and K639) and MIC19 (K77, K86, K121, and K136) were cross-linked to themselves (e.g., a peptide containing K281 was linked to a second peptide containing K281), suggesting that at least part of the MICOS complex multimerizes, potentially aligning as ATP synthase multimers during the establishment of cristae morphology (47). These findings were supported by previously reported MIC60 dimer, trimer, and tetramer formation (48) and suggested that two regions in the intermembrane space domain of MIC60 (around K281 and K639) were involved in multimer formation (Fig. S1D). Site-specific mapping of cross-linked interactions on MIC60 identified three MICOS proteins (MIC10, MIC13, and MIC19) binding close to the C-terminus of MIC60 (amino acids 639–725) (Fig. S1D), a region known to be required for crista junction formation (49). MIC19 was observed in three nonredundant links to the MIC60 C-terminus (to MIC60 K498, K515, and K639) (Fig. S1D). These findings establish putative binding interfaces within MIC60 that enable the protein to act as a scaffold for the MICOS complex in general. We also identified a link between MIC60 and the dynamin-like protein optic atrophy 1 (Opa1), MIC60 K119 to Opa1 K710 (Fig. S1D), that identifies an interfacial region for these proteins near the N terminus (K119) of MIC60. As a final point, we observed interactions between the MICOS/MIB complex protein MIC27 and subunits ATPA, ATP5F1, and ATP5J of the F1 domain of ATP synthase, including two ATP synthase stator domain proteins, ATP5F1 and ATP5J (50, 51). These ATP synthase interactions with MICOS/MIB provide structural insight (stator binding) consistent with the reported roles of MICOS/MIB complexes in coordinating with OXPHOS complexes, including ATP synthase, to define the architecture of the inner mitochondrial membrane.

OXPHOS complexes (complexes I–IV and ATP synthase) are critical for ATP production in mitochondria. We observed cross-links within the OXPHOS complexes that showed excellent

agreement with previous structural data (Fig. S2). These included a homo-multimeric link between two molecules of QCR2 with K159 observed linked to itself (K159–K159) with a Cα–Cα distance of 22.8 Å (murine QCR2 was overlaid on a yeast complex III dimer structure), well within the empirically derived maximum linkable distance (35 Å) of BDP-NHP (24, 35, 52, 53) (Fig. 2.2A and Fig. S3A). We further compared cross-links against the empirical structures for OXPHOS complexes II and IV as well as electron transport flavoproteins ETFA and ETFB (Fig. 2.2B–D) based on conserved lysine residues in the empirical structures. In each of these examples, we observed the Cα–Cα distances between cross-linked lysines to be less than 35 Å (Fig. 2.2).

Extending *in situ* analysis to another OXPHOS complex, we mapped cross-linked lysine sites across ATP synthase (Complex V). We identified cross-linked residues within each of the major extramembrane domains of the complex: rotor, stator, and ATPA/B (Fig. S2). We further observed that 13% (41 of 318) of cross-linked relationships within ATP synthase were between ATPA/B and the stator (Fig. 2.2E). These cross-links provide distance constraints to refine molecular interactions between ATP synthase subunits and information on the relationship between ATP8 and other complex V subunits (Fig. 2.2E). It has been proposed that ATP8 serves a fundamental role in the assembly and/or production of ATP by F-ATPases (54). XL-MS (54) and cryo-EM (55) studies on ATP synthase complexes purified from bovine and Pichia angusta, respectively, indicate that ATP8 interacts with subunits of the stator, providing structural stability to the peripheral stalk. The structure of ATP8 is predicted to consist of a short N-terminal domain exposed in the intermembrane space (IMS) followed by a transmembrane helix and a flexible, disordered C-terminal tail that extends up from the membrane into the mitochondrial matrix. In purified bovine ATP synthase, two sites were previously

identified as linking residues K46 and K54 of ATP8 to subunits b (AT5F1), d (ATP5H), and F6 (ATP5J) in the stator (K120, K24, and K73 respectively) (54). We identified four cross-linked residues in ATP8 (K46, K48, K54, and K57) linked to six other ATP synthase subunits, including the stator subunits ATP5H (subunit d: K25, K85, K95, K117, K148, and K149), ATP5J (subunit F6: K99 and K105), and AT5F1 (subunit b: K162), the rotor subunits ATPD (K136) and ATP5E (K50), and the core subunit ATPA (K498) (Fig. 2.2E and Fig. S4). Furthermore, mapping of a homology model of ATP8 to cryo-EM–derived structures of ATP synthase in multiple rotational states (55) revealed that links between ATP8 (K46 and K48) and the rotor subunit ATPD (K136) are possible only with ATP synthase rotational state 3. In contrast, the link between ATP8 (K48) and the rotor subunit ATP5E (K50) was possible only in rotational state 1 (Fig. 2.2E). These cross-links confirmed existing XL-MS data obtained from purified bovine ATP synthase in murine ATP synthase from functional mitochondria (54) and established interactions within the rotor and core subunits that are rotational state dependent. We also observed cross-linked interactions between the ATP synthase inhibitor ATIF1 and the F1 domain proteins ATPA and ATPB (Fig. S5). Using a full-length model of the murine ATIF1 structure, we docked the inhibitor to an empirical ATP synthase F1-domain structure containing ATIF1 protein fragments (PDB ID code: 4Z1M) (56). Three of five links between ATIF1 and ATPA/B were well within the cross-linker Cα–Cα distance threshold (ATPA–ATIF1: 25.8 Å; ATPB–ATIF1: 13.8 Å and 29.7 Å). However, the predicted ATIF1 model contained an extended C-terminal, α-helix that is not present in the empirical structure (Fig. S5). When the extended helix was overlaid on protein fragments from the empirical structure, we observed two cross-links between the C-terminus of ATIF1 and ATP synthase subunit ATPB with Cα–Cα distances greater than 50 Å, longer than the BDP-NHP linker. The long Cα–Cα distances suggested that

the ATIF1 C-terminal α-helix may have a flexible conformation that would not be visible by X-ray crystallography but would allow binding to the external surface of ATPB and could be arrested by chemical cross-linking (Fig. S5). Identification of potentially dynamic or transient interactions are particularly interesting, because it was established previously that cross-linked peptide abundances change in a conformation-dependent manner (35); thus future studies could harness the ATIF1–ATPA/B links to elucidate condition- and conformation-specific flexing of the ATIF1 helix.

Building on such dynamic complex interactions, we observed multiple intercomplex links between respirasome supercomplex components Complex I and Complex III that facilitated cross-link-distance-constrained, rigid-body docking. Even before they were mapped to the docked model, these cross-links provided evidence of the assembly of an OXPHOS supercomplex within whole, functional mitochondria. The resulting docked model of the Complex I [PDB ID code: 5LDW (57)]–Complex III [PDB ID code: 1KYO (58)] supercomplex (Fig. 2.3) (59) indicated that both Complex III monomers interact simultaneously with Complex I: QCR2 from one Complex III monomer and QCR6 from the second Complex III monomer interacted with Complex I's NDUA2 (in the matrix) and NDUB4 (in the intermembrane space), respectively (Fig. 2.3A and Fig. S6).

We compared the XL-MS–based supercomplex model with a recently published ovine cryo-EM structure (PDB ID code: 5J8K) (21). We note that the XL-MS–based supercomplex was assembled without prior knowledge of the cryo-EM structure. Strikingly, after blind assembly of the supercomplex, the final *in situ* XL-MS model strongly agreed with the cryo-EM structure for Complex I and Complex III (rmsd = 1.3 Å and 2.4 Å, respectively). We did not observe links between complex III and complex IV, as is consistent with studies that showed these two

complexes do not co-immunoprecipitate from Black-6 murine mitochondria, such as those used here, because of a mutation in the scaffolding protein SCAF1 (60). The *in situ* cross-linked peptides from whole, respiring mitochondria presented here establish a final conformation of Complex I–Complex III that is highly similar to the cryo-EM model and a set of powerful molecular probes that can be used in the future to quantify conditional response on supercomplex assembly in functional mitochondria (35).

Furthermore, we identified cross-linked sites between subunits of Complex I and ATP synthase of the OXPHOS system (Fig. S2). As discussed in a recent review (61), supercomplexes between ATP synthase and complexes of the respiratory chain are known to form, but there are conflicting reports on the association of Complex I and Complex V (62-64). The links identified between Complexes I and V support the existence of this interaction in respiring mitochondria, but the structural implications of these cross-links will require further studies that take into account the role of cristae formation and large mitochondrial membrane topologies. Current structural knowledge of Complex I places NDUA8 and NDUS5 on the IMS face of the complex, opposite the mitochondrial matrix where the ATP synthase components ATPO, ATB, and ATF5 reside in fully assembled complexes. However, it is not yet known when these links form or if this interaction occurs only during certain stages of complex assembly. Nonetheless, the links identified here provide valuable evidence that could be used to probe the interactions of either the subassemblies of the complexes or the fully assembled Complex I and Complex V. These links could help shed light on the hypothesis that ATP synthase dimers form the mitochondrial permeability transition pore (mPTP) (65) and the relationship between Complex I activity and the mPTP (66-69).

The work presented here focused on a small subset of interaction models that can be derived from cross-linked peptides, including those identified between ATP8, ATIF1, and ATP synthase components, the MICOS complex, and between subunits of Complexes I and III. These links highlight a few of the more than 2,400 cross-linked peptide pairs presented. However, the full dataset also includes preliminary findings for other protein complexes such as interprotein interaction interfaces involving the mitochondrial RNA polymerase, POLRMT. Previous work has shown that, in addition to a direct role in mitochondrial transcription, POLRMT is involved in mitochondrial translation and ribosome biogenesis (70). In the current study we identified cross-linked sites between murine POLRMT and the mitochondrial translation initiation factor IF-2 that are consistent with these proposed secondary functions (70). Last, each of the cross-linked peptide pairs identified here has the potential to serve as a molecular probe for the future study of dynamic *in vivo* protein conformations and interactions (35, 71).

To allow rapid, simple dissemination of these data for future studies, we developed tools to allow non–XL-MS experts to take advantage of the mitochondrial interactome data presented here. First, we generated two databases to enable (i) targeted quantitative analysis of protein–protein relationships by parallel reaction monitoring (PRM) (71) and (ii) large-scale identification of new datasets by spectral matching (Fig. S7) (27, 72). Importantly, neither PRM nor spectral library matching requires specialized instrumentation to identify and quantify XL-MS interactions, so these techniques can be transferred rapidly between laboratories and core facilities (71), allowing wide dissemination of XL-MS–based analysis of mitochondrial proteins. Second, to enable widespread use of these data by the community, we developed a flexible web tool (github.com/mammmals/cross-link-PRMtransitionForm) (71) to allow users to generate

PRM transitions for any cross-linked peptide interaction identified in this study using any user-selected cross-linker or desired modification.

The work here highlights the utility of *in situ* XL-MS to determine protein interactions in complex, native conditions. These data are complementary to current structural biology techniques and offer several key benefits for the research community. First, this interactome provides evidence for mitochondrial protein interactions and complex interfaces that should be of high value to the community in general (e.g., MICOS/MIB site interactions). Second, the interactome provides evidence for the presence and orientation of OXPHOS supercomplexes from intact, respiring mitochondria. Finally, the identified cross-linked peptides will enable future studies to target and quantify protein and complex conformational changes, including site-specific perturbation of interaction interfaces, *in situ*.

2.4 Methods

Mitochondrial isolation protocol

In total, 11 murine mitochondrial biological replicates were isolated from four mouse tissues [heart, brain, liver, and skeletal muscle (leg)] as described (40, 73).

Mouse tissues were excised from mice, and the aortas were removed from the hearts. Tissues were rinsed briefly in ice-cold isolation medium (0.2–0.3 M sucrose, 10–30 mM Hepes sodium salt, 0.2 mM EDTA/2 mM EGTA, pH 7.2–7.4) or PBS to remove residual blood. Tissues were minced on ice and resuspended in fresh isolation medium. Heart tissues were digested with trypsin (10 μg/mL) and incubated on ice for 10 min. Trypsin digestion was stopped by the addition of isolation medium containing trypsin inhibitor (0.5 mg/mL) and BSA (1 mg/mL). The suspension was centrifuged for 1 min at 1,500 × g at 4 °C, and the supernatant was discarded.

The pellets were resuspended in fresh isolation medium containing 1 mg/mL BSA. The samples were transferred to a Teflon-glass tube and homogenized on ice with a Teflon pestle. The homogenates were centrifuged for 10 min at 800 × g at 4 °C. The supernatants were collected and centrifuged for 15 min at 8,000–10,000 × g at 4 °C. After the removal of supernatant, the pellet was resuspended in isolation medium. The pellet was centrifuged for 15 min at 8,000 - 10,000 × g at 4 °C and was resuspended in isolation medium. The protein concentrations of resuspended mitochondria were quantified using a Lowry assay and/or a BCA assay (Pierce).

Mitochondrial Respiration Using Seahorse XF24 Analyzer.

The OCR of isolated cardiac mitochondria was measured with an XF24 Extracellular Flux Analyzer (Seahorse Bioscience) according to the manufacturer's protocol (www.primetech.co.jp/Portals/0/db/product/Seahorse/No.12_TechBrief-Iso-mito=6P=_wF.pdf). The Seahorse utility plate was hydrated with calibration buffer and incubated at 37 °C for 24 h before respiration experiments. Mitochondria were seeded in XF 24-well cell-culture microplates at 1.5–2 μg protein per well in 1× mitochondrial assay solution (70 mM sucrose, 220 mM mannitol, 10 mM potassium dihydrogen phosphate, 5 mM magnesium chloride, 2 mM HEPES, 1 mM EGTA, 0.2% BSA, pH 7.35) containing substrates (10 mM pyruvate and 2 mM malate). The plate with seeded mitochondria was incubated for 10 min at 37 °C. The plate then was incubated in a Seahorse Analyzer, and a baseline OCR was measured. Fifty microliters of 40-mM ADP (4 mM final concentration), 55 μL of 25-μg/mL oligomycin A (2.5 μg/mL final concentration), 60 μL of 40-μM carbonyl cyanide-4-(trifluoromethoxy)phenylhydrazone (FCCP) (4 μM final concentration), and 65 μL of 40-μM antimycin A (4 μM final concentration) were added sequentially into each well, and changes in OCR were measured.

Synthesis of the BDP-NHP cross-linker

The mass spectrometrically cleavable cross-linker BDP-NHP was synthesized as described (24). BDP-NHP was synthesized using solid phase peptide synthesis. Fluorenylmethyloxycarbonyl chloride (FMOC)-protected amino acids were serially bound (order:biotin-Lys, branch-Lys, Asp, Pro) to a glycine-SASRIN bead support using an AAPPTec peptide synthesizer. After the attachment of proline, succinic anhydride was added. The full molecule at this point can be ordered from AnaSpec or another peptide synthesis company at a final cost of ~$2.94 per micromole of cross-linker. Synthesis is finished by esterification with NHP-trifluoroacetic acid. After drying, BDP-NHP was dissolved in anhydrous DMSO ([BDP-NHP] ~200 mM) and stored at −80 °C until use.

Cross-linking of mitochondria and preparation for LC-MS/MS/MS.

Purified mitochondria were resuspended in cross-linking buffer (170 mM Na2PO4, pH 8.0) and were cross-linked with 5 mM of BDP-NHP for 30 min at room temperature with constant mixing at 700 rpm on an Eppendorf Thermomixer R (Fisher Scientific). After the cross-linking reaction finished, mitochondria were washed twice with cross-linking buffer alone to remove excess cross-linker. Cross-linked mitochondria then were resuspended in 8 M urea, 50 mM Tris·Cl (pH 8.0), and 150 mM NaCl to lyse the organelles. Mitochondria were disrupted by three 20-s pulses with a sonicating probe at 50% intensity. Mitochondrial proteins were reduced with 5 mM β mercaptoethanol for 30 min at room temperature, alkylated with 15 mM iodoacetamide for 30 min in the dark at room temperature, and digested with sequencing grade trypsin (1:200 dilution; Promega) at 37 °C overnight. Digested peptides were desalted with a C18 Sep-Pak cartridge, and the eluted peptides were dried to completion before being resuspended in SCX buffer A [5

mM KH2PO4, (pH 2.6), 30% (vol/vol) ACN]. Resuspended peptides were injected into a Phenomenex Luna SCX column and were fractionated using a 97.5-min gradient of buffer B [5 mM KH2PO4 (pH 2.6), 30% (vol/vol) ACN, 350 mM KCl] as follows: 0% buffer B at 0 min, 5% B at 7.5 min, 60% B at 47.5 min, 100% B at 67.5 min, 100% B at 77.5 min, 0% B at 77.51 min, and 0% B at 97.5 min. Fractions were taken every 5 min starting at 17.5 min and were pooled into six pools as follows: fractions 1–5, fractions 6–7, fraction 8, fraction 9, fraction 10, and fractions 11–14. Fraction pools were dried to a final volume of ∼2 mL in a vacuum centrifuge, and the pH was adjusted to 8.0 with 1.5 M NaOH. Pooled cross-linked peptides were enriched by the addition of 200 μL of monomeric avidin bead slurry (Ultralink; Pierce) and were incubated at room temperature on an orbital shaker at maximum speed. Cross-linked peptides were washed with 100 mM ammonium bicarbonate, pH 8.0, and eluted with 70% (vol/vol) ACN/1% formic acid before being dried to completion in a vacuum centrifuge and stored at −80 °C until analyzed.

LC-MS/MS/MS, ReACT, and data analysis

Samples were resuspended in 5% (vol/vol) ACN/2% (vol/vol) formic acid and injected in technical duplicate into an in-house–pulled 45-cm C8 (Reprosil, 5 μm, 120 Å) column protected by a 2-cm C8 trapping column. Cross-linked peptides were identified using ReACT-based instrument methods (24). ReACT targets high charge state precursor ions ($z \geq 4$) in MS1 scans for low-energy fragmentation. Low-energy (normalized collision energy = 25) fragments in the subsequent MS2 scan then were queried for masses (i.e., released peptides) that sum to the total precursor mass plus the addition of the reporter ion species at 752.41 m/z. This summation occurs in real time in the instrument control software, and masses that satisfy the equation

precursor m/z = reporter m/z + peptide 1 m/z + peptide 2 m/z within a 20-ppm tolerance are fragmented further to render MS3 spectra that can be searched using canonical search methods analogous to data-dependent acquisition searching. Released peptide spectra (precursors in MS2, fragments in MS3) were searched against a target-decoy database constructed from the MitoCarta 2.0 database of annotated mitochondrial proteins from mice (43). Spectra were searched using Comet on the MS3 spectral pairs for each targeted relationship (74). Comet parameters were searched using default parameters with the following modifications: peptide mass tolerance: 20.0 ppm; enzyme: trypsin; variable modifications: 15.9949 M (methionine oxidation); 197.032422 K (cross-linker stump mass); 42.010565 K (acetyl-lysine); fragment bin tolerance: 1.0005; fragment bin offset: 0.4; MS level: 3.

The peptide spectral match FDR was filtered to be less than 5% based on PeptideProphet e-value scoring (24, 75); notably, the FDR for fully identified cross-linked relationships was significantly lower than this limit. The final relationship FDR across all tissue mitochondrial samples in this study was 1.91% (162 identified decoy relationships out of 8,467 total identified relationships). The protein FDR for the entire atlas was 5.6% (20 reverse proteins out of 358 total proteins). PPI networks were displayed using Cytoscape. The large-scale network of mitochondrial interactions will be available on XLinkDB 2.0 (53). A fully interactive version of the network in Fig. 2.1C is also available in Dataset S2.

A spectral library was generated using the cross-linked identifications observed in this study, as described previously (29). Briefly, SpectraST 5.0 was used to assemble a library from all searched mzXML files and the output of ReACT analysis. The example in Fig. S7 comes from searching an individual mzXML file from the dataset against the full spectral library. This spectral library is available in Dataset S3.

Structure prediction, protein modeling, and protein–protein docking

Structure prediction was done for individual proteins using their canonical UniProt amino acid sequence and the Phyre2 protein-fold recognition server (76). Protein models for mouse structures were compared with other models of mammalian (e.g., bovine, human) or eukaryotic (e.g., yeast) structures based on the rmsd. To dock the large protein supercomplexes, we determined conserved residues corresponding to cross-linked lysines from our study within previously established empirical structures (Complex I: PDB ID code 5LDW; Complex III: PDB ID code 1KYO). We then submitted these structures with distance constraints (0–35 Å) for the conserved residues to PatchDock (59). For the NDUA2 structure (Fig. S4A) that did not contain a conserved K13 residue, R16 was used in its place, and the distance constraint was extended (40 Å). Structures were displayed using ICM Brower Pro (MolSoft) or NGL Viewer (77). Modeled structures are available in Dataset S4.

2.5 Figures

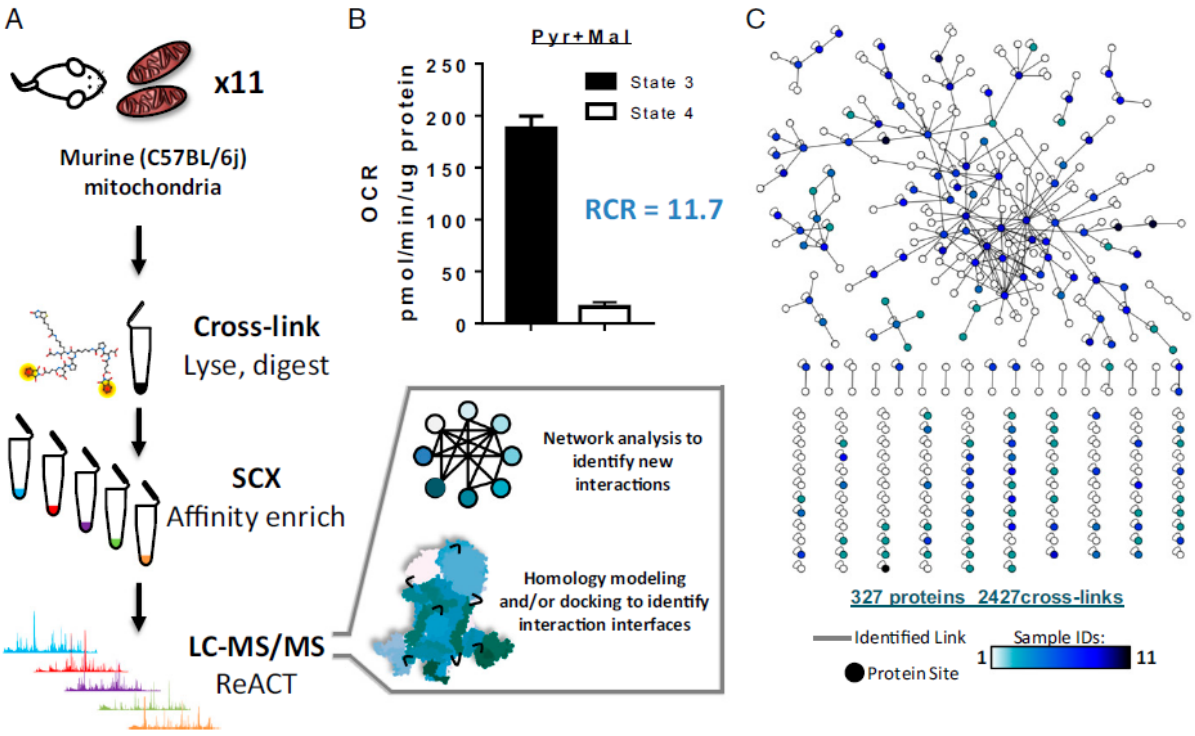

Figure 2.1: Determination of cross-linked protein interactions in functional mouse mitochondria.

(A) Functional mitochondria were cross-linked and lysed, and protein lysates were digested with trypsin, followed by SCX fractionation on the cross-linked peptides. Pooled SCX fractions were enriched with monomeric avidin to capture the biotin-containing cross-linker covalently bound to two peptides. Cross-linked peptides were identified by MS/MS and ReACT (24). (B) The OCR of isolated mitochondria with pyruvate and malate as substrates was measured. After the baseline measurements, 50 µL of 40-mM ADP (4 mM final concentration) and 55 µL of 25 µg/mL oligomycin A (2.5 µg/mL final concentration), a complex V inhibitor, were injected sequentially. The changes in OCR after the addition of ADP (state 3) and then oligomycin A (State 4) were measured by Seahorse XF24. The RCR is expressed as State 3 OCR/state 4 OCR. Data were expressed as the SD from five technical replicates. (C) Protein interactions as

determined by large-scale chemical cross-linking analysis of functional mouse heart mitochondria. Nodes represent individual proteins; edges (lines) represent all cross-links identified between two proteins. Nodes are colored according to the number of samples in which each protein interaction was observed. An interactive network depicting site-to-site interactions is available in Dataset S2.

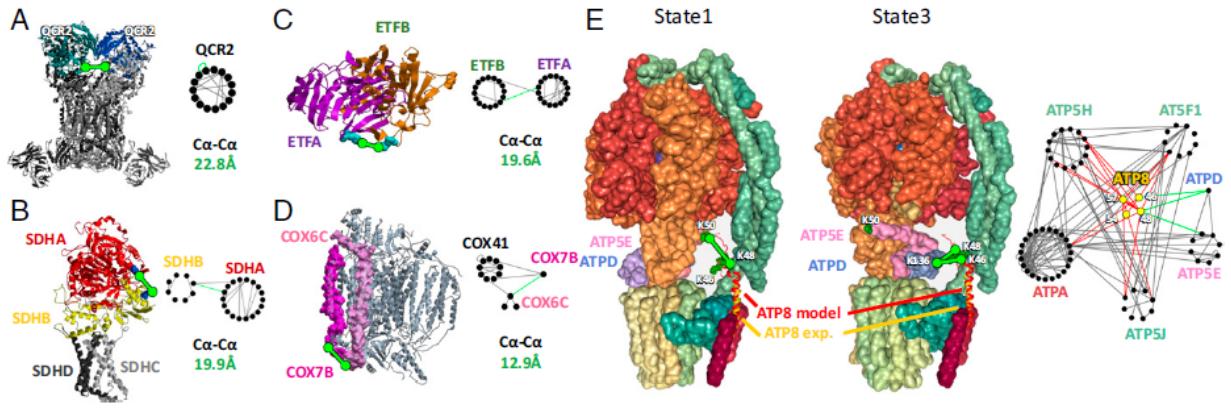

Figure 2.2: Cross-linked sites mapped to empirical protein structures.

Sites of cross-linking identified in empirical structures are shown along with site–site interaction networks. Cross-links are depicted as space-filled residues and green lines. Cα–Cα distances for the links are shown. Network nodes represent individual cross-linked sites; edges represent identified cross-links. Cross-links highlighted in each structure are shown as green edges in the network (78). (A) Complex III dimer (monomers shown in light gray and dark gray). Homology model of mouse QCR2 overlaid on the yeast complex III structure (PDB ID code: 1KYO). The mouse QCR2 proteins for monomers one and two are shown in blue and teal, respectively. (B) Homology models of mouse SDHA and SDHB were overlaid on the porcine complex II structure (PDB ID code: 4YXD) (79). Identified cross-linked lysines are highlighted in blue. (C) The ETFA–ETFB complex structure (PDB ID code: 1EFV) (78) from human, with conserved lysine sites highlighted in teal. Mouse ETFA (purple) K139 corresponds to human K139, and mouse ETFB (orange) K26 corresponds to human R26. (D) Complex IV structure from bovine with COX7B (magenta) and COX6C (pink) highlighted (PDB ID code: 3ASO) (80). Mouse COX7B K75 (corresponding to bovine K51) and mouse COX6C K68 (corresponding to bovine K65) link the proteins on the IMS side of the complex. (E) The Phyre2 model of ATP8 (red) was superimposed on a helix assigned to ATP8 (yellow) in cryo-EM–derived structures (55) of ATP

synthase in rotational state 3 (PDB ID code: 5LQX) and rotational state 1 (PDB ID code: 5LQZ). Cross-linked sites (green space-filled residues) between APT8 (K46 and K48) and ATPD (K136) are compatible with state 3, whereas the cross-link between ATP8 (K48) and ATP5E (K50) is compatible only with state 1. Cross-linked sites involving ATP8 and six other ATP synthase subunits are indicated in the subnetwork and are displayed on a structure in Fig. S4.

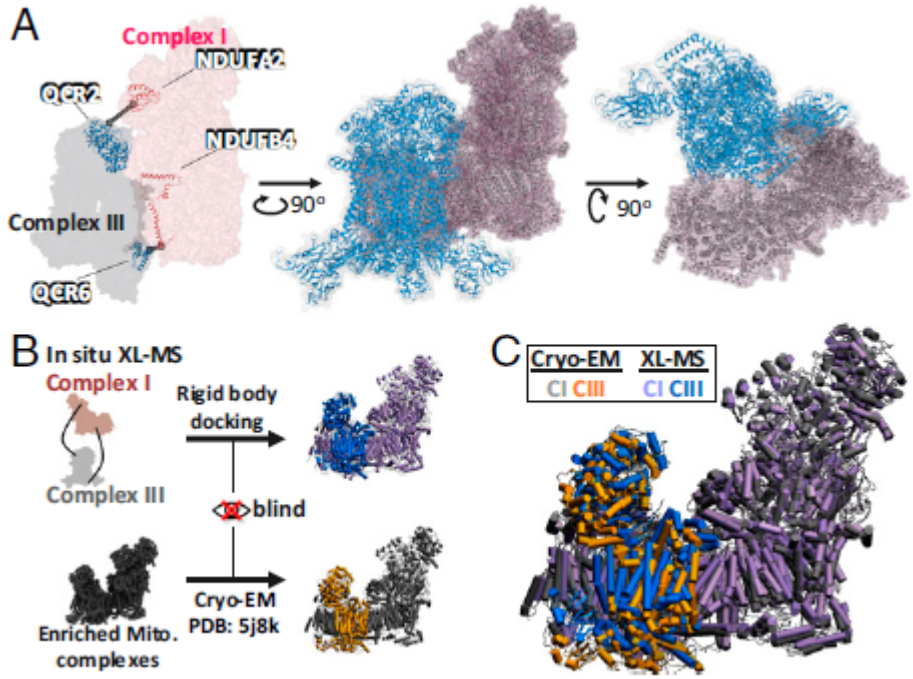

Figure 2.3: Determination of supercomplex structures from functional mitochondria.

(A) Supercomplex model from rigid body docking (59) of Complex I (NDUA2, NDUA4) and Complex III (QCR2, QCR6) using cross-linked peptide distance constraints (NDUA2–QCR2; NDUA4–QCR6). Complex I is shown in pink, and Complex III is shown in blue. Ribbon models of intercomplex cross-linked proteins are shown within the surface model in the left panel, and the distance constraints used are displayed as gray lines. (B) Workflow for the comparison of a recently published cryo-EM structure (PDB ID code: 5J8K) (21) and the XL-MS–based supercomplex model. The XL-MS–based model was generated without prior knowledge of the cryo-EM model. (C) Comparison of the *in situ* XL-MS docked supercomplex with the cryo-EM supercomplex model (PDB ID code: 5J8K). Structures were aligned based on Complex I. Complex I rmsd = 1.3 Å; complex III rmsd = 2.4 Å.

Supplementary information and additional resources of this chapter are included in the following publication:

Mitochondrial protein interactome elucidated by chemical cross-linking mass spectrometry

Devin K. Schweppe, Juan D. Chavez, Chi Fung Lee, Arianne Caudal, Shane E. Kruse, Rudy Stuppard, David J. Marcinek, Gerald S. Shadel, Rong Tian, and James E. Bruce.

2.6 References

1. D. C. Wallace, A Mitochondrial Paradigm of Metabolic and Degenerative Diseases, Aging, and Cancer: A Dawn for Evolutionary Medicine. *Annual Review of Genetics* **39**, 359-407 (2005).
2. A. Anitha *et al.*, Brain region-specific altered expression and association of mitochondria-related genes in autism. *Molecular Autism* **3**, 12 (2012).
3. S. Waldbaum, M. Patel, Mitochondria, oxidative stress, and temporal lobe epilepsy. *Epilepsy Research* **88**, 23-45 (2010).
4. E. Lionaki, M. Markaki, K. Palikaras, N. Tavernarakis, Mitochondria, autophagy and age-associated neurodegenerative diseases: New insights into a complex interplay. *Biochimica et Biophysica Acta (BBA) - Bioenergetics* **1847**, 1412-1423 (2015).
5. E. M. Mejia, L. K. Cole, G. M. Hatch, Cardiolipin metabolism and the role it plays in heart failure and mitochondrial supercomplex formation. *Cardiovascular & hematological disorders drug targets* **14**, 98-106 (2014).
6. M. G. Rosca *et al.*, Cardiac mitochondria in heart failure: decrease in respirasomes and oxidative phosphorylation. *Cardiovascular Research* **80**, 30-39 (2008).
7. M. K. C. Hesselink, V. Schrauwen-Hinderling, P. Schrauwen, Skeletal muscle mitochondria as a target to prevent or treat type 2 diabetes mellitus. *Nature Reviews Endocrinology* **12**, 633-645 (2016).
8. D. C. M. Simoes *et al.*, Glucocorticoid and Estrogen Receptors Are Reduced in Mitochondria of Lung Epithelial Cells in Asthma. *PLOS ONE* **7**, e39183 (2012).
9. S. Vyas, E. Zaganjor, M. C. Haigis, Mitochondria and cancer. *Cell* **166**, 555-566 (2016).

10. R. K. Lane, T. Hilsabeck, S. L. Rea, The role of mitochondrial dysfunction in age-related diseases. *Biochimica et Biophysica Acta (BBA) - Bioenergetics* **1847**, 1387-1400 (2015).

11. D. J. Pagliarini *et al.*, A Mitochondrial Protein Compendium Elucidates Complex I Disease Biology. *Cell* **134**, 112-123 (2008).

12. V. K. Mootha *et al.*, Integrated Analysis of Protein Composition, Tissue Diversity, and Gene Regulation in Mouse Mitochondria. *Cell* **115**, 629-640 (2003).

13. H. Schägger, K. Pfeiffer, Supercomplexes in the respiratory chains of yeast and mammalian mitochondria. *The EMBO Journal* **19**, 1777-1783 (2000).

14. K. Shinzawa-Itoh *et al.*, Purification of Active Respiratory Supercomplex from Bovine Heart Mitochondria Enables Functional Studies. *The Journal of Biological Chemistry* **291**, 4178-4184 (2016).

15. E. Kugelberg, Mitochondria adapt to bacteria. *Nature Reviews Immunology* **16**, 465-465 (2016).

16. E. Kugelberg, Immunometabolism: Mitochondria adapt to bacteria.

17. C. F. Lee *et al.*, Normalization of NAD+ Redox Balance as a Therapy for Heart Failure. *Circulation* (2016).

18. K. N. Papanicolaou, B. O'Rourke, D. B. Foster, Metabolism leaves its mark on the powerhouse: recent progress in post-translational modifications of lysine in mitochondria. *Frontiers in Physiology* **5**, 301 (2014).

19. V. Giorgio *et al.*, Dimers of mitochondrial ATP synthase form the permeability transition pore. *Proceedings of the National Academy of Sciences* **110**, 5887-5892 (2013).

20. K. N. Alavian *et al.*, An uncoupling channel within the c-subunit ring of the F_1F_0 ATP synthase is the mitochondrial permeability transition pore. *Proceedings of the National Academy of Sciences* **111**, 10580-10585 (2014).

21. J. A. Letts, K. Fiedorczuk, L. A. Sazanov, The architecture of respiratory supercomplexes. *Nature* **537**, 644-648 (2016).

22. X. Tang, G. R. Munske, W. F. Siems, J. E. Bruce, Mass Spectrometry Identifiable Cross-Linking Strategy for Studying Protein−Protein Interactions. *Analytical Chemistry* **77**, 311-318 (2005).

23. F. Liu, D. T. S. Rijkers, H. Post, A. J. R. Heck, Proteome-wide profiling of protein assemblies by cross-linking mass spectrometry. *Nature Methods* **12**, 1179-1184 (2015).

24. C. R. Weisbrod *et al.*, In Vivo Protein Interaction Network Identified with a Novel Real-Time Cross-Linked Peptide Identification Strategy. *Journal of Proteome Research* **12**, 1569-1579 (2013).

25. C. Yu, W. Kandur, A. Kao, S. Rychnovsky, L. Huang, Developing New Isotope-Coded Mass Spectrometry-Cleavable Cross-Linkers for Elucidating Protein Structures. *Analytical Chemistry* **86**, 2099-2106 (2014).

26. X. Tang, J. E. Bruce, A new cross-linking strategy: protein interaction reporter (PIR) technology for protein-protein interaction studies. *Molecular bioSystems* **6**, 939-947 (2010).

27. X. Wu *et al.*, In vivo protein interaction network analysis reveals porin-localized antibiotic inactivation in Acinetobacter baumannii strain AB5075. *Nature Communications* **7**, 13414 (2016).

28. M. R. Hoopmann *et al.*, Kojak: Efficient Analysis of Chemically Cross-Linked Protein Complexes. *Journal of Proteome Research* **14**, 2190-2198 (2015).

29. D. K. Schweppe *et al.*, Spectral Library Searching To Identify Cross-Linked Peptides. *Journal of Proteome Research* **15**, 1725-1731 (2016).

30. D. K. Schweppe, J. D. Chavez, J. E. Bruce, XLmap: an R package to visualize and score protein structure models based on sites of protein cross-linking. *Bioinformatics* **32**, 306-308 (2016).

31. M. Fioramonte *et al.*, Analysis of secondary structure in proteins by chemical cross-linking coupled to MS. *Proteomics* **12**, 2746-2752 (2012).

32. F. Stengel, R. Aebersold, C. V. Robinson, Joining Forces: Integrating Proteomics and Cross-linking with the Mass Spectrometry of Intact Complexes *. *Molecular & Cellular Proteomics* **11** (2012).

33. Arti T. Navare *et al.*, Probing the Protein Interaction Network of Pseudomonas aeruginosa Cells by Chemical Cross-Linking Mass Spectrometry. *Structure* **23**, 762-773 (2015).

34. Devin K. Schweppe *et al.*, Host-Microbe Protein Interactions during Bacterial Infection. *Chemistry & Biology* **22**, 1521-1530 (2015).

35. Juan D. Chavez, Devin K. Schweppe, Jimmy K. Eng, James E. Bruce, *Cell Chemical Biology* **23**, 716-726 (2016).

36. L. Yang *et al.*, In Vivo Application of Photocleavable Protein Interaction Reporter Technology. *Journal of Proteome Research* **11**, 1027-1041 (2012).

37. H. Zhang *et al.*, Identification of Protein-Protein Interactions and Topologies in Living Cells with Chemical Cross-linking and Mass Spectrometry. *Molecular & Cellular Proteomics* **8**, 409-420 (2009).

38. C. Zheng *et al.*, Cross-linking Measurements of In Vivo Protein Complex Topologies *. *Molecular & Cellular Proteomics* **10** (2011).

39. J. D. Chavez, C. R. Weisbrod, C. Zheng, J. K. Eng, J. E. Bruce, Protein Interactions, Post-translational Modifications and Topologies in Human Cells. *Molecular & Cellular Proteomics* **12**, 1451-1467 (2013).

40. E. A. Boehm, B. E. Jones, G. K. Radda, R. L. Veech, K. Clarke, Increased uncoupling proteins and decreased efficiency in palmitate-perfused hyperthyroid rat heart. *American Journal of Physiology-Heart and Circulatory Physiology* **280**, H977-H983 (2001).

41. G. Karamanlidis *et al.*, Mitochondrial Complex I Deficiency Increases Protein Acetylation and Accelerates Heart Failure. *Cell Metabolism* **18**, 239-250 (2013).

42. Martin D. Brand, David G. Nicholls, Assessing mitochondrial dysfunction in cells. *Biochemical Journal* **435**, 297-312 (2011).

43. S. A.-O. Calvo, K. R. Clauser, V. K. Mootha, MitoCarta2.0: an updated inventory of mammalian mitochondrial proteins.

44. Brendan J. Floyd *et al.*, Mitochondrial Protein Interaction Mapping Identifies Regulators of Respiratory Chain Function. *Molecular Cell* **63**, 621-632.

45. H. Nury *et al.*, Structural basis for lipid-mediated interactions between mitochondrial ADP/ATP carrier monomers.

46. M. A. Huynen, M. Mühlmeister, K. Gotthardt, S. Guerrero-Castillo, U. Brandt, Evolution and structural organization of the mitochondrial contact site (MICOS) complex and the

mitochondrial intermembrane space bridging (MIB) complex. *Biochimica et Biophysica Acta (BBA) - Molecular Cell Research* **1863**, 91-101 (2016).

47. M. Harner *et al.*, The mitochondrial contact site complex, a determinant of mitochondrial architecture. *The EMBO Journal* **30**, 4356-4370 (2011).

48. R. Rabl *et al.*, Formation of cristae and crista junctions in mitochondria depends on antagonism between Fcj1 and Su e/g. *Journal of Cell Biology* **185**, 1047-1063 (2009).

49. C. Körner *et al.*, The C-terminal domain of Fcj1 is required for formation of crista junctions and interacts with the TOB/SAM complex in mitochondria. *Molecular Biology of the Cell* **23**, 2143-2155 (2012).

50. J. R. Friedman, A. Mourier, J. Yamada, J. M. McCaffery, J. Nunnari, MICOS coordinates with respiratory complexes and lipids to establish mitochondrial inner membrane architecture. *eLife* **4**, e07739 (2015).

51. W. Kühlbrandt, Structure and function of mitochondrial membrane protein complexes. *BMC Biology* **13**, 89 (2015).

52. J. D. Chavez *et al.*, Quantitative interactome analysis reveals a chemoresistant edgotype. *Nature Communications* **6**, 7928 (2015).

53. D. K. Schweppe *et al.*, XLinkDB 2.0: integrated, large-scale structural analysis of protein cross-linking data. *Bioinformatics* **32**, 2716-2718 (2016).

54. J. Lee *et al.*, Organization of Subunits in the Membrane Domain of the Bovine F-ATPase Revealed by Covalent Cross-linking *. *Journal of Biological Chemistry* **290**, 13308-13320 (2015).

55. K. R. Vinothkumar, M. G. Montgomery, S. Liu, J. E. Walker, Structure of the mitochondrial ATP synthase from Pichia angusta determined by electron cryo-microscopy. *Proceedings of the National Academy of Sciences* **113**, 12709-12714 (2016).

56. J. V. Bason, M. G. Montgomery, A. G. W. Leslie, J. E. Walker, How release of phosphate from mammalian F1-ATPase generates a rotary substep. *Proceedings of the National Academy of Sciences* **112**, 6009-6014 (2015).

57. J. Zhu, K. R. Vinothkumar, J. Hirst, Structure of mammalian respiratory complex I. *Nature* **536**, 354-358 (2016).

58. C. Lange, C. Hunte, Crystal structure of the yeast cytochrome bc1 complex with its bound substrate cytochrome c. *Proceedings of the National Academy of Sciences* **99**, 2800-2805 (2002).

59. D. Schneidman-Duhovny, Y. Inbar, R. Nussinov, H. J. Wolfson, PatchDock and SymmDock: servers for rigid and symmetric docking. *Nucleic Acids Research* **33**, W363-W367 (2005).

60. E. Lapuente-Brun *et al.*, Supercomplex Assembly Determines Electron Flux in the Mitochondrial Electron Transport Chain. *Science* **340**, 1567 (2013).

61. L. Biasutto, M. Azzolini, I. Szabò, M. Zoratti, The mitochondrial permeability transition pore in AD 2016: An update. *Biochimica et Biophysica Acta (BBA) - Molecular Cell Research* **1863**, 2515-2530 (2016).

62. N. V. Dudkina, S. Sunderhaus, E. J. Boekema, H.-P. Braun, The higher level of organization of the oxidative phosphorylation system: mitochondrial supercomplexes. *Journal of Bioenergetics and Biomembranes* **40**, 419 (2008).

63. K. M. Davies *et al.*, Macromolecular organization of ATP synthase and complex I in whole mitochondria. *Proceedings of the National Academy of Sciences* **108**, 14121-14126 (2011).

64. K. M. Au - Davies *et al.*, Visualization of ATP Synthase Dimers in Mitochondria by Electron Cryo-tomography. *JoVE*, e51228 (2014).

65. P. Bernardi, A. Rasola, M. Forte, G. Lippe, The Mitochondrial Permeability Transition Pore: Channel Formation by F-ATP Synthase, Integration in Signal Transduction, and Role in Pathophysiology. *Physiological Reviews* **95**, 1111-1155 (2015).

66. B. Li *et al.*, Inhibition of complex I regulates the mitochondrial permeability transition through a phosphate-sensitive inhibitory site masked by cyclophilin D. *Biochimica et Biophysica Acta (BBA) - Bioenergetics* **1817**, 1628-1634 (2012).

67. E. Fontaine, P. Bernardi, Progress on the Mitochondrial Permeability Transition Pore: Regulation by Complex I and Ubiquinone Analogs. *Journal of Bioenergetics and Biomembranes* **31**, 335-345 (1999).

68. E. Fontaine, O. Eriksson, F. Ichas, P. Bernardi, Regulation of the Permeability Transition Pore in Skeletal Muscle Mitochondria: Modulation By Electron Flow Through The Respiratory Chain Complex I. *Journal of Biological Chemistry* **273**, 12662-12668 (1998).

69. A. M. Porcelli *et al.*, Respiratory Complex I Dysfunction Due to Mitochondrial DNA Mutations Shifts the Voltage Threshold for Opening of the Permeability Transition Pore toward Resting Levels *. *Journal of Biological Chemistry* **284**, 2045-2052 (2009).

70. Y. V. Surovtseva, G. S. Shadel, Transcription-independent role for human mitochondrial RNA polymerase in mitochondrial ribosome biogenesis. *Nucleic Acids Research* **41**, 2479-2488 (2013).

71. J. D. Chavez *et al.*, A General Method for Targeted Quantitative Cross-Linking Mass Spectrometry. *PLOS ONE* **11**, e0167547 (2016).

72. H. Lam *et al.*, Development and validation of a spectral library searching method for peptide identification from MS/MS. *Proteomics* **7**, 655-667 (2007).

73. R. Au - Marcu, C. K. Au - Neeley, G. Au - Karamanlidis, B. J. Au - Hawkins, Multi-parameter Measurement of the Permeability Transition Pore Opening in Isolated Mouse Heart Mitochondria. *JoVE*, e4131 (2012).

74. J. K. Eng, M. R. Jahan Ta Fau - Hoopmann, M. R. Hoopmann, Comet: an open-source MS/MS sequence database search tool.

75. A. Keller, A. I. Nesvizhskii, E. Kolker, R. Aebersold, Empirical Statistical Model To Estimate the Accuracy of Peptide Identifications Made by MS/MS and Database Search. *Analytical Chemistry* **74**, 5383-5392 (2002).

76. L. A. Kelley, S. Mezulis, C. M. Yates, M. N. Wass, M. J. E. Sternberg, The Phyre2 web portal for protein modeling, prediction and analysis. *Nature Protocols* **10**, 845-858 (2015).

77. A. S. Rose, P. W. Hildebrand, NGL Viewer: a web application for molecular visualization. *Nucleic Acids Research* **43**, W576-W579 (2015).

78. D. L. Roberts, F. E. Frerman, J.-J. P. Kim, Three-dimensional structure of human electron transfer flavoprotein to 2.1-Å resolution. *Proceedings of the National Academy of Sciences* **93**, 14355-14360 (1996).

79. D. K. Inaoka *et al.*, Structural Insights into the Molecular Design of Flutolanil Derivatives Targeted for Fumarate Respiration of Parasite Mitochondria. *International Journal of Molecular Sciences* **16**, 15287-15308 (2015).

80. M. Suga *et al.*, Distinguishing between Cl- and O22- as the bridging element between Fe3+ and Cu2+ in resting-oxidized cytochrome c oxidase. *Acta Crystallographica Section D* **67**, 742-744 (2011).

Chapter 3: Chemical cross-linking mass spectrometry analysis of protein conformations and supercomplexes in heart tissue

3.1 Abstract

While modern structural biology technologies have greatly expanded the size and type of protein complexes that can now be studied, the ability to derive large-scale structural information on proteins and complexes as they exist within tissues is practically nonexistent. Here, we demonstrate the application of cross-linking mass spectrometry to identify protein structural features and interactions in tissue samples, providing systems-structural-biology insight into protein complexes as they exist in the mouse heart. This includes insights into multiple conformational states of sarcomere proteins, as well as interactions among OXPHOS complexes indicative of supercomplex assembly. The extension of cross-linking mass spectrometry analysis into the realm of tissues opens the door to increasing our understanding of protein structures and interactions within the context of the greater biological system.

3.2 Rationale

Cardiovascular diseases are the principal cause of death globally, resulting in more than 17 million deaths in 2013 (1). Complex diseases such as heart failure are not readily replicated in cell culture models, and the lack of structural information on proteins and complexes that exist within the heart limits understanding of relevant disease pathways and new therapy developments. With recent advances in mass spectrometry based proteomics and the emergence of cross-linking mass spectrometry (XL-MS) methods, molecular structural information in the form of distance restraints between cross-linked residues has been obtained on purified proteins and protein complexes (2-4). The advent of MS cleavable cross-linkers (5, 6) (recently reviewed

by Sinz (7)) has enabled XL-MS analysis of samples of increasing complexity including cell lysates (8, 9). However, opportunities for unique biological insight are offered by XL-MS application to intact cellular systems, where protein concentration is several hundred mg/mL (10, 11) and molecular crowding (12) and subcellular compartmentalization influence protein structures and interactions. XL-MS methods based on protein interaction reporter (PIR) technologies (13) have advanced applications to enable systems-level study of protein conformations and interactions in isolated functional organelles (14), intact virus particles (15, 16), and live cells (17-19) These capabilities allow systems structural biology measurements and even quantitative interactome measurements in stable phenotypic and dynamic pharmacological comparisons (20, 21). A key advantage of *in vivo* XL-MS is that structural information is obtained on proteins within native environments where cellular compartmentalization, influence of macromolecular crowding on protein structures and interactions, concentrations of cofactors, and interaction partners are at or near normal physiological levels. On the other hand, while cultured cells provide significant insight into many physiological properties, replication of organ-level disease states such as cardiomyopathy and heart failure in cell culture models has remained elusive. Large-scale XL-MS has not previously been applied to derive protein structural information directly from tissues, in part due to the bewildering complexity of tissue samples. Here, we demonstrate the feasibility of applying XL-MS to tissue, highlighting the resulting systems-level structural analysis of protein conformations and interactions as they exist within the heart. Future quantitative XL-MS tissue analyses could help elucidate key molecular details that underpin heart failure and other pathologies.

3.3 Results and Discussion

Here, we demonstrate the initial systems structural biology measurements with murine heart tissue samples using XL-MS. These efforts reveal more than 2,000 cross-linked peptide pairs, each of which provides a structural constraint on protein conformations and complexes that exist within the heart (Dataset S1). Each link identifies a pair of Lys residues that must have existed in relative proximity to one another hundreds of billions of times in order to be detected by MS. In this way each link identified here provides structural information on proteins and protein complexes as they existed within the biological system of the heart tissue, hence the term systems structural biology.

To obtain such information, heart tissue was isolated from mice, dissected into 1 mm^3 cubes, and subjected to chemical cross-linking with the PIR cross-linker BDP-NHP (Fig S1) (17). Following the cross-linking reaction, samples were either processed as a whole-heart sample or subjected to subcellular fractionation to isolate mitochondria. Both the whole-heart and isolated mitochondrial samples were subjected to protein extraction, enzymatic digestion, and enrichment of the in-tissue cross-linked peptide pairs before analysis using a realtime MS3 technique termed ReACT (19) (Fig S2). In total, Comet searching of ReACT-generated MS3 spectra identified 2,663 non-redundant cross-linked peptide pairs with an estimated false discovery rate (FDR) of 2.4% (see STAR Methods and Figs S2 and S3 for more details on FDR). These links contain 2,026 non-redundant Lys-Lys linkages in 316 proteins, identifying 419 non-redundant protein-protein interactions (including self-interactions) (Dataset S1). The interaction network is available online in XlinkDB (22, 23) (network name = ChavezCellSystems2017_BruceLab) as well as in Fig S4.

Cardiac muscle consists of specialized highly ordered cytoskeletal structures known as sarcomeres, which are composed of interleaved thick myosin filaments and thin filaments

comprised of actin, tropomyosin, and troponin (Fig S5A). Because sarcomeric proteins exist as dynamic, interdependent, complex proteins with conformations and interactions critical for normal cardiac function, structural knowledge of these proteins obtained directly from heart tissue could yield unique insight into normal and dysfunctional states. Cross-linked peptide pairs from all major sarcomeric proteins were detected, enabling site directed model assembly of the myosin, actin, troponin, and tropomyosin complex onto which 53 interprotein Lys-Lys links were mapped (Fig 3.1A).Myosin 6 (MYH6) is the primary constituent of thick filaments in the sarcomere, providing the ATP-driven motor arm that binds to and pulls on actin in the thin filaments, resulting in sarcomere contraction. A total of 572 cross-linked peptide pairs involving MYH6, including 103 interprotein linkages to 22 different proteins, were identified (Fig S5B). MYH6 is a large (224 kDa) and flexible molecule, existing in an ensemble of conformational states regulated in part by the myosin light chain subunits (MLRV and MYL3) changing the angles about three hinge regions in MYH6 (24, 25). Data from fluorescence and electron paramagnetic resonance-based spectroscopic studies reveal more conformational diversity of the myosin complex than is currently available in models derived from crystallography or cryo electron microscopy (cryo-EM)(26), highlighting the need for data acquired by complementary techniques capable of sampling the complex under dynamic and physiological conditions (27, 28).

Cross-linking captures structural information on the ensemble of conformations, as evident with 10 links (colored yellow) involving MLRV or MYL3 and MYH6 clustered around the three flexible hinge regions of MYH6 (Fig 3.1A). These links are inconsistent (Ca-Ca > 42 A°) with the rigor state model (29) in Fig 3.1A, suggesting that they represent a different conformation of the MYH6 machinery. Three of the over-distance links between MYH6 and MLRV do fall

within an acceptable distance when mapped to a conformation of MYH6 in the OFF state. There are many known disease-related mutations that occur throughout MYH6, and troponin subunits that are linked to cardiomyopathies (30, 31). For myosin to bind actin and induce muscle contraction, calcium is required to bind to the calcium binding subunit of troponin (TNNC1), which causes a conformational shift moving the inhibitory subunit of troponin (TNNI3) and exposing the myosin binding site on actin (32, 33). In contrast to skeletal muscle, cardiomyocytes rely on release of intracellular calcium from the sarcoplasmic reticulum for contraction to occur. This calcium-induced conformational shift is illustrated by the cross-links observed between K165 TNNI3 and K330 of α-actin (ACTA) and K43 of TNNC1 and K330 of ACTA, which are not possible (Ca-Ca distance >42 A°) with the calcium-saturated structural model of troponin (Fig 3.1B), and would only be possible in a calcium-depleted state for which no structural model is available in the PDB. Furthermore, the links between the troponin subunits and K330 of ACTA are mutually exclusive, with seven links identified between 3 MYH6 and ACTA indicating the cross-linking of different conformations within the sarcomere contraction cycle. The cross-linked residues identified between these sarcomeric proteins will serve as probes for specific protein conformations and interactions in future quantitative XL-MS studies, enabling dynamic measurements between diseased and healthy heart tissue.

Due to the extraordinary energy requirements of the heart, cardiomyocytes contain the highest concentration of mitochondria of any cell in the body, comprising 30% of the cellular volume (34). The mitochondrial oxidative phosphorylation complexes (OXPHOS) provide chemical energy for the heart through generation of ATP. The electron transport chain, consisting of OXPHOS Complexes I–IV, transfer electrons from NADH to reduce molecular oxygen and in the process generate a proton gradient across the mitochondrial inner membrane to power ATP

synthase (Complex V). In total, 208 cross-linked Lys residues involved in 319 site-to-site linkages were identified across the five OXHPOS complexes (Fig S6). OXPHOS complexes can be extracted as supercomplexes composed of various combinations of CI to CV (35). Supercomplexes consisting of CI, CIII, and CIV are referred to as respirasomes, as they can carry out respiration in the presence of ubiquinone and cytochrome c, and have been of intense interest in the structural biology field (35). Recently several cryo-EM structures of respirasomes consisting of CI-$CIII_2$-CIV have been made available (36-39). Beyond this, respirasomes have been proposed to assemble into even higher-order structures and respiratory strings (36, 37, 39, 40). Such higher-order complexes are challenging to study, as membrane extraction is likely to disrupt increasingly larger structures. However, XL-MS provides a complementary approach to study these complexes, as protein interaction information is preserved through covalent bond formation on complexes within their native environment.

XL-MS experiments with murine heart tissues described here resulted in identification of multiple links between OXPHOS complexes, defining the existence of larger supercomplex assemblies consistent with the circular Sus scrofa model proposed by Wu et al (39) and single-particle EM results, suggesting the presence of CI_2-$CIII_2$ in potato (40). For instance, lysine sites linking CI and CIII (NDUA2 K13, K75, and K98 to QCR2 K250) and between CI and CIV (NDUA9K189 to COX5A K68) in murine heart XL-MS data were compared with homologous sites on a recent cryo-EM-derived structural model for the purified S. scrofa CI-$CIII_2$-CIV supercomplex (39). The observed links between CI and CIII agree with the supercomplex model (red lines in Fig 3.2A); however, the cross-linked sites between CI and CIV are well beyond possible linking distance when mapped to the CI-$CIII_2$-CIV model (yellow line in Fig 3.2A). NDUA9 exists in the matrix arm of CI, whereas in all current CI-$CIII_2$-CIV supercomplex

models, CIV is located on the opposite end of the CI membrane arm. However, cross-linked site-directed docking of CI-CIV with CI-$CIII_2$-CIV resulted in a circular model of the supercomplex comprising CI2-$CIII_2$-CIV_2 with a two-fold axis of symmetry centered on the CIII dimer (Fig 3.2B). It is certainly possible and likely that a variety of supercomplex assemblies exist within heart tissue, and while the circular model shown in Fig 3.2B is consistent with all intercomplex links between CI, CIII, and CIV, we cannot rule out the possibility that a different conformation resulted in the observed CI-CIV linkage. Regardless of the conformation, the link between NDUA9 and COX5A can be used as a structural probe for the CI-CIV interaction in future quantitative studies aimed at supercomplex assembly. Thus, XL-MS data from murine heart tissue supports the proposed existence of higher-order supercomplex assemblies consisting of two copies each of CI, CIII, and CIV within heart tissue, which could function more efficiently during electron transfer due to reduced distance for diffusion of intermediate electron carriers, CoQ and Cytochrome C, between complexes (39). Importantly, each of the more than 2,000 links contained in Fig S4 and Dataset S1 can now be used to quantify supercomplex assemblies and many other interactions in tissues from normal and failing heart tissues to elucidate their roles in mitochondrial function and heart disease. As Wu et al. (39) indicate, further investigations with noninvasive methods are required to better visualize how respiratory strings and large complex assemblies are formed on the inner mitochondrial membrane. Although the XL-MS method presented here cannot be considered noninvasive, the systems-level information derived by this approach can help fulfill this need.

As was demonstrated with cultured cells, quantitative measurements of cross-linked sites can reveal conformational and interaction changes that underpin relevant functional changes in phenotypic and pharmacological comparisons (21, 41, 42). Here, we show that XL-MS enables

systems structural biology studies at the tissue level. For disease states that cannot readily be replicated in cultured cells, this systems structural biology method provides unique molecular insight into relevant protein conformations and interactions in tissues. Each identified cross-linked peptide pair provides a useful molecular probe that can be used to quantify changes in protein conformations or protein-protein interactions in tissues, and to possibly help identify molecular interactions that can serve as new targets for mitochondrial-targeting therapies for cardiovascular or other diseases.

3.4 Methods

Animal model

This study utilized four mice, strain C57BL/6NCrl (IMSR_CRL:27). Two female mice were harvested at 14.4 weeks of age (DOB: 10/17/2017, harvested 1/26/2017) each weighing over 24 g with no signs of illness. Two male mice were harvested at 12 weeks of age (DOB: 04/28/17, harvested 07/21/17) weighing 26 g with no signs of illness. Mice from both harvest dates were littermates housed in the same cage (group housing all C57Bl6/6NCrl) and chosen randomly into the experimental group. Mice were maintained on a standard rodent diet and water available ad libitum in a vivarium with a 12 h light/dark cycle at 22C. All procedures involving animal use were performed with the approval of Institutional Animal Care and Use Committee of the University of Washington.

Isolation of heart tissue

Mice were deeply anesthetized with pentobarbital at dose > 270mg/kg intraperitoneally. Deep anesthesia was confirmed by lack of response to toe pinch and decreased respiratory rate. The

chest cavity was opened, and the heart was rapidly excised and placed into 5ml of ice-cold mitochondrial isolation medium (MIM) buffer (300 mM sucrose, 10 mM HEPES, 0.2 mM EDTA, pH 7.4). All traces of blood were rinsed away with fresh MIM buffer. The aorta, atria, and any additional tissue were removed. The heart was transferred to a pre-chilled 60mm dry petri dish and maintained on ice. The heart tissue was minced with a razor blade on the dry petri dish to achieve a homogenous tissue size distribution of approximately 1 mm cubes.

Synthesis of chemical cross-linker

The PIR cross-linker BDP-NHP (19), is a peptide based molecule synthesized by solid phase peptide synthesis. The peptide sequence is: Succinate-Asp-Pro-Lys(Pro-Asp-Succinate)-Lys(Biotin)-Gly. For this study it was obtained from AnaSpecsynthesized on Clt resin. To form the reactive cross-linker molecule the succinate groups are converted to N hydroxyphthalamide (NHP) esters. To accomplish this, the BDP on resin is reacted with a twelve-fold molar excess of trifluoroacetate N-hydroxyphthalamideester (TFA-NHP). TFA-NHP is synthesized by dissolving 5.86 g of NHP in a four-fold molar excess (20 mL) of trifluoroaceticanhydride in a 50mL round bottom flask. The reaction is carried out for 1.5 h under an atmosphere of dry N_2 gas with constant mixing by a magnetic stir bar. After 1.5 h, excess TFA is removed using a rotary evaporator set to 30 mbar and a water bath set to 60C. After two hours of rotary evaporation, the water bath is exchanged for an ice bath to crystalize the TFA-NHP. The product is a white crystalline solid obtained in quantitative yield. To synthesize the active form of the cross-linker BDP-NHP, the resin with cross-linker bound is swollen with a minimal volume (~4 mL/ g resin) of dimethyl formamide (DMF). A twelve-fold molar excess of NHP (3.11 g for 1 g of Clt resin containing 1 mmole BDP) is dissolved in 10 mL of dry pyridine and added to the resin. The

reaction is carried out for20 min with constant mixing at room temperature. After 20 min the reaction mixture is loaded onto a Poly-Prep chromatography column (Bio-Rad) and the liquid is removed by vacuum filtration. The resin is then washed extensively with DMF (5 x 10 mL) followed by 5 x 5mL washes with dichloromethane (DCM). The cross-linker is then cleaved from the resin by incubating with 5mL of 95% TFA,5% DCM for 1 h. Following cleavage, the BDP-NHP is precipitated in diethyl ether, pelleted by centrifugation and dried by vacuum centrifugation. The product is then weighed and dissolved in dimethyl sulfoxide (DMSO) at a concentration of 200-300 mM and stored at -80C until use. The chemical structure of BDP NHP is shown in Fig S1.

Chemical cross-linking

Minced mouse heart tissue was centrifuged at 1500 g for 3 min at 4C and supernatant was removed. Tissue was suspended in 0.25 mL of 170 mM Na_2HPO_4 pH 8.0. The PIR cross-linker BDP-NHP (d0 light or d8 heavy isotope forms) was added to final concentration of 10 mM from a 258 mM stock solution in DMSO. The sample was mixed on a Thermomixer at 800 rpm for 30 min at room temperature. The tissue was then centrifuged at 1500 g for 3 min and the supernatant was removed. Cross-linked tissue was then either frozen at -80C or subjected to further processing for mitochondrial isolation as described below.

Mitochondrial isolation from XL heart tissue

Cross-linked heart tissue was suspended in 4 mL of MIM buffer containing 4 mg/mL fatty acid free bovine serum albumin (BSA) and transferred to a glass homogenization tube. The tissue was homogenized using 4-6 passes at 1200-1400 rpm with a teflon pestle. The homogenate was

transferred to a 15 mL tube and centrifuged at 800 g for 10 min at 4C to pellet nuclei and tissue debris. The supernatant was transferred into two 2 mL tubes and centrifuged at 8000 g for 15 min at 4C. The supernatant was removed by aspiration and the two mitochondrial pellets were each suspended in 1 mL MIM buffer and combined to a single tube. The sample was then centrifuged at 8000 g for 15 min at 4C and the supernatant removed to obtain the mitochondrial pellet.

Protein extraction from XL heart tissue

Frozen cross-linked mouse heart tissue was transferred with the aid of 0.5 mL of 0.1M NH_4HCO_3, to a stainless steel cryogrinding jar cooled to -196C with liquid nitrogen. Using a Retsch MM 400 mixer mill, the sample was cryoground for five three minute cycles at 30 Hz and cooled with liquid N_2 between cycles. The resulting frozen powder was transferred to a 15mL tube and 1mL of 8M urea in 0.1 M Tris pH 8.0 was added. Sample viscosity was reduced by sonication using a GE – 130 ultrasonic processor, followed by reduction and alkylation of cysteine residues by incubation with 5 mM Tris(2-carboxyethyl)phosphine (TCEP) (Fisher Scientific) for 30 minutes followed by a 45-min incubation with 10 mM iodoacetamide (Fisher Scientific). To reduce the urea concentration to less than 1M the samples were diluted by a factor of 10 with fresh 0.1M Tris buffer pH 8.0. The protein concentration was measured using the Pierce Coomassie protein assay (Thermo). A fraction of the total protein content (0.37 mg) was set aside for generation of a stage 1 database (described below) while the rest of the protein in the sample was digested with a 1:200 ratio of sequencing grade modified trypsin (Promega) to protein and was incubated at 37C for 18 h. Enrichment of XL Peptide Pairs Digested peptides were desalted with a C18 Sep-Pak cartridge, and the eluted peptides were dried to completion before being resuspended in SCX buffer A [7 mM KH_2PO_4, (pH 2.6), 30% (vol/vol) ACN].

Resuspended peptides were injected into a Phenomenex Luna SCX column and were fractionated using a 97.5-min gradient of buffer B [7 mM KH_2PO_4 (pH 2.6), 30% (vol/vol) ACN, 350 mM KCl] as follows: 0% buffer B at 0 min, 5%B at 7.5 min, 60% B at 47.5 min, 100% B at 67.5 min, 100% B at 77.5 min, 0% B at 77.51 min, and 0% B at 97.5 min. Fractions were taken every 5 min starting at 17.5 min and were pooled into six pools as follows: fractions 1–5,fractions 6–7, fraction 8, fraction 9, fraction 10, and fractions 11–14. Fraction pools were dried to a final volume of ~2mL in a vacuum centrifuge, and the pH was adjusted to 8.0 with 1.5M NaOH. Pooled cross-linked peptides were enriched by the addition of 200 mL of monomeric avidin bead slurry (Ultralink; Pierce) and were incubated at room temperature on an orbital shaker at maximum speed. Cross-linked peptides were washed with 100mM ammonium bicarbonate, pH 8.0, and eluted with 70% (vol/vol) ACN/1% formic acid before being dried to completion in a vacuum centrifuge and stored at -80C until analyzed.

LC-MS^3 analysis of XL peptide pairs

Samples containing PIR cross-linked peptides were analyzed in technical triplicate by liquid chromatography mass spectrometry using a Waters NanoAcquity UPLC coupled to a Thermo Velos-FTICR mass spectrometer and a real-time adaptive, targeted mass spectrometry method developed for PIR cross-linked peptides (ReACT). Peptides were loaded onto a 3 cm x 100 mm inner diameter fused silica trap column packed with a stationary phase consisting of Michrom Magic C8, 5 mm diameter, 200 Å pore size particles (Bruker) with a flow rate of 2 mL/min of mobile phase consisting of 98% solvent A (H2O containing 0.1% formicacid) and 2% solvent B (ACN containing 0.1% formic acid) for 10 min. Peptides were then fractionated over a 60 cm x 75 mm inner diameter fused silica analytical column packed with Michrom Magic C8, 5 mm

diameter, 100-Å pore size particles by applying a linear gradient from 95% solvent A, 5% solvent B to 60% solvent A, 40% solvent B over either 120 or 240 minutes at a flow rate of 300 nL/min. Eluting peptide ions were ionized by nano-electrospray ionization by applying a positive 2 kV potential to a laser pulled spray tip at the end of the analytical column. The Velos-FTICR mass spectrometer was operated utilizing ReACT where a high resolution MS1 scan is acquired in the ICR cell at a resolving power of 50,000 at 400 m/z. Ions with a charge state of four or greater were selected for low energy CID fragmentation using a normalized collision energy (NCE) of 25 followed by high resolution MS2 analysis in the ICR cell at a resolving power of 50,000 at 400 m/z where an ‘‘on-the-fly’’ check of the observed fragment ion masses against the PIR mass relationship (Mass Precursor = Mass Reporter Ion + Mass Peptide 1 + Mass Peptide 2) is performed. Masses that satisfied the PIR relationship within a tolerance of 20 ppm mass error triggered subsequent low resolution MS3 analyses of the released cross-linked peptide ions in the Velos ion trap mass analyzer operated at normal unit resolution. For details on processing of data generated on the Velos-FTICR see the section: Database searching of ReACT MS3 spectra below.

Generation of a Stage 1 database of putative cross-linked proteins

100 mL of UltraLink monomeric avidin slurry was added to 0.37 mg of cross-linked protein extracted from PIR cross-linked heart tissue and incubated at room temperature for 30 min. The monomeric avidin beads were washed 5 times with 1mL of 0.1 M NH_4HCO_3 pH 8.0 before eluting PIR reactive proteins using 100 μL of 8M urea containing 2mM biotin in 0.1M NH_4HCO_3 pH 8.0. Disulfide bonds in the eluted proteins were reduced with 5mM TCEP for 30 minutes followed by alkylation with 10mM iodoacetamide for 45 min. Samples were diluted 10x

with 0.1 M NH_4HCO_3 pH 8.0 before overnight digestion with a 1:200 ratio of trypsin at 37C. The peptide samples were then desalted using C18 SepPak cartridges, followed by concentration and removal of acetonitrile by vacuum centrifugation using an EZ2-Plus evaporator. The sample volume was adjusted to 100 mL with 0.1% formic acid before being analyzed by data dependent LC-MS/MS using an Easy-nLC (Thermo) coupled to a Q-Exactive Plus mass spectrometer (Thermo). Peptides were separated by reversed-phase chromatography using in-house packed C18 columns. Peptides were loaded onto a 3-cm x 100-mm inner diameter fused silica trap column packed with a stationary phase consisting of ReproSil C18, 5-mm diameter, 200 Å pore size particles (Dr. Maisch GmbH) with a flowrate of 2 mL/min of mobile phase consisting of 98% solvent A (H2O containing 0.1% formic acid) and 2% solvent B (ACN containing 0.1% formic acid) for 10 minutes. Peptides were then fractionated over a 60-cm x 75-mm inner diameter fused silica analytical column packed with ReproSil C18, 5-mm diameter, 100 Å pore size particles (Dr. Maisch GmbH) by applying a linear gradient from 90% solvent A, 10% solvent B to 60% solvent A, 40% solvent B over 120 minutes at a flow rate of 300 nL/min. Eluting peptide ions were ionized by nano-electrospray ionization by applying a positive 2 kV potential to a laser pulled spray tip at the end of the analytical column. The Q-Exactive Plus mass spectrometer operated using a data dependent analysis method consisting of a MS1 scan at 70,000 resolving power at m/z 200 followed by MS2 scans at 17,500 resolving power on the 20 most abundant ions in the MS1. Ions selected for MS2 were isolated using a 1.6 m/z isolation window, and fragmented by higher-energy collisional dissociation (HCD) using a normalized collision energy of 27. Additional MS2 settings included an automatic gain control (AGC) setting of 50,000 ions, a maximum ion accumulation time of 50 ms, charge state exclusion settings to not select ions with charge states of one, more than eight or unassigned and a dynamic

exclusion time of 30 s. Mass spectral data acquired on the Q-Exactive plus was searched against the mouse UniProt database containing both forward and reverse protein sequences (downloaded 01/07/2017, containing 33,670 total sequences) using Comet (version 2016.01 rev. 2) (43). Default parameters were used unless stated otherwise. The mass error tolerance was set to 20 ppm for the precursor mass allowing for standard 13C error offsets (-1/0/1/2/3). Carbamidomethylated cysteine was specified as a static modification while methionine oxidation and lysine acetylation were included as variable modifications. Resulting peptide spectrum matches were filtered at 1% FDR. A total of 13,619 peptide sequences were identified corresponding to 2063 proteins. The stage 1database used to search the ReACT generated MS3 spectra, as described below, consisted of the forward and reverse sequences of these 2063 proteins.

Database searching of ReACT MS3 spectra

Comet was used to search the MS3 spectra generated from ReACT against the stage 1 database containing the forward and reverse sequences for 2063 putatively cross-linked proteins (4126 total sequences) using the following parameters: 20 ppm mass error tolerance for the precursor mass allowing for standard 13C error offsets. Each peptide sequence was required to contain the residual PIR cross-linker mass modification on Lys residues. The residual cross-linker mass differed for the full heart sample cross-linked with the light isotope cross-linker d0-BDP (197.032422 Da) and the post-XL isolated mitochondria sample cross-linked with heavy isotope labeled d8-BDP (201.0575293 Da). Carbamidomethylated cysteine was specified as a static modification, while methionine oxidation and lysine acetylation were included as variable modifications. Fragment ion tolerance was set to 1.005 Da. Peptide spectral matches (PSMs) to

the MS3 spectra were mapped back to the PIR mass relationships identified in the MS2 spectra during the ReACT analysis. Comet assigns each PSM an expectation value, or E-value, which is a statistical measure that standardizes the reporting of peptide identifications. The Comet E-value is calculated by applying a linear least-squares regression on the log transform of the cumulative distribution function of the histogram of the cross-correlation score (xcorr) and extrapolating the point at which the top scoring peptide intersects the least-squares fit line (43). The E-value can be interpreted as the number of peptides that are expected to score as well as the top scoring peptide by chance in the search (44). Based on the principle described by Trnka et al. that cross-linked peptide pair identifications are only as confident as the worst scoring of the two peptides (45), an E-value threshold of 0.2 or less was applied to the greater E-value for each cross-linked peptide pair. This resulted in a dataset with an estimated FDR of 0.76% (81/10600) at the PSM level, 2.4% (64/2663) at the non-redundant peptide pair level, and (63/2026) 3.1% FDR at the non-redundant site-to-site level. Here, non-redundant cross-linked peptide pairs are defined as each pair of peptides with a unique primary sequence, including unique modifications. For example the cross-linked peptide pair AVGEK189EVR_K68GMNTLVGYDLVPEPK and AVGEK189EVR_K68GM[147.04]NTLVGYDLVPEPK are counted as two non-redundant pairs due to the site of oxidation (indicated by the mass 147.04 Da) on the third residue of the second peptide. Both of these peptide pairs identify the same Lys-Lys linkage and collapse to a single entry in the reported in the 2,026 non-redundant Lys-Lys pairs. A PTM, such as methionine oxidation, results in a different mass and so the modified peptide pair analyzed and identified independently in the LC-MS workflow. Modified cross-linked peptide pairs contain unique masses, are analyzed separately, and represent unique probes that could be useful for studying the structures of the linked proteins. PTMs such as methionine oxidation could alter a protein

structure or its interactions and in that sense should be listed separately so that future studies using cross-linked peptide pairs as probes for conformations or interactions can take that into account. For more details on the estimation of FDR see the Quantification and Statistical Analysis section below.

Structural analysis and modeling

For assembly of the sarcomere protein complex shown in Figure 1, structural information from the PDB models: 5H53, 5CJ1, 4XA4,5CHX, 5CJ0, 1J1E, and 5JLH was utilized. Clustal Omega v1.2.4 was used to align the protein sequences in the PDB structures to the homologous mouse protein sequences obtained from UniProt. A series of structural superposition and manual docking utilizing cross-link distance constraints was carried out using ICM Molsoft MolBrowser Pro v. 3.8-6. PDB 5H53 contains structural information for the myosin motor (MYH6), the essential myosin light chain (MYL3), the regulatory myosin light chain (MLRV) and two monomers of actin (ACTA). The coiled-coil domain for MYH6 was modeled by superposition of overlapping structural data from PDB files 5CJ1, 5CJ0, 5CHX and 4XA4 and aligning this with residues 836-845 of myosin in 5H53. Tropomyosin (TPM1) was incorporated into the model by aligning the actin chains of 5JLH with those in 5H53. Structural information for the troponin complex proteins TNNC1, TNNT2, and TNNI3 was obtained from PDB 1J1E. Data from cross-links (TPM1 K168- TNNT2 K223, TPM1 K168 - TNNT2 K271,TPM1 K168 - TNNI3 K107, TNNT2 K286 – K330 ACTA, TNNI3 K165 – ACTA K330, TNNC1 K43 – ACTA K330, and TNNT2 K286 –MYH6 K352) between the three troponin proteins and TPM1, ACTA and MYH6 were utilized as distance constraints to dock 1J1E onto the assembled myosin, actin, tropomyosin complex by maximizing the number of links that fell below the distance constraint of 42 Å. The

resulting docked structure was evaluated for consistency with published models for the interaction of troponin with the thin filament (32, 33).The heterodimeric complex of the trifunctional enzyme proteins ECHA and ECHB was constructed by generating homology models for ECHA and ECHB using Phyre2 (46) on intensive mode. Rigid body molecular docking of the ECHA and ECHB models was accomplished using PatchDock (47) utilizing the cross-links between ECHA and ECHB with a distance constraint of 42 Å. A total of 3 models resulted from PatchDock and the top scoring model is displayed in Figure S2.The model of the circular CI_2-$CIII_2$-CIV_2 supercomplex was assembled using the atomic coordinates from PDB 5GUP. CI was docked to the CIII using the three links between NDUA2 and QCR2 (NDUA2 K13, K75, and K98 to QCR2 K250). A second copy of CI was superimposed symmetrically about the CIII dimer and CIV was docked into the CI_2CIII_2 complex using the cross-link between COX5A K68 and NDUA9 K189 as a distance constraint with an upper limit of 42 Å. A total of 16 models resulted from PatchDock and the top scoring model is displayed in Figure 2B.

Estimation of false discovery rate for ReACT MS3 identifications

Comet generated PSMs to MS3 spectra acquired by ReACT were mapped back to the PIR relationship (Mass Precursor = MassReporter Ion + Mass Peptide 1 + Mass Peptide 2) identified during the LC-MS acquisition. This step is performed entirely base on scan number as MS3 spectra on released peptides are only generated following the acquisition of an MS2 spectrum that satisfies the PIR mass relationship with a mass tolerance of less than 20 ppm. Initially PSMs are filtered to only include those with a Lys residue internal to the sequences (not C-term Lys) that is modified by the cross-linker (197.032422 Da). All PSMs containing an internal cross-linked residue, irrespective of E-value, are matched to the PIR relationships detected during the

MS acquisition. This results in four possibilities for cross-linked peptide pair sequences: 1) both peptides are assigned forward sequences (fwd_fwd), 2) first peptide assigned a forward sequence and second peptide assigned a reverse sequence (fwd_rev), 3) first peptide assigned a reverse sequence and second peptide assigned a forward sequence (rev_fwd), and 4) both peptides assigned reverse sequences (rev_rev).The complete unfiltered list of assignments is available in Dataset S1. Following matching of PSMs to the PIR relationships, the assigned peptide pairs are sorted in ascending order according to the worst scoring (largest E-value) of the two PSMs. This is the most conservative approach relying on the principle described by Trnka et al.(45) that the assignment of a cross-linked peptide pair is only as good as the worst scoring PSM for the pair. With the sorted list of cross-linked peptide pair assignments, the false discovery rate is estimated by taking the ratio of the sum of decoy assignments to target assignments:(fwd_rev + rev_fwd + rev_rev)/(fwd_fwd). For the current study a maximum E-value threshold of 0.2 was applied resulting in an FDR of 0.76% at the PSM level. As recently highlighted by Fisher and Rappsilber (48), FDR for cross-linked peptides can be estimated at different levels, namely: PSM level, non-redundant peptide pair level, non-redundant site-site level and protein-protein level. As redundancy is removed between each level correct assignments will tend to collapse on each other while decoy assignments tend to accumulate leading to an increase in the estimated FDR at each level. One way to control for this is to calculate FDR for cross-linked peptide pairs that have multiple PSMs, as decoy assignments tend to be random and only have single PSMs, the FDR will drop while maintaining a large percentage of correct assignments. This is illustrated in Figure S1D. Beyond evaluating the FDR on the entire data set, the FDR can also be estimated for individual subsets of cross-linked peptide pairs, namely intra-protein, inter-protein, and homo-dimer cross-links. Homo-dimer cross-links are a special case where two peptides with

overlapping sequences, which originate and occur only once within a given protein sequence are cross-linked together. These homo-dimer cross-links serve to unambiguously identify homo-oligomeric protein interactions. As can be seen in Figures S3A–S3D, all decoy assignments passing the E-value threshold occur in the inter-protein class resulting in effectively 0% FDR in the intra-protein and homo-dimer link classes at our E-value threshold of less than or equal to 0.2. While slightly enriched in decoy hits, the estimated FDR for the inter-protein linkages is also acceptably low at 3.9% at the PSM level.

Data software and availability:

The complete set of mass spectrometry data is available through Proteome Exchange PRIDE Archive accession number PXD007673.

3.5 Figures

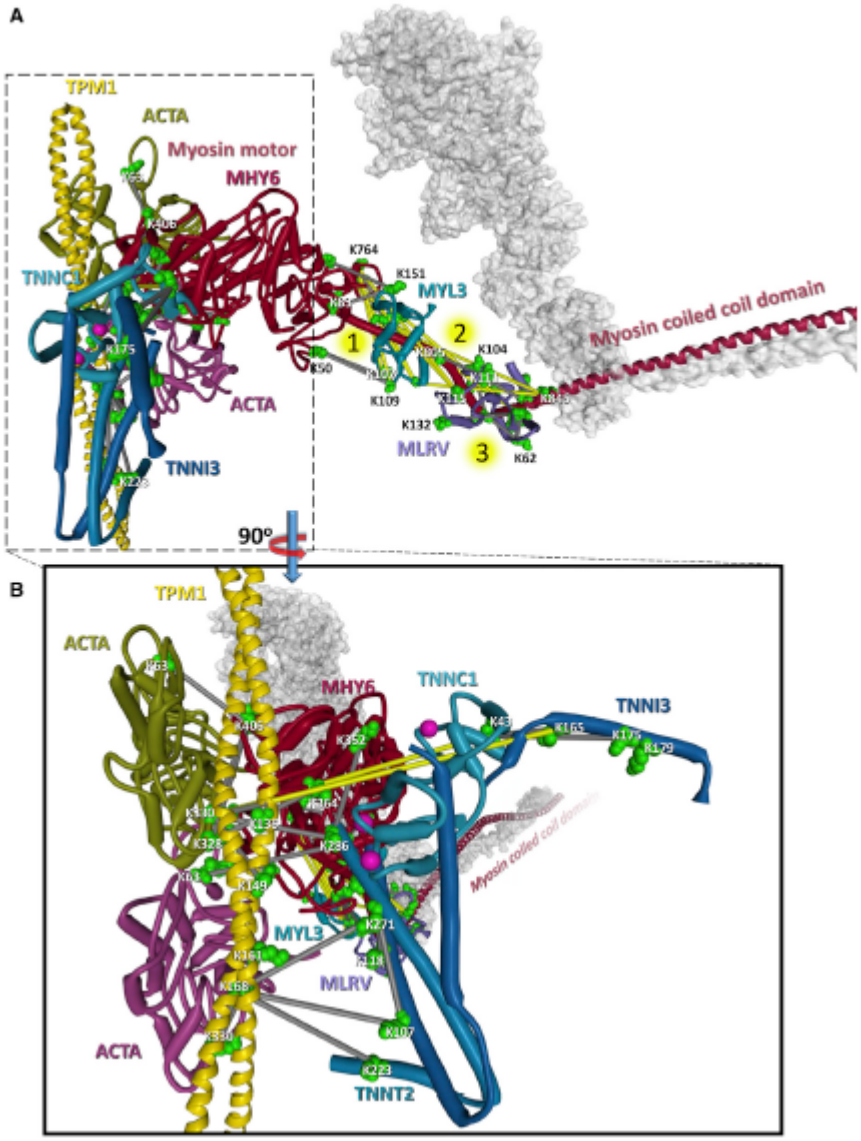

Figure 3.1: Cross-linking-Derived Model for Sarcomere Protein Complexes

(A) Structural model of sarcomere protein interactions including the thick filament proteins: myosin motor (MYH6, red), myosin essential light chain (MYL3, teal blue), myosin regulatory light chain (MLRV, blue-violet), and the thin filament proteins: actin (ACTA green and red-violet), tropomyosin (yellow), and the three troponin subunits (TNNC1, light blue; TNNT2, blue; TNNI3, dark blue). The model utilizes structural information from structures PDB: 5H53, 5CJ1,

4XA4, 5CHX,5CJ0, 1J1E, and 5JLH. The second MYH6 molecule is represented by a gray semi-transparent structure. Cross-linked sites are indicated by green space-filled residues, and links between residues are displayed as gray bars (Ca-Ca distance <42 Å) or yellow bars (Ca-Ca distance >42 Å). A total of 10 cross-links (2 MYH6-MLRV and 8 MYH6-MYL3) exceed 42 Å. These links are clustered around three flexible hinge regions indicated by numbered yellow circles in the MYH6 light chain binding domain. It is likely that these links are representative of the conformational flexibility of the myosin motor and are formed from a different conformation than the rigor state model shown here. Forty-six homodimer cross-linked peptide pairs were also identified in the coiled-coil domain of MYH6 (see Dataset S1). (B) Zoomed inset of a 90° rotation of the structure shown in (A). Calcium ions bound to TNNC1 are shown as magenta spheres. The yellow links between K165 of TNNI3 and K330 of ACTA and K43 of TNNC1 and K330 of ACTA exceed the possible cross-linkable distance and are not compatible with the calcium-saturated structure of troponin (PDB: 1J1E), and are instead indicative of the calcium-depleted state of troponin in which TNNI3 changes conformation to interact with ACTA, effectively blocking the myosin interaction site (32, 33). See also Dataset S1 and Figure S5.

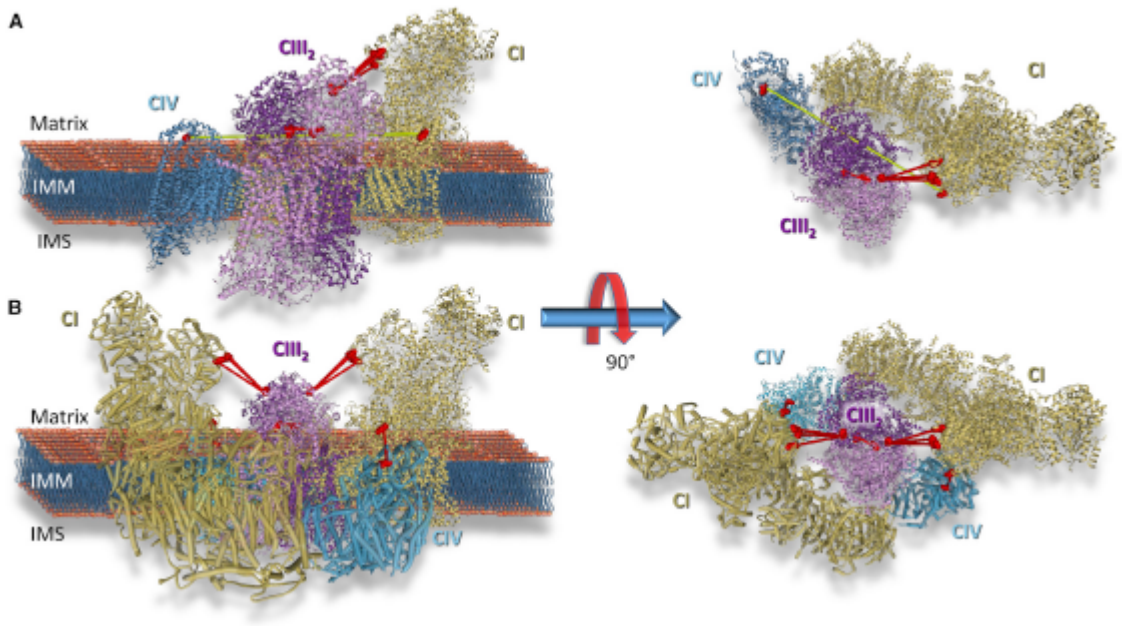

Figure 3.2: Cross-linking-Derived Model for Respirasome Supercomplex CI_2-$CIII_2$-CIV_2

(A) Cryo-EM-derived structure of respirasome CI-$CIII_2$-CIV (PDB: 5GUP) with cross-links identifying interactions between CI (gold ribbon) and CIII (purple ribbon) (NDUA2 K13, K75, and K98 linked to QCR2 K250), CIII homodimer (QCR2 K159 linked to QCR2 K159), and CI and CIV (teal-blue ribbon) (COX5A K189 linked to NDUA9 K68) displayed. Cross-linked sites are shown as space-filled residues. Residues connected by red lines agree with the structure while residues connected by a yellow line exceed the maximum cross-linkable distance (42 Å). (B) Structure of a circular representation of the respirasome CI_2-$CIII_2$-CIV_2, which agrees with all observed cross-linked sites. See also Dataset S1 and Figure S6.

Supplementary information and additional resources of this chapter are included in the following publication:

Chemical Cross-linking Mass Spectrometry Analysis of Protein Conformations and Supercomplexes in Heart Tissue

Juan D. Chavez, Chi Fung Lee, Arianne Caudal, Andrew Keller, Rong Tian, James E. Bruce

3.6 References

1. G. A. Roth *et al.*, Demographic and epidemiologic drivers of global cardiovascular mortality. *N Engl J Med* **372**, 1333-1341 (2015).
2. Z. A. Chen *et al.*, Architecture of the RNA polymerase II–TFIIF complex revealed by cross-linking and mass spectrometry. *The EMBO journal* **29**, 717-726 (2010).
3. A. Leitner *et al.*, The Molecular Architecture of the Eukaryotic Chaperonin TRiC/CCT. *Structure* **20**, 814-825 (2012).
4. A. Tosi *et al.*, Structure and Subunit Topology of the INO80 Chromatin Remodeler and Its Nucleosome Complex. *Cell* **154**, 1207-1219 (2013).
5. J. W. Back *et al.*, A new cross-linker for mass spectrometric analysis of the quaternary structure of protein complexes. *Journal of the American Society for Mass Spectrometry* **12**, 222-227 (2001).
6. X. Tang, G. R. Munske, W. F. Siems, J. E. Bruce, Mass Spectrometry Identifiable Cross-Linking Strategy for Studying Protein−Protein Interactions. *Analytical Chemistry* **77**, 311-318 (2005).
7. A. Sinz, Cross-linking Mass Spectrometry Goes In-Tissue. *Cell Systems* **6**, 10-12 (2018).
8. F. Liu, D. T. S. Rijkers, H. Post, A. J. R. Heck, Proteome-wide profiling of protein assemblies by cross-linking mass spectrometry. *Nature Methods* **12**, 1179-1184 (2015).
9. D. Tan *et al.*, Trifunctional cross-linker for mapping protein-protein interaction networks and comparing protein conformational states. *eLife* **5**, e12509 (2016).
10. M. B. Elowitz, M. G. Surette, P.-E. Wolf, J. B. Stock, S. Leibler, Protein Mobility in the Cytoplasm of Escherichia coli. *Journal of Bacteriology* **181**, 197-203 (1999).
11. J. Malmström *et al.*, Proteome-wide cellular protein concentrations of the human pathogen Leptospira interrogans. *Nature* **460**, 762-765 (2009).
12. R. J. Ellis, Macromolecular crowding: obvious but underappreciated. *Trends in Biochemical Sciences* **26**, 597-604 (2001).

13. X. Tang, J. E. Bruce, A new cross-linking strategy: protein interaction reporter (PIR) technology for protein-protein interaction studies. *Molecular bioSystems* **6**, 939-947 (2010).

14. D. K. Schweppe *et al.*, Mitochondrial protein interactome elucidated by chemical cross-linking mass spectrometry. *Proceedings of the National Academy of Sciences* **114**, 1732-1737 (2017).

15. J. D. Chavez *et al.*, Cross-linking Measurements of the Potato leafroll virus Reveal Protein Interaction Topologies Required for Virion Stability, Aphid Transmission, and Virus–Plant Interactions. *Journal of Proteome Research* **11**, 2968-2981 (2012).

16. S. L. DeBlasio *et al.*, Visualization of Host-Polerovirus Interaction Topologies Using Protein Interaction Reporter Technology. *Journal of Virology* **90**, 1973-1987 (2016).

17. J. D. Chavez, C. R. Weisbrod, C. Zheng, J. K. Eng, J. E. Bruce, Protein Interactions, Post-translational Modifications and Topologies in Human Cells. *Molecular & Cellular Proteomics* **12**, 1451-1467 (2013).

18. Arti T. Navare *et al.*, Probing the Protein Interaction Network of Pseudomonas aeruginosa Cells by Chemical Cross-Linking Mass Spectrometry. *Structure* **23**, 762-773 (2015).

19. C. R. Weisbrod *et al.*, In Vivo Protein Interaction Network Identified with a Novel Real-Time Cross-Linked Peptide Identification Strategy. *Journal of Proteome Research* **12**, 1569-1579 (2013).

20. J. D. Chavez *et al.*, Quantitative interactome analysis reveals a chemoresistant edgotype. *Nature Communications* **6**, 7928 (2015).

21. Juan D. Chavez, Devin K. Schweppe, Jimmy K. Eng, James E. Bruce, *Cell Chemical Biology* **23**, 716-726 (2016).

22. D. K. Schweppe *et al.*, XLinkDB 2.0: integrated, large-scale structural analysis of protein cross-linking data. *Bioinformatics* **32**, 2716-2718 (2016).

23. C. Zheng *et al.*, XLink-DB: Database and Software Tools for Storing and Visualizing Protein Interaction Topology Data. *Journal of Proteome Research* **12**, 1989-1995 (2013).

24. J. H. Brown *et al.*, Visualizing key hinges and a potential major source of compliance in the lever arm of myosin. *Proceedings of the National Academy of Sciences* **108**, 114-119 (2011).

25. O. Pylypenko, A. M. Houdusse, Essential "ankle" in the myosin lever arm. *Proceedings of the National Academy of Sciences* **108**, 5-6 (2011).

26. D. D. Thomas, D. Kast, V. L. Korman, Site-Directed Spectroscopic Probes of Actomyosin Structural Dynamics. *Annual Review of Biophysics* **38**, 347-369 (2009).

27. A. C. Knowles *et al.*, Orientation of the Essential Light Chain Region of Myosin in Relaxed, Active, and Rigor Muscle. *Biophysical Journal* **95**, 3882-3891 (2008).

28. W. M. Shih, Z. Gryczynski, J. R. Lakowicz, J. A. Spudich, A FRET-Based Sensor Reveals Large ATP Hydrolysis–Induced Conformational Changes and Three Distinct States of the Molecular Motor Myosin. *Cell* **102**, 683-694 (2000).

29. T. Fujii, K. Namba, Structure of actomyosin rigour complex at 5.2 Å resolution and insights into the ATPase cycle mechanism. *Nature Communications* **8**, 13969 (2017).

30. A. N. Chang, M. S. Parvatiyar, J. D. Potter, Troponin and cardiomyopathy. *Biochemical and Biophysical Research Communications* **369**, 74-81 (2008).

31. J. R. Moore *et al.*, Understanding Cardiomyopathy Phenotypes Based on the Functional Impact of Mutations in the Myosin Motor. *Circulation Research* **111**, 375-385 (2012).

32. N. M. Cordina *et al.*, Ca2+-Induced PRE-NMR Changes in the Troponin Complex Reveal the Possessive Nature of the Cardiac Isoform for Its Regulatory Switch. *PLOS ONE* **9**, e112976 (2014).

33. S. Takeda, A. Yamashita, K. Maeda, Y. Maéda, Structure of the core domain of human cardiac troponin in the Ca^{2+}-saturated form. *Nature* **424**, 35-41 (2003).

34. J. Schaper, E. Meiser, G. Stämmler, Ultrastructural morphometric analysis of myocardium from dogs, rats, hamsters, mice, and from human hearts. *Circulation Research* **56**, 377-391 (1985).

35. D. Milenkovic, J. N. Blaza, N.-G. Larsson, J. Hirst, The Enigma of the Respiratory Chain Supercomplex. *Cell Metabolism* **25**, 765-776 (2017).

36. J. Gu *et al.*, The architecture of the mammalian respirasome. *Nature* **537**, 639-643 (2016).

37. J. A. Letts, K. Fiedorczuk, L. A. Sazanov, The architecture of respiratory supercomplexes. *Nature* **537**, 644-648 (2016).

38. J. S. Sousa, D. J. Mills, J. Vonck, W. Kühlbrandt, Functional asymmetry and electron flow in the bovine respirasome. *eLife* **5**, e21290 (2016).

39. M. Wu, J. Gu, R. Guo, Y. Huang, M. Yang, Structure of Mammalian Respiratory Supercomplex I1III2IV1. *Cell* **167**, 1598-1609.e1510 (2016).

40. J. B. Bultema, H.-P. Braun, E. J. Boekema, R. Kouřil, Megacomplex organization of the oxidative phosphorylation system by structural analysis of respiratory supercomplexes from potato. *Biochimica et Biophysica Acta (BBA) - Bioenergetics* **1787**, 60-67 (2009).

41. J. D. Chavez *et al.*, A General Method for Targeted Quantitative Cross-Linking Mass Spectrometry. *PLOS ONE* **11**, e0167547 (2016).

42. X. Zhong *et al.*, Large-Scale and Targeted Quantitative Cross-Linking MS Using Isotope-Labeled Protein Interaction Reporter (PIR) Cross-Linkers. *Journal of Proteome Research* **16**, 720-727 (2017).

43. J. K. Eng, T. A. Jahan, M. R. Hoopmann, Comet: An open-source MS/MS sequence database search tool. *Proteomics* **13**, 22-24 (2013).

44. J. K. Eng, B. Fischer, J. Grossmann, M. J. MacCoss, A Fast SEQUEST Cross Correlation Algorithm. *Journal of Proteome Research* **7**, 4598-4602 (2008).

45. M. J. Trnka, P. R. Baker, P. J. J. Robinson, A. L. Burlingame, R. J. Chalkley, Matching Cross-linked Peptide Spectra: Only as Good as the Worse Identification. *Molecular & Cellular Proteomics* **13**, 420-434 (2014).

46. L. A. Kelley, S. Mezulis, C. M. Yates, M. N. Wass, M. J. E. Sternberg, The Phyre2 web portal for protein modeling, prediction and analysis. *Nature Protocols* **10**, 845-858 (2015).

47. D. Schneidman-Duhovny, Y. Inbar, R. Nussinov, H. J. Wolfson, PatchDock and SymmDock: servers for rigid and symmetric docking. *Nucleic Acids Research* **33**, W363-W367 (2005).

48. L. Fischer, J. Rappsilber, Quirks of Error Estimation in Cross-Linking/Mass Spectrometry. *Analytical Chemistry* **89**, 3829-3833 (2017).

Chapter 4: Mitochondrial interactome quantitation reveals structural changes in metabolic machinery in failing murine heart

4.1 Abstract

Advancements of cross-linking mass spectrometry (XL-MS) for structural analysis of proteins bridges the gap between purified systems and native tissue environments. Here, isobaric quantitative protein interaction reporter technology (iqPIR) was utilized to further extend XL-MS to the first system-wide comparative study of mitochondrial proteins from healthy and diseased murine hearts. The failing heart interactome includes 602 statistically significant cross-linked peptide pairs altered in the disease condition. Structural insight into ketone oxidation metabolons, OXPHOS machinery, and nucleotide transporter hybrid-conformations, support mitochondrial remodeling in failing heart while bringing forth new hypotheses for pathological mechanisms. Application of quantitative cross-linking technology in tissue provides molecular-level insight to complex biological systems difficult to model in cell culture, thus providing a valuable resource for study of human diseases.

4.2 Rationale

Mitochondria contain over 1,100 proteins that orchestrate diverse cellular functions, from intermediary metabolism and energy production to signaling and cell death (1, 2). Extensive genomic and proteomic approaches have resulted in a curated compendium of mitochondrial proteins with their sub-organellar localization (1). Advancements in cryo-electron microscopy, X-ray crystallography and NMR have greatly increased understanding of protein function and have enabled structure visualization of purified mitochondrial proteins and complexes with sizes unimaginable only a few years ago (3-7). However, within its native cellular or subcellular

environment, protein function is dynamically-regulated by the presence of other proteins, post-translational modifications, substrates, cofactors, and transient conformational changes that are not directly measured with conventional techniques.

Chemical cross-linking combined with mass spectrometry (XL-MS) methods have emerged to provide structural insight from complex samples (8). A cross-linker approach based on peptide synthesis chemistry to introduce MS cleavable features and affinity tags referred to as Protein Interaction Reporter (PIR) technology (9) has enabled interactome-level structural studies with isolated functional mitochondria (10), intact virus particles (11), live cells (12, 13), and even whole tissue samples (14), providing unique structural insights on protein interaction landscapes. While identification of *in vivo* protein-protein interactions (PPIs) and conformational features from cross-linked peptides increases knowledge about how proteins function within cells, quantitation of cross-linked peptide level changes during perturbation reveal molecular features that confer functional changes at the systems-level. For instance, quantitation of PIR cross-linked peptide levels in cells using SILAC (15) revealed functional differences relevant to acquired resistance to topoisomerase I inhibition therapy (16). Moreover, quantitative PIR applications to cellular pharmacological studies revealed interactome changes that are drug-concentration dependent and mechanism-of-action specific (13, 17). Thus, quantitative cross-linking technologies enable visualization of interactome changes in living systems relevant to functional changes that could be informative in pathological comparisons. Recently, PIR technologies were further advanced to include isobaric quantitative capabilities that can enable quantitative interactome studies for systems without need for SILAC (18), as is employed here for failing heart mitochondrial interactome studies.

Due to the extraordinary energy requirements of the heart, cardiomyocytes contain the highest concentration of mitochondria of any cell in the body across mammalian species (19, 20). Concurrently, mitochondrial dysfunction is a well-known maladaptive mechanism in the progression of heart failure. In this study, the feasibility of applying isobaric quantitative PIR (iqPIR) (18) XL-MS technology to mitochondria from healthy and failing mouse hearts is demonstrated. For the first time, integrated measurements of protein interactions, conformations, and surface accessibility allowing for comparative network analysis was enabled directly in tissue. These advancements provide the unique opportunity to study chronic, organ-level conditions, where cell modeling does not holistically recapitulate the bewildering complexity of disease. Of the total ~3,800 non-redundant cross-linked peptide pairs detected, 90% of cross-linked peptide pairs are quantified in at least one biological replicate. Statistical analysis revealed 602 cross-linked peptide pairs were significantly altered in failing hearts compared to sham controls, corresponding to altered catalytic pockets, hybrid conformations, and higher-order protein assemblies. This study provides molecular-level insight into basic mitochondrial function, and serves as a systems-level resource for generating new hypotheses for disease progression.

4.3 Results and Discussion

Quantitation of mitochondrial protein interactome in failing hearts

A workflow was developed to assess mitochondrial protein interactome in failing hearts using iqPIR technology (Fig 4.1A). Heart failure was induced by transverse aortic constriction (TAC, n=6) surgery in mice. Sham-operated (Sham) animals were used as controls (n=6). TAC hearts demonstrated a decline in left ventricular fractional shortening (Fig 4.1B) and increased chamber

size (Fig S1A-B) compared to Sham. At harvest, TAC mice showed significant cardiac hypertrophy (Fig 4.1C) and clear signs of pulmonary congestion (Fig S1C-D), indicating the development of heart failure.

Dissected TAC or Sham cardiac tissue was cross-linked with 2-plex iqPIR cross-linker with either Reporter Heavy (RH) or Stump Heavy (SH) iqPIR versions. TAC and Sham cross-linked samples were then mixed pairwise in a 1:1 ratio based on equal amount of total proteins. Thus, a total of 6 pairs of biological replicates were generated including 3 pairs of forward samples (RH labeled TAC combined with SH labeled sham) and 3 pairs of reverse samples (SH labeled TAC combined with RH labeled sham). The forward/reverse labeling strategy was used to evaluate if there was any quantitation bias caused by labeling direction.

In total, 3,792 non-redundant cross-linked peptide pairs were identified from 6 pairs of TAC/Sham heart samples at an estimated FDR of 1% or less, corresponding to 2,734 lysine residue pairs and 507 protein pairs. The failing heart interactome network is available online in XLinkDB (21) (xlinkdb.gs.washington.edu, network table name = CaudalCellCommunity2021_Bruce). From the total coverage, over 90% (3607/3792) of the cross-linked peptide pairs were quantified in at least one of 6 pairs of biological replicates. All quantified cross-link ratios were plotted against the p-value of each ratio (Figure 4.1D), which determined statistical outliers (significance threshold p-value= 2.5×10^{-6}). The data were further processed by applying a statistical t-test and Bonferroni correction to all quantified cross-linked peptides, then further filtered to a maximum of 2 missing ratios out of 6 pairs of biological replicates.

A final number of 602 cross-links were quantified showing statistically significant differences between TAC and Sham hearts (Supplemental Table 1). The heat map containing 602 cross-

links was generated using NG-CHM BUILDER (22) with Euclidean distance and complete linkage selected for hierarchical clustering (Figure 4.1E). A total of 316 cross-linked peptides were decreased while 286 cross-linked peptides were increased in TAC.

iqPIR cross-linkers employ reactive esters to covalently react with surface accessible lysine residues. Dead-end (DE) labeled peptides are generated when only one ester reacts with a lysine residue, while the other ester is hydrolyzed. This feature is useful as a read-out for the surface accessibility of proteins, and an indirect survey of relative protein level changes. Since PPI levels can be affected by endogenous protein levels, DE-labeled peptide quantitation and intra-cross-linked peptides were used to estimate protein abundance for each cross-linked peptide pair as demonstrated previously by Chavez et al (18). For each non-redundant cross-link pair, the mean Log2 ratios for Protein A and Protein B were calculated from all DE peptides (Supplemental Table 1, Fig S1E). In addition, reproducibility of the data was evaluated by applying linear regression to 6 pairs of biological replicates on a pair-wise basis. R-squared values were calculated and shown in Fig 4.1F. Despite the known individual variations in the TAC model, strikingly high data correlation and consistency were observed across all 15 comparisons of 6 TAC/Sham pairs. It is worth noting that each sample is 1:1 mix of cross-linked proteins from two different animals thus regression fitting of two samples involved 4 different animals. The correlations of forward and forward labeling samples (average R^2=0.54) are similar to those of forward and reverse labeling samples (average R^2=0.45) (Supplemental Table 2), which further confirmed the consistency and reproducibility of iqPIR quantitation results. The subset of cross-linked peptide pairs displaying statistically different ratios in TAC were further analyzed by interaction network analysis (Fig S1F). Comprehensive views of pathways and proteins exhibiting large statistical changes (Log 2 ratios are generally ≥1 or ≤-1) led to key highlights of

TAC-induced structural changes that will be further discussed in greater detail in the following sections.

Active conformational states of ketone oxidation proteins enriched in TAC

Recent studies demonstrated an increase in ketone consumption by failing hearts (23-25). Enzymes for ketone oxidation, D-β-hydroxybutyrate dehydrogenase (BDH) and Succinyl-CoA:3-oxoacid-CoA transferase (SCOT1), were upregulated in the failing heart but mechanisms driving the flux of ketone oxidation were not fully understood (24-26). Circulating ketones, primarily generated by the liver, are taken up by cardiomyocytes and metabolized via three consecutive reactions catalyzed by BDH, SCOT1 and Acetyl-CoA acetyltransferase (THIL) to produce acetyl-CoA for further oxidation in the TCA cycle (Fig 4.2A). Consistent with increased expression of ketone metabolism proteins in failing myocardium (24, 25), DE quantitation of BDH, SCOT1 and THIL were increased in the iqPIR dataset (Supplemental Table 1). However, quantification of cross-linked lysine residues in SCOT1 and THIL did not match the changes of DE suggesting the presence of protein structural changes beyond changes to abundance (Fig 4.2B).

SCOT1, encoded by the *Oxct1* gene, is a tetramer of two inter-connected homodimers (Fig 4.2C). It transfers a Coenzyme A (CoA) moiety from succinyl-CoA to acetoacetate to form acetoacetyl-CoA and succinate (Fig 2A). The reaction involves E344 in the active site, which sits between two binding pockets for succinate/acetoacetate (residues 321-329, Loop A) and CoA (residues 374-386, Loop B), respectively (27). Four non-redundant cross-linked peptide pairs in SCOT1 were increased during TAC (Fig 2B, S2A). Cross-linked peptides containing K286, K296, K418, and K421 were mapped onto the SCOT1 structure (human SCOT1 PDB: 3DLX)

and pinpointed a key surface near Loop A (Fig 2C). During catalysis, the C-terminal undergoes a 17 degree angle domain rotation where Loop A must conform in order to alleviate steric clashing with the static N-terminal (27). We hypothesize that the rotation renders the cross-linking of the four peptide pairs possible. Thus, increases in the cross-linked peptide pairs suggest a greater fraction of SCOT1 assumes an active conformational state in TAC. As K286 and K296 reside in a relatively disordered region of SCOT1, where detailed structural information is unavailable. However, large conformational change in the C-terminal domain, where the four cross-linked peptide pairs reside, is observed when apo (PDB: 3OXO, chain A) and substrate-bound (PDB: 3OXO, chain E) porcine SCOT1 monomers are aligned (Fig S2B) (28, 29) supporting the notion that active enzyme assumes distinct conformation in the region. In humans, naturally occurring mutations in Loop A, such as G324E and L327P, result in SCOT1 loss-of-function (30), indicating the importance of flexible conformations observed in this region.

The homodimer link between SCOT1 K296-K296 increased ~2-fold in TAC (p-value=$2.13E^{-13}$) indicating increased interaction between two monomeric units of SCOT1 (Fig 2A). However, the K296-K296 distance mapped onto the human tetramer structure (PDB:3DLX) (Figure S2C) is~66Å, which exceeds the span possible by iqPIR cross-linkers (Cα-Cα<42Å). These results suggested that SCOT1 exists in an alternative conformation or higher order assembly which is increased in TAC. To determine if this is the case, human SCOT1 tetramers were subjected to molecular docking (31). With no distant constraints, docking results from 6 of the top 10 solutions (Fig 4.2D, S3A) consistently placed this region at the interface between two tetramers. The N-terminal domain is relatively static (Fig S2B) during catalysis, yet the cross-linked peptide pair K214-K274 exhibited decreasing quantitation during TAC (Fig 2C). Higher-order

docking solutions of SCOT1 place K214 and K274 buried at the oligomeric interface between two tetramers in three solutions (Fig S3B). In these conformations, either K214 or K274 would be inaccessible to cross-linking, which further supports possible enrichment of SCOT1 oligomer in TAC.

In contrast to SCOT1, the cross-link between K242-K260 in THIL decreased in TAC despite a moderate increase of DE (mean Log2 ratio=0.19, Fig 2B). This peptide pair was mapped to lysine residues located on adjacent monomers of the human crystal structure (Fig 4.2E, Substrate-bound THIL PDB 2IBW). Residue K260 (conserved human K263) helps form the CoA binding pocket and provides the only salt-bridge contact with the 3'phosphate moiety (32). Post-translational modification (PTM) at either K242 or K260 provides one possible explanation for decreased cross-linking. However, previous reports demonstrated that hyperacylation at K260 suppressed THIL activity (33, 34) Increased ketone oxidation, as observed in heart failure (23-25), would likely increase salt-bridge occupancy by forming the K260-CoA interaction necessary for catalysis and consequently, decrease cross-linking accessibility (Figure S3C).

Taken together, quantitative iqPIR analysis confirmed the upregulation of ketone metabolism proteins as previously reported, and furthermore, suggest possible mechanisms for active protein conformations in the failing hearts. These findings provide greater insight on how ketone metabolism is potentially adapted in the failing heart that could enable future therapeutic developments.

Decreased interaction between NDUA4 and C6XB1 affects CIV activity in TAC

Mitochondrial respiration, assessed by oxygen consumption rate (OCR), was reduced in TAC hearts (Fig 4.3A-B). Multiple mechanisms have been proposed for impaired OCR, among which

altered function of electron transport chain (ETC) has been proposed (19). Quantitative mitochondrial interactome data analysis revealed five cross-linked lysine pairs between NDUA4 and CX6B1 (human COX6B isoform 1) in Complex IV that were significantly decreased in TAC (Fig 4.3C, Supplemental Table 3). Complex IV (Cytochrome C oxidase, CIV) is the terminal end of the electron transport chain, which accepts two electrons from Cytochrome C (CYC) to reduce oxygen into water. Due to its high sensitivity to detergent conditions (35, 36) interaction between NDUA4 and other subunits of Complex IV has been difficult to assess. Since iqPIR cross-linkers were applied directly to heart tissue to secure PPIs with covalent bonds, the disruption of detergent-sensitive interactions such as those of NDUA4 was avoided with this approach. Identification of multiple NDUA4 inter-protein cross-linked peptide pairs provides direct and definitive evidence that NDUA4 exists as a component of CIV in cardiac mitochondria and provides insight into the NDUA4-CX6B1 interaction. Cross-linked peptides containing residues K10, K13, and K85 of CX6B1 and K56, K74 and K76 of NDUA4 were mapped to disordered regions of both proteins residing in the IMS (Fig 4.3D, PDB: 5Z62) making further structural analysis challenging. Mutations in CX6B1 R20 which disrupt a salt-bridge with D17 (37) are hypothesized to cause instability of CIV leading to encephalomyopathy and hypertrophic cardiomyopathy in patients (38). R20 is likely stabilized by a salt-bridge with nearby NDUA4 D60, although this side-chain is only partially resolved in the structure (Figure S4A, PDB: 5Z62). However, Complex IV activity was found to be significantly decreased in TAC (Figure S4B) raising the possibility that NDUA4-CX6B1 interaction modulated CIV function. Furthermore, as NDUA4 blocks the CIV dimerization interface, its presence maintains CIV primarily as a monomer thus facilitating Complex I-III_2-IV respirasome assembly (35). Alterations in the interaction between NDUA4 and other subunits of CIV could therefore affect

respirasome formation. Decreased CI-$CIII_2$-CIV respirasome has been previously reported in heart failure (39). Thus, quantitative mitochondrial interactome analysis reveals remodeling of Complex IV structure as a new contributor to impaired mitochondrial respiration within the failing heart.

Enrichment of an intermediate state of ADP/ATP carrier detected in TAC

Exchange of ATP and ADP between mitochondria and cytosol is achieved by the mitochondrial ADP/ATP carrier (ADT), a highly conserved, abundant, and extensively studied translocase (40). ADT is a dual gated transporter that interconverts between at least two known distinct structural conformations (Fig 4.4A). During a normal cycle, the cytoplasm-open state (C-state) faces the IMS and the gate to the mitochondrial matrix is closed via a series of salt-bridges, allowing for the release of a bound ATP and the binding of a new cytosolic ADP (40). The binding of ADP induces a conformational shift to the matrix-open state (M-state) in which the gate to the IMS is closed by formation of new salt-bridges and a hydrophobic plug (41). The M-state releases cytosolic ADP in exchange for a newly charged ATP and the cycle repeats. These conformational changes permit the transport of large nucleotide solutes across small protein carriers while preventing proton leak throughout the exchange process (42). Mammalian ADT exists in four isoforms which exhibit tissue-dependent but overlapping expression patterns. Quantitative iqPIR analysis revealed increased levels of seven non-redundant cross-linked peptide pairs of ADT1 in TAC (Fig 4.4B, S4C). It should be noted that other ADT isoforms and multimeric ADT structures may also be present that could explain increases in these observed links (Figure S4D), but ADT1 is the predominant isoform in cardiac and skeletal muscle (43). Cross-links between K23-K92, K23-K94, K23-K96 and K23-K199 are compatible with the C-

state (40) of ADT1 because all lysine residues are solvent exposed in this conformation (Fig 4.4C, S4B, bovine ADT1 PDB: 1OKC, Supplemental Video 1). However, these links are not compatible with the M-state because K92, K94, K96, and K199 must penetrate occluded volume of the protein in this conformation. Moreover, K96 and K199 form salt bridge interactions with D196 and D292 that contribute to the ADT1 gate closure to the IMS (Fig 4.4D, S4E, TtAac ADT1 PDB: 6GCI, Supplemental Video 1). Although the K23 and K33 cross-link is compatible with distance constraints, it is known that K33 partakes in the hydrogen-bond network needed to stabilize the C-state by forming a salt-bridge with D232 (40) (Fig S4F). On the other hand, cross-links between K23-K33, K23-K147, and K33-K147 are compatible only with the M-state (Fig 4D, S4D). Thus, increases of all seven links would indicate that both C-state and M-state have increased in TAC. This is, however, unlikely given the mutual exclusivity of M- and C-states and the observation of no large change in ADT1 protein levels (Log2 TAC/Sham= 0.5). Functionally, increased enrichment of C-state in failing hearts, in which ATP production is known to be impaired, is also counter-intuitive. Collectively, increases in these seven cross-linked peptide pairs and ADT1 protein level measurements in TAC hearts cannot be explained by either a shift between C-state and M-state of ADT1 in heart failure.

Perhaps a more likely explanation is the existence of an alternative state of ADT1, with which all quantified cross-links are compatible, and this new conformation has increased in TAC. To satisfy all the cross-links in one single state, lysine residues involved in gating at either C- or M-state must be accessible to cross-linkers. This new conformation could be consistent with the P-state which was recently proposed to be simultaneously open to both the IMS and the matrix, synonymous with non-selective mPTP conductance (41, 42). Although there is currently no known structural evidence, the non-selective P-state is hypothesized to provide an open channel

where the lysine residues responsible for gating are not involved in salt bridge formation and thus, may be available for cross-linking. Thus, our results provide novel structural evidence that heart failure is associated with increased conformational enrichment of ADT1 that is non-functional for ADP/ATP translocation but likely possesses non-selective conductivity (44).

In this study, iqPIR technology achieved one of the highest levels of cross-linking complexity resolved from tissue thus far. Our comparative studies of mitochondria in normal and failing hearts yield quantitative changes in 98 mitochondrial proteins, providing a system's view of protein structure remodeling in heart failure. Among the 602 cross-linked peptide pairs that showed statistically significant level differences in TAC vs. Sham hearts, enrichment of active ketone oxidation enzymes, altered interactions among Complex IV subunits and novel conformational enrichment of the ADP/ATP transporter were revealed in TAC hearts. These findings advance mitochondrial and heart failure research in several ways. First, the data elucidate new structural information on key players in mitochondrial function, providing a basis for developing future therapies. Second, the results enable generation of novel hypotheses for mechanisms of mitochondrial maladaptation in disease. Most importantly, the quantitative interactome dataset provides a valuable resource for exploration and visualization of changes in many other proteins not discussed here that may be important for improved understanding of mitochondrial function and heart failure pathology.

Using iqPIR technology as a discovery-based approach in this study, conformational and interaction changes in mitochondrial proteins and complexes were observed that possess direct functional relevance to metabolic changes in heart failure. Identification of SCOT1 oligomer metabolons and increased active conformational states of SCOT1 and THIL in the present study are corroborated by previously reported metabolic changes in failing hearts. Therefore, this

agreement serves as affirmation of the utility of quantitative *in vivo* cross-linking and mass spectrometry as a means to gain greater molecular-level insight on changes in heart failure. Importantly, changes in ketone metabolism has been thus far attributed to substrate and enzyme abundance in heart failure with no information on regulatory mechanisms (26). Our results provide new insight into metabolic remodeling, suggesting that active conformations exist beyond mere increases in protein levels.

The first direct evidence for the NDUA4 existence as a CIV subunit within cardiac tissue was provided by PIR technology (14). The present iqPIR data further confirms that interaction and enables the first quantitation of the NDUA-CX6B1 interaction in failing and control heart tissues with five non-redundant Lys-Lys residue pairs between NDUA4 and CX6B1. The decrease in NDUA4-CX6B1 interactions and concomittant decrease in CIV activity in heart failure samples suggests this interaction could serve as a potential modulator of CIV activity. NDUA4 is thought to maintain CIV monomeric population by occupying the CIV dimerization interface. Decreased NDUA4-CX6B1 cross-links, coincident with decreased CIV activity in TAC, supports the hypothesis that monomer and respirasome populations are functionally active populations (35). It remains unclear whether destabilization of NDUA4 during TAC results in consequential alterations of CIV dimeric pools, and what role this population, if any, may have in disease pathology (45). Nonetheless, the present observation that NDUA4-CX6B1 interactions decrease in heart failure presents a new, previously unrecognized target for future studies and possible therapies that stabilize this interaction as treatment to restore or prevent CIV functional decline in heart failure.

Mitochondrial ADP/ATP carrier (ADT) has long been proposed to contribute a pore-forming component of the mitochondrial permeability transition pore (mPTP) (42, 46). However, several

decades of genetics and physiological studies have yielded ambiguous evidence. Transient opening of mPTP has physiological function such as regulating mitochondrial calcium homeostasis or reactive oxygen species signaling while prolonged mPTP contributes to cell death under stress conditions including heart failure (43). Our results provide critical structural information consistent with recently proposed P state of ADT which opens to both matrix and inter-membrane space (43). It remains unclear whether the P-state is static, or is resultant from rapid interconversion between two incompletely gated structures. Nonetheless, increased presence of such a state compromises nucleotide translocation function and increases mitochondrial proton leaks leading to impaired energetics. In support of this notion, a mitochondrial-targeted tetrapeptide, elamipretide (SS-31), is shown to bind K23 of ADT1 and reduces proton leak in mitochondria of aging animals (47). Thus, changes in the conformational state of ADT warrants further investigation both as a disease mechanism and a therapeutic target. In summary, we demonstrate that iqPIR and mass spectrometry constitute a powerful technology to quantify protein structural changes at the systems-level in tissues. Application of this technology to animal models of heart failure generated a new mitochondrial protein interactome that revealed novel mechanisms that underpin potential therapies.

4.4 Methods

Key resources table

REAGENT or RESOURCE	SOURCE	IDENTIFIER
Chemicals, Peptides, and Recombinant proteins		
iqPIR cross-linker	AnaSpec, Chavez et al 2020	Peptide sequence: Gly-GlyLys(biotin)-Lys-Pro_2-Asp_2-$succinate_2$-N-hydroxyphthalimide $(NHP)_2$
Deposited Data		
LC-MS data deposited into PRIDE	https://www.ebi.ac.uk/pride/archive/	Accession No: PXD027757
Cross-link data deposited into XLinkDB	http://xlinkdb.gs.washington.edu/xlinkdb/index.php	Network Name: CaudalCellCommunity2021_Bruce
Experimental Models: Organisms/Strains		
Mouse: C57BL6/NCrl	Charles River Laboratories	IMSR_CRL:27
Software and Algorithms		
Comet v. 2018	Eng et al 2013	
Mango	Moir et al 2018	
Xlink Prophet	Keller et al 2002	

Resource availability

Lead contacts

Further information and requests for resources and reagents should be directed to and will be fulfilled by the lead contacts, Rong Tian (rongtian@uw.edu) and James E. Bruce (jimbruce@uw.edu).

Data and software availability

Cross-linking data has been deposited at XlinkDB and is publicly available as of the date of publication. DOI is listed in the key resources table. The mass spectrometry proteomics data have been deposited to the ProteomeXchange Consortium via the PRIDE (49) partner repository with the dataset identifier: PXD027757. Any additional information required to reanalyze the data reported in this paper is available from the lead contacts upon request.

Experimental models and subject details

All protocols concerning animal use were approved by the Institutional Animal Care and Use Committee at University of Washington. This study utilized 12 wild-type mice, strain C67Bl6/NCrl (IMSR_CRL:27). Female and male mice have different responses to pressure overload. TAC surgery causes a mild and variable phenotype in female. Thus, only male mice were used in this study. Adult (>10 weeks old, weighing 24-26g) male mice were chosen randomly into experimental groups. Mice were housed in a vivarium with a 12 hr light/dark cycle at 22°C. Mice were maintained on ad libitum standard rodent diet and water.

Transverse aortic constriction (TAC) surgery

Male mice aged 10-12 weeks, weighing 24-28g underwent TAC or Sham surgery as previously described (50). Mice were anesthetized with 4% isoflurane and intubated with a 20-gauge canula. Mice were ventilated at 2.5% isoflurane at 135 breaths per minute by a small animal TOPO ventilator (Kent Scientific, Torrington, CT). The aortic arch was exposed and separated from the thymus via left thoracotomy. A 27-gauge blunt needle was held near the aorta (between the brachiocephalic and left common carotid arteries). A constriction of the transverse aorta was generated by tying a 6-0 Ethilon ligature against the blunt needle. The needle was then promptly removed. The lungs were inflated and the chest was closed by 5-0 polypropylene suture. The animal was removed from the ventilation system and given SR buprenorphine (subcutaneous, 0.5mg/kg) analgesic and 0.9% saline (intraperitoneal, 0.2ml) for hydration after mice regained consciousness (2hrs after ventilation). Sham operated mice underwent all the same procedures as TAC, excluding ligature of the aorta. Mice were randomly assigned to TAC and Sham procedures, and researcher was blind to operation until after echocardiogram analysis was performed. Combined mortality (acute and chronic) was less than 25%.

Transthoracic echocardiography

Mice were anesthetized and maintained with 0.8%-2% isofluorane in 95% oxygen at rates of 550-600 beats per minute as done previously(51). Trans-thoracic echocardiography was conducted 4 weeks post-TAC and Sham surgery with Vevo 2100 high-frequency, high resolution digital imaging system (VisualSonics) with a MS400 Microscan Transducer. A parasternal long-axis view was used to collect M-mode images for analysis of fractional shortening, ejection fraction, and other functional parameters.

Cross-linking of cubed heart tissue

Mice were euthanized by cervical dislocation. The chest cavity was opened, and the heart was rapidly excised and placed into ice-cold, mitochondria isolation medium (MIM: 70mM sucrose, 220mM mannitol, 5mM MOPS, 1.6mM carnitine hydrochloride, 1mM EDTA, 0.025% fatty acid-free BSA, pH 7.4 with 5M KOH) to flesh out blood. The aorta and atria were removed. The myocardium was weighed (heart weight). The heart was transferred to a pre-chilled 60mm dry petri dish and maintained on ice. Heart tissue was finely minced with a razor blade to a homogenous tissue size distribution of approximately $1mm^2$ cubes.

Heart tissue was centrifuged at 1500 x g for 5 min at 4°C, and MIM was replaced with cross-linking buffer (170 mM Na2HPO4, pH 8). iqPIR (18) is a novel technology recently developed for quantitation of cross-linked peptide pairs using isobaric stable isotopes selectively incorporated into the PIR cross-linker, which enables MS^2-based interactome quantitation in a way analogous to how TMT (52) or iTRAQ (53) is used for proteome quantitation. Briefly, reporter heavy (RH) or stump heavy (SH) iqPIR cross-linkers were applied to different samples

individually first, then TAC/Sham cross-linked sample pairs were pooled together for further downstream sample processing and data acquisition. This strategy greatly decreases sample handling errors and reduces instrument time for data acquisition. Identical cross-linked peptide pairs from TAC and sham samples have identical masses and LC retention times, yet produce different and distinct quantitative isotope signatures in MS^2 spectra. The intensities of TAC- or Sham-distinct isotope labeled peptide and fragment ions in each MS^2 spectrum enable relative quantitation of cross-linked peptides in TAC and Sham samples. The samples were mixed for 30 min at room temperature on a Thermomixer at 800 rpm. The tissue was centrifuged at 1500 x g for 5 min at 4°C and the supernatant was removed. Cross-linked tissue was then further subjected to modified mitochondrial isolation as described below.

Mitochondrial isolation from cross-linked heart tissue

Cross-linked heart tissue was washed in fresh MIM and centrifuged at 1500 x g for 5 min at 4°C. Subsequent steps are the same as regular mitochondrial isolation protocol below. However, resulting fractions and supernatants were collected after each step. All fractions were frozen in -80°C after isolation and saved for processing.

Protein extraction from cross-linked mitochondria

Frozen fractions were transferred to a stainless steel cryogrinding jar cooled to -196°C with liquid nitrogen in 0.1M NH_4HCO_3. The samples were cryoground for five 3 min cycles at 30 Hz using a Retch MM 400 mixer mill. Between cycles, the cryogrinder was cooled with liquid nitrogen between cycles. The resulting frozen powder was transferred to a falcon tube where 8M urea (in 0.1M Tris, pH 8.0) was added. Samples were sonicated using a GE-130 ultasonic

processor, followed by reduction of cysteine residues by incubation with 5mM Tris (2-carboxyethyl) phosphine (TCEP, Fisher Scientific) for 30 min followed by alkylation with 45 min incubation with 10mM iodoacetamide (Fisher Scientific). Urea concentration was reduced to less than 1M by diluting the samples by a factor of 10 with fresh 0.1M Tris Buffer (pH 8.0). The protein concentration was measured using the Pierce Coomassie protein assay (Thermo Scientific).

Protein digestion and enrichment of cross-linked peptides

The procedures for protein digestion, desalting, and enrichment of cross-linked peptides by strong cation exchange chromatography (SCX) and biotin-capture were followed as described in a previous publication (54). Briefly, extracted protein were digested with trypsin (200:1 in weight ratio) overnight at 37°C and then quenched with acidification of digest to pH ~3 by adding TFA. The digest was then desalted using Sep-Pak cartridges and fractionated on SCX using a flow rate of 1.5 mL/min and 97.5-min gradient with an increasing percentage of SCX solvent B (solvent A: 7 mM KH_2PO_4, pH 2.6, 30% (vol/vol) acetonitrile and solvent B: 7 mM KH_2PO_4, pH 2.6, 350 mM KCl, 30% (vol/vol) acetonitrile). The SCX fractions were adjusted to pH 8.0 and then subjected to biotin capture by adding monomeric avidin UltraLink resin (Thermo Scientific) to each pooled fraction. After 3 times of washing the avidin beads with 0.1 M NH_4HCO_3, pH 8.0, the cross-linked peptides were eluted with 70% (vol/vol) acetonitrile, 1% (vol/vol) formic acid (FA) and then dried in a speed vacuum. The dried samples were reconstituted in 0.1% FA and ready for LC-MS/MS analysis.

LC-MS/MS

Cross-linked peptide samples were analyzed in technical duplicate by liquid chromatography mass spectrometry using an Easy-nLC (Thermo Scientific) coupled to a Q Exactive Plus mass spectrometer (Thermo Scientific). Each analysis used a 3 µL injection of sample onto a 3 cm x 100 µm inner diameter fused silica trap column packed with a stationary phase consisting of 5 µm Reprosil C8 particles with 120 Å pores (Dr. Maisch GmbH) with a flow rate of 2 µL/ min of mobile phase consisting of solvent A (H2O containing 0.1% formic acid) for 10 minutes. Peptides were then fractionat-ed over a 60 cm x 75 µm inner diameter fused silica analytical column packed with 5 µm Reprosil C8 particles with 120 Å pores by applying a linear gradient from 95% solvent A, 5% solvent B (acetonitrile containing 0.1% formic acid) to 60% solvent A, 40% solvent B over either 120 or 240 minutes at a flow rate of 300 nL/min. Eluting peptide ions were ionized by electrospray ionization by applying a positive 2.2 kV potential to a laser pulled spray tip at the end of the analytical column. The mass spectrometer was operated using a top five data dependent acquisition method with a resolving power setting of 70,000 for MS^1 and MS^2 scans. Additional settings include an AGC target value of 1e6 with a maximum ion time of 100 ms for the MS^1 scans and an AGC value of 5e4 with a maximum ion time of 300 ms for the MS^2 scans. Charge state exclusion parameters were set to only allow ions with charge states from 4+ to 7+ to be selected for MS^2. Ions selected for MS^2 were isolated with a 3 m/z window and fragmented by HCD using a normalized collision energy setting of 30. Ions for which MS^2 was performed were then dynamically excluded from further selection for MS^2 for 30 s.

Heat map analysis

Perseus (version 1.6.15.0) (55) was used for statistical data analysis of cross-link quantitation ratios. Data was first filtered based on 70% of total valid values across all biological replicates

and then applied with T-test using Benjamini-Hochberg FDR at 0.05. T-test q-values less than 0.05 were considered significant. Heatmaps were generated using NG-CHM GUI software (version 2.20.0) (22) with Euclidean distance and complete linkage selected for both row and column hierarchical clustering.

Mitochondrial isolation from cardiac tissue

Hearts were excised from mice, the aortas and atria were removed. Heart tissues were rinsed briefly in ice-cold mitochondria isolation medium (70mM sucrose, 220mM mannitol, 5mM MOPS, 1.6mM carnitine hydrochloride, 1mM EDTA, 0.025% fatty acid-free BSA, pH 7.4 with 5M KOH) with the addition of 2 mM taurine, to remove residual blood. Tissues were minced on ice and resuspended in fresh MIM, followed by trypsin digestion (10ug/ml) and incubated on ice for 10 min. Trypsin digestion was stopped by the addition of trypsin inhibitor (0.5mg/ml) and additional BSA (1 mg/ml) to MIM. The suspension was centrifuged for 1 min at 1,500 x g at 4°C, and the supernatant was discarded. The tissue pellets were resuspended in fresh MIM containing 1mg/ml BSA, and transferred to a Teflon-glass tube and homogenized on ice with a Teflon pestle. The homogenates were centrifuged for 10 min at 800 x g at 4°C. The supernatants were collected and centrifuged for 10 min at 8,000 x g at 4°C. The supernatant was discarded and the mitochondrial pellets were resuspended in MIM to wash. The resuspension was centrifuged for 10 min at 8,000 x g at 4°C, and the supernatant discarded. The mitochondrial pellet was resuspended to a concentrated volume for protein quantification by BCA Assay (Pierce).

Mitochondrial respiration using Seahorse XFe24 analyzer

The oxygen consumption rate (OCR) of isolated cardiac mitochondria was measured with an XF24e Flux Analyzer (Seahorse Bioscience, Agilent) based off the manufacturer's protocol(56). The Seahorse utility plate was hydrated with calibration buffer and incubated overnight at 37°C prior to respiration experiments. The mitochondria were seeded in 24-well microplates at 1-2ug protein per well in 1x mitochondrial assay solution (70mM sucrose, 220mM mannitol, 10mM KH_2PO_4, 5mM $MgCl_2$, 2mM HEPES, 1mM EGTA, 0.2% BSA, pH 7.35 at room temperature) containing substrates and centrifuged for 2,000 x g for 20 min at 4°C. Respiration buffer was added to each well to a final volume of 500ul, then the plate was placed in a non-CO2 incubator for 10 min at 37°C. The plate was incubated the Seahorse Analyzer and a baseline oxygen consumption rate (OCR) was measured. Sequential injections of inhibitors (final concentration 4mM ADP, 2.5 ug/mL oligomycin, 4uM carbonyl cyanide-4-(trifluoromethoxy)phenylhydrazone, and 4uM antimycin A) were added into each well and changes in OCR were measured. For Complex I-supported respiration, 10mM pyruvate and 2mM malate were given to mitochondria seeded at 2ug/well.

Molecular docking calculation

Crystal structures of tetrameric of human SCOT1 (PDB: 3DLX) were subjected to rigid body molecular docking using online platform, SymmDock (31). Without applying distance constraints, the ten highest scoring solutions were analyzed with the biomolecular visualization tool, Pymol. Residues and sidechains surrounding K296 (human 284-286 and 297-299) are shown as yellow spheres because residues 296-296 are unresolved in all solved structures. The putative interface between SCOT1 structures consistently puts regions surrounding K296 of opposite tetramers nearby (within 42Å distance in 6 of the top 10 solutions).

Cytochrome C oxidase and citrate synthase activity from heart tissue homogenate

Citrate synthase (CS) and Cytochrome C Oxidase (COX) activities were determined in heart tissue homogenates at 30°C using a protocol adapted from previously published methods (57). Briefly, for CS activity frozen cardiac tissue (25mg) was homogenized at 4°C in CelLytic™ MT Cell Lysis Reagent (C3228) and then incubated on ice for 30 minutes. The samples were then centrifuged at 10,000 x g for 10 minutes at 4°C and protein concentration determined. CS activity was analyzed in 100mM Tris buffer containing 0.1% Triton X-100, pH 8.0 as previously described (57).

For COX activity, 25mg of cardiac tissue was homogenized at 4°C in 50 mM potassium phosphate buffer containing 1 mM EDTA, and 0.1%Triton X-100 (pH 7.4; final concentration, 5 mg tissue/mL). The samples were incubated on ice for 30 minutes followed by centrifugation at 10,000 x g for 10 minutes at 4°C. COX activity was analyzed in 100mM potassium phosphate buffer as previously described (57).

Quantification and statistical analysis

Assessment of cardiac and mitochondrial function

The numbers of independent experiments are specified in the relevant figure legends. Data are expressed as the mean ± standard error of the mean (SEM). Statistical comparisons between two groups were conducted by unpaired, two-tailed Student's *t*-test. $P<0.05$ was considered to be statistically significant. Statistical analysis was performed with Prism 9.0 software (GraphPad).

LC-MS/MS data analysis

The LC-MS/MS results were analyzed for identification and quantitation of iqPIR cross-linked peptide pairs as previously described (18). Briefly, LC-MS/MS data raw files were converted to .mzXML format using the ReADW tool in the Trans Proteomic Pipeline software suite (58). Mango (59) was used to search for PIR mass relationships and Comet (60) was used to search the mzXML files against the mouse Mitocarta 2 database (61) consisted of both forward and reverse protein sequences (2,084 total sequences). The resulting pepXML files were then analyzed with XLinkProphet (62) and filtered for estimated 1% FDR at the non-redundant cross-link level. For dead-end peptides, PeptideProphet (63) was applied to filter Comet search results at < 1% FDR. All cross-links passing the threshold were used for quantitation. Light (SH) and heavy (RH) isotope peptide precursors and their fragment peaks containing the stump group were deconvoluted and their peak intensities were extracted to calculate Log2 ratios. The final ratio for each cross-linked peptide pair is the normalized mean value from all contributing ion ratios to the same cross-link from different charge states, different scans, and separate replicate runs with outliers removed, where normalization is achieved by subtracting from each cross-link Log2 ratio the median value of all cross-link Log2 ratios. Finally, the cross-link Log2 ratio p-value reflecting its likelihood of being 0 is calculated based on a statistical t-test using the Log2 ratio mean value, standard deviation, and number of contributing quantified ions. Protein quantitation was estimated by combining together normalized Log2 ratios of all intra-protein cross-links and dead-end peptides corresponding to the protein. The mean Log2 ratio of all contributing ratios (intra-protein cross-link and dead-end) was used after excluding outliers.

4.4 Figures

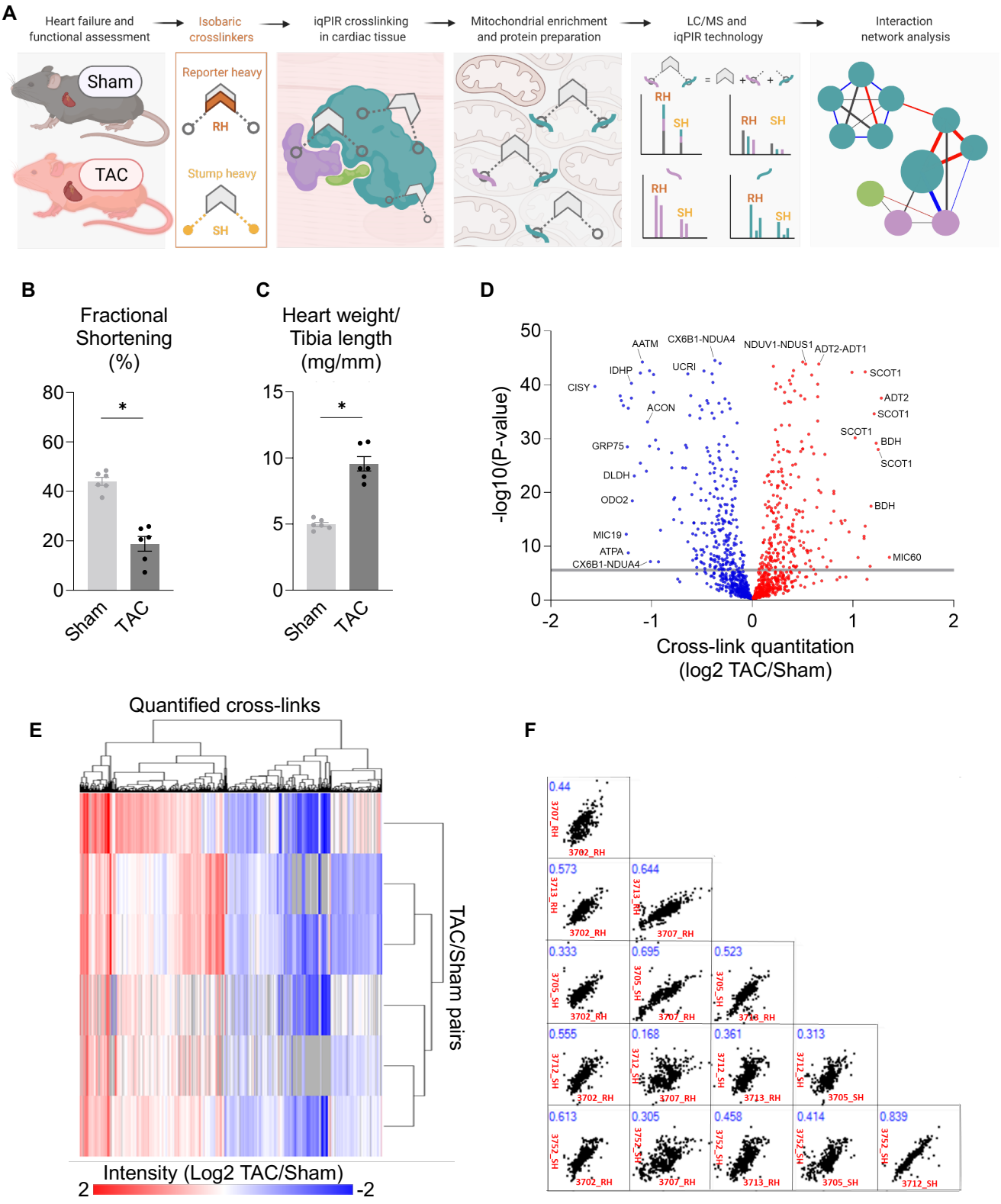
A
Heart failure and functional assessment
Isobaric crosslinkers
iqPIR crosslinking in cardiac tissue
Mitochondrial enrichment and protein preparation
LC/MS and iqPIR technology
Interaction network analysis
Sham
TAC
Reporter heavy
RH
Stump heavy
SH
B
Fractional Shortening (%)
Sham
TAC
C
Heart weight/ Tibia length (mg/mm)
Sham
TAC
D
-log10(P-value)
Cross-link quantitation (log2 TAC/Sham)
AATM
CX6B1-NDUA4
NDUV1-NDUS1
ADT2-ADT1
IDHP
UCRI
CISY
ACON
GRP75
DLDH
ODO2
MIC19
ATPA
CX6B1-NDUA4
SCOT1
ADT2
SCOT1
SCOT1
BDH
SCOT1
BDH
MIC60
E
Quantified cross-links
TAC/Sham pairs
Intensity (Log2 TAC/Sham)
2
-2
F

Figure 4.1: Quantitation of mitochondrial protein interactome in failing hearts

(A) Schematic of quantitative failing heart interactome pipeline. Briefly, TAC and Sham hearts were excised and subjected to stump-heavy and reporter-heavy iqPIR cross-linking reaction followed by mitochondrial enrichment. Samples were pooled for downstream processing and data acquisition by LC/MS. Identical cross-linked peptide pairs from TAC and Sham samples have identical masses yet produce distinct quantitative isotope signatures in MS^2 spectra, and their intensities enable relative quantitation of cross-linked peptides. Illustration created with BioRender.com.

(B) Assessment of cardiac function measured by fractional shortening (%) using echocardiography in TAC and Sham groups four-weeks post-surgery.

(C) Cardiac hypertrophy measured by ratio of heart weight (mg) to tibia length (mm) harvest.

(D) Volcano plot of quantified cross-link lysine ratios (Log2 TAC/Sham) versus statistical significance. Significance threshold set to p=2.5x10-6 (-log10=5.6). Blue circles indicate cross-linked peptide ratios with decreasing quantitation, while red circles indicate cross-linked peptide ratios with increasing quantitation (relative to TAC).

(E) Heat map illustration of quantified cross-linked peptide pairs showing significant changes between TAC and Sham groups, filtered for values present in at least 4/6 biological replicates.

(F) Pair-wise scatter plots of 6 pairs of biological replicates. Correlation of Log2 ratios of two biological replicates as shown in X-axis and Y-axis was evaluated with linear regression. R-squared value marked in blue font on top left of each figure.

For (B-C), all data are n=6, AVG+/-SEM, * denotes $p<0.05$ by Student's t test.

Figure 4.2

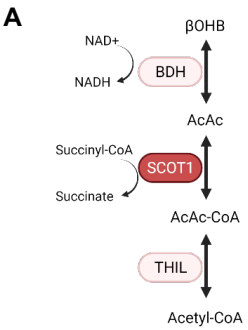

B

Cross-linked peptide pair			Log2 ratio (TAC/Sham)	
Protein	LysA	LysB	**Mean XL**	Mean DE
SCOT1	296	421	**1.25**	0.87
SCOT1	286	418	**1.02**	0.87
SCOT1	296	418	**0.99**	0.87
SCOT1	286	421	**1.12**	0.87
SCOT1	296	296	**1.05**	0.87
SCOT1	214	274	**-1.69**	0.87
THIL	260	242	**-1.47**	0.19

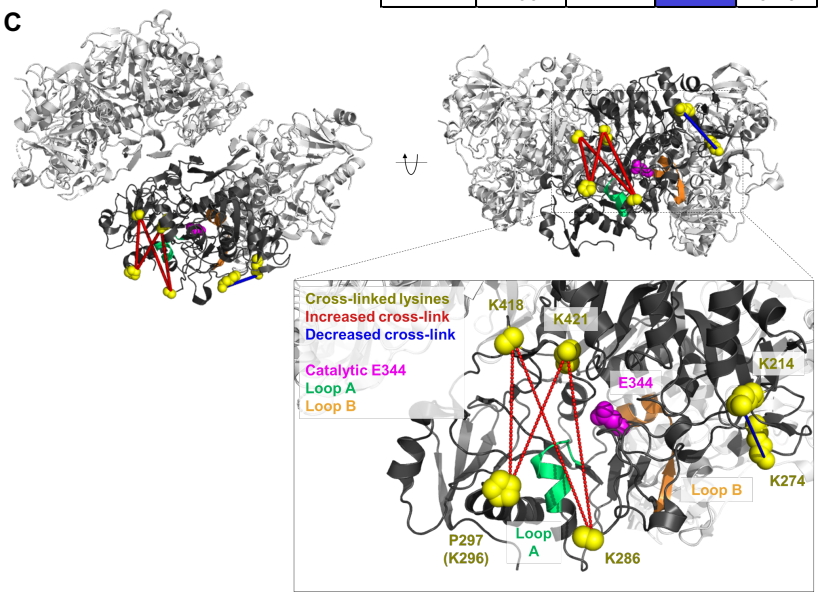

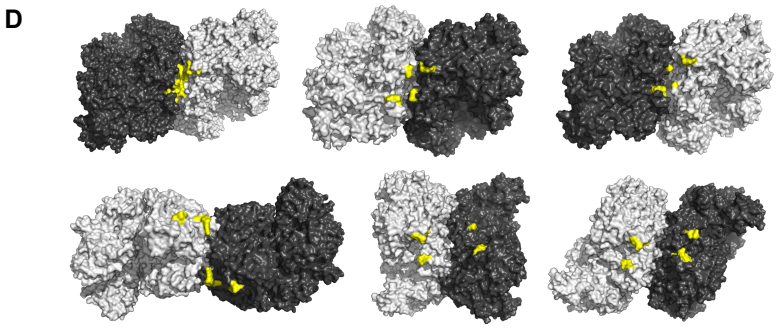

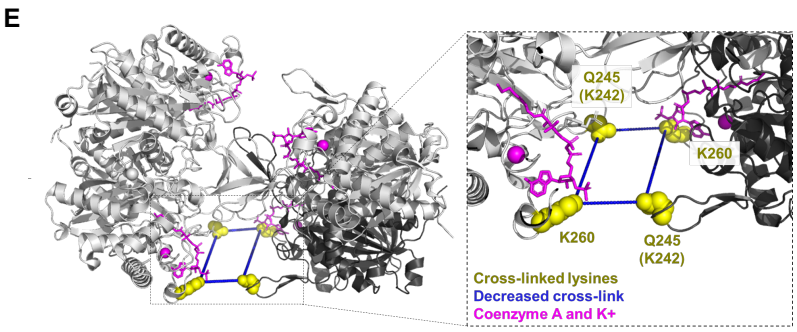

Figure 4.2: Active conformational states of ketone oxidation proteins enriched in TAC

(A) Schematic of ketone oxidation pathway.

(B) Table summarizing the mean cross-linking ratio and DE ratio for cross-linked peptide pairs exhibiting quantitative changes in ketone oxidation machinery.

(C) Human SCOT1 tetrameric structure (PDB: 3DLX) shown in grey. Monomeric unit is shown in black centered around the catalytic E344 (magenta). Cross-linked lysine side-chains (K286, K296/P297, K418, and K421, shown as yellow spheres) surround Loop A and together form four cross-links found to increase in TAC. Loop A (CoA binding site, residues 321-329, chain shown in green) is a dynamic region that must undergo conformational change to prevent steric clashing of N- and C-termini during catalysis. Decreasing cross-linked peptide pair, K214-K274, is also shown (yellow spheres) near Loop B (Succinate/Acetoacetate binding site, residues 374-386 chain shown in orange). P297 is shown due to missing density of K296.

(D) Six solutions (from top ten highest scoring) from molecular docking of two human SCOT1 tetramers (grey and black, PDB: 3DLX) using Symmdock (31) indicative of higher order oligomerization. Residues surrounding K296 (missing density) are shown in yellow, and are consistently docked in close proximity (Cα- Cα<42Å) to each other, providing evidence for K296-K296 cross-link being between two SCOT1 tetramers.

(E) Human THIL (PDB: 2IBW) tetrameric structure with bound CoA and KCl (magenta) highlighting the decreased cross-link between K260-K242/Q245 (sidechains shown as yellow spheres). K260 forms the only direct contact with CoA. K242 resides in the anionic loop meant to capture incoming substrate. Mouse K242 is equivalent to human Q245.

Figure 4.3

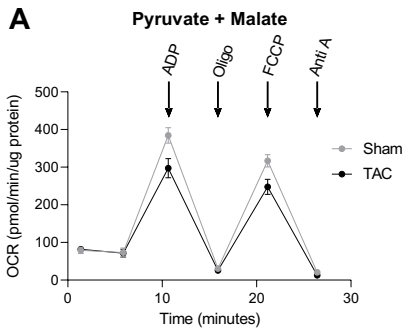

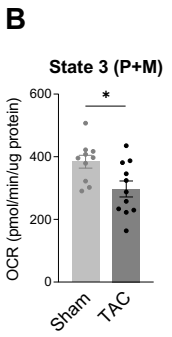

C

Cross-linked peptide pair				Log 2 ratio (TAC/Sham)		
ProteinA	ProteinB	LysA	LysB	**Mean XL**	Mean DE A	Mean DE B
CX6B1	NDUA4	85	56	**-1.01**	-0.41	-0.27
CX6B1	NDUA4	10	74	**-0.55**	-0.41	-0.27
CX6B1	NDUA4	10	76	**-0.49**	-0.41	-0.27
CX6B1	NDUA4	13	74	**-0.49**	-0.41	-0.27
CX6B1	NDUA4	13	76	**-0.44**	-0.41	-0.27

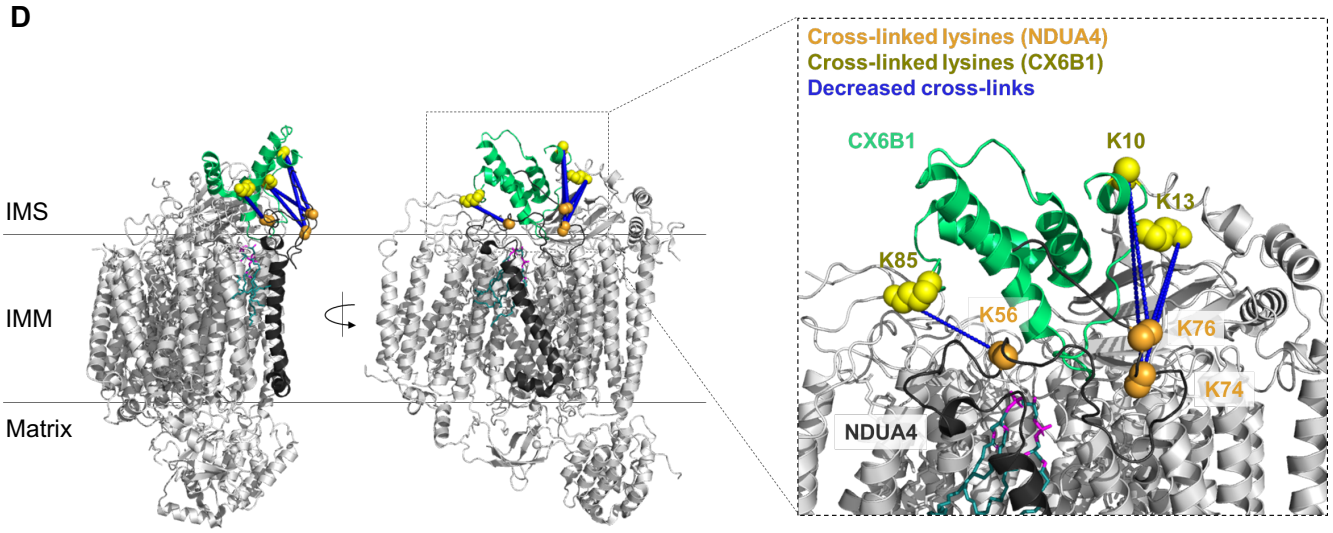

Figure 4.3: Decreased interaction between NDUA4 and C6XB1 affects CIV activity in TAC

(A) Oxygen consumption rate of mitochondria isolated from TAC and Sham hearts given pyruvate/malate substrates followed by sequential injections of ADP, Oligomycin, FCCP, and Antimycin A, measured by Seahorse XFe24 Analyzer.

(B) State III-driven respiration of isolated mitochondria (after addition of ADP).

(C) Table summarizing the mean cross-linking ratio and DE level ratio for cross-linked peptide pairs exhibiting quantitative changes in NDUA4 and CX6B1 subunits of CIV.

(D) Monomeric Complex IV (grey, PDB: 5Z62). Interactions between NDUA4 (black) and CX6B1 (green) subunits are shown. Cross-linked lysine sidechains are shown as yellow (CX6B1) or orange (NDUA4) spheres. Cross-links exhibit a structural scaffold on the IMS-facing interface of CIV, which are decreased in TAC. Cardiolipin bound to CIV is shown in teal.

For (A-B), all data are n=10-11, AVG+/-SEM, *denotes $p<0.05$ by Student's t test.

Figure 4.4

A

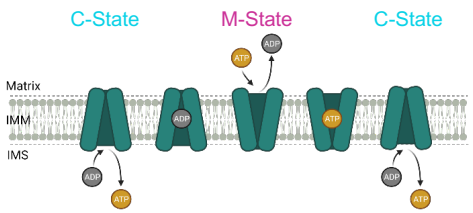

B

Cross-linked peptide pair			Log2 ratio (TAC/Sham)		C-state		M-state	
Protein	LysA	LysB	**Mean XL**	Mean DE	Euclidean distance	Jwalk SASD	Euclidean distance	Jwalk SASD
ADT1	92	23	**0.74**	0.5	22.6	23.78	20.08	99
ADT1	94	23	**0.55**	0.5	28.13	31.94	24.1	61.38
ADT1	96	23	**0.79**	0.5	27.32	29.61	25.47	99
ADT1	199	23	**0.65**	0.5	27.96	32.09	22.62	99
ADT1	33	23	**1.03**	0.5	13.52	16.64	14.41	17.78
ADT1	147	23	**0.65**	0.5	23.53	66.86	27.25	30.92
ADT1	147	33	**0.65**	0.5	19.12	99	24.51	31.65

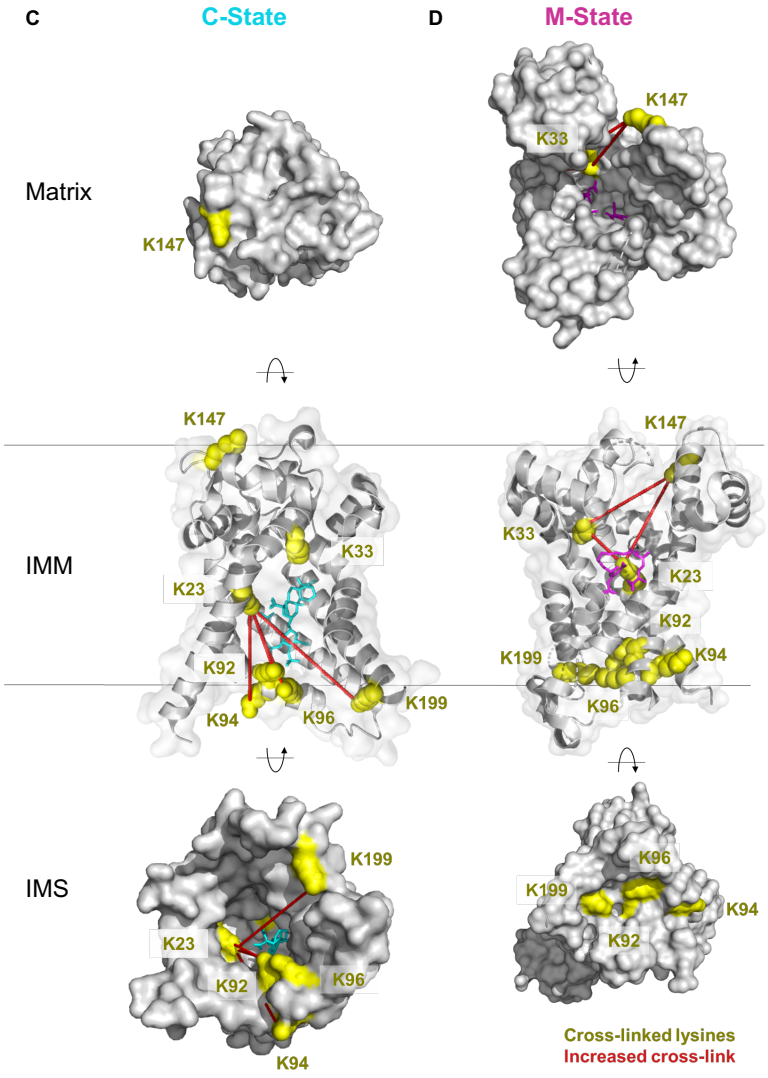

Figure 4.4: Enrichment of an intermediate state of ADP/ATP carrier detected in TAC

(A) Schematic of ADT cycling between two dominant conformational states. The cytoplasmic-facing state (C-state) delivers ATP to the cytosol and binds ADP. Binding of ADP induces a conformational change to the matrix-facing state (M-state), which returns ADP to the mitochondria and binds a newly charged ATP.

(B) Table summarizing mean cross-linking ratio and DE level ratio for each cross-linked peptide pair detected in ADT1 exhibiting changes in TAC. Euclidean distance (EI) and Solvent Accessible Surface distance (Jwalk SASD) (48) are listed for each cross-linked peptide pair when mapped onto both C-state and M-state of ADT1. Highlighted values satisfy iqPIR molecular distance constraint (EI<42Å, Jwalk SASD<51Å).

(C) Cross-linked peptide pairs (yellow lysine side chains) mapped onto the C-state conformation of bovine ADT1 (PDB: 1OKC). In this conformation, K23, K92, K94, K96, and K199 are available and can satisfy cross-linking distance constraints. K147 and K33 are not accessible in the M-state. Carboxyatractyloside (CATR) stabilizes the C-state and is shown in cyan.

(D) Cross-linked peptide pairs (yellow lysine side chains) mapped onto the M-state of ADT1 (TtAac PDB: 6GCI) where residues K92, K94, K96 and K199 form the gate closed to the matrix, and are inaccessible for cross-linking.Three cross-links are possible and shown between K23-K33, K23-K147, and K33-K147. Bongkrekic acid (BKA) stabilizes the M-state and is shown in magenta.

Supplemental Figure 1

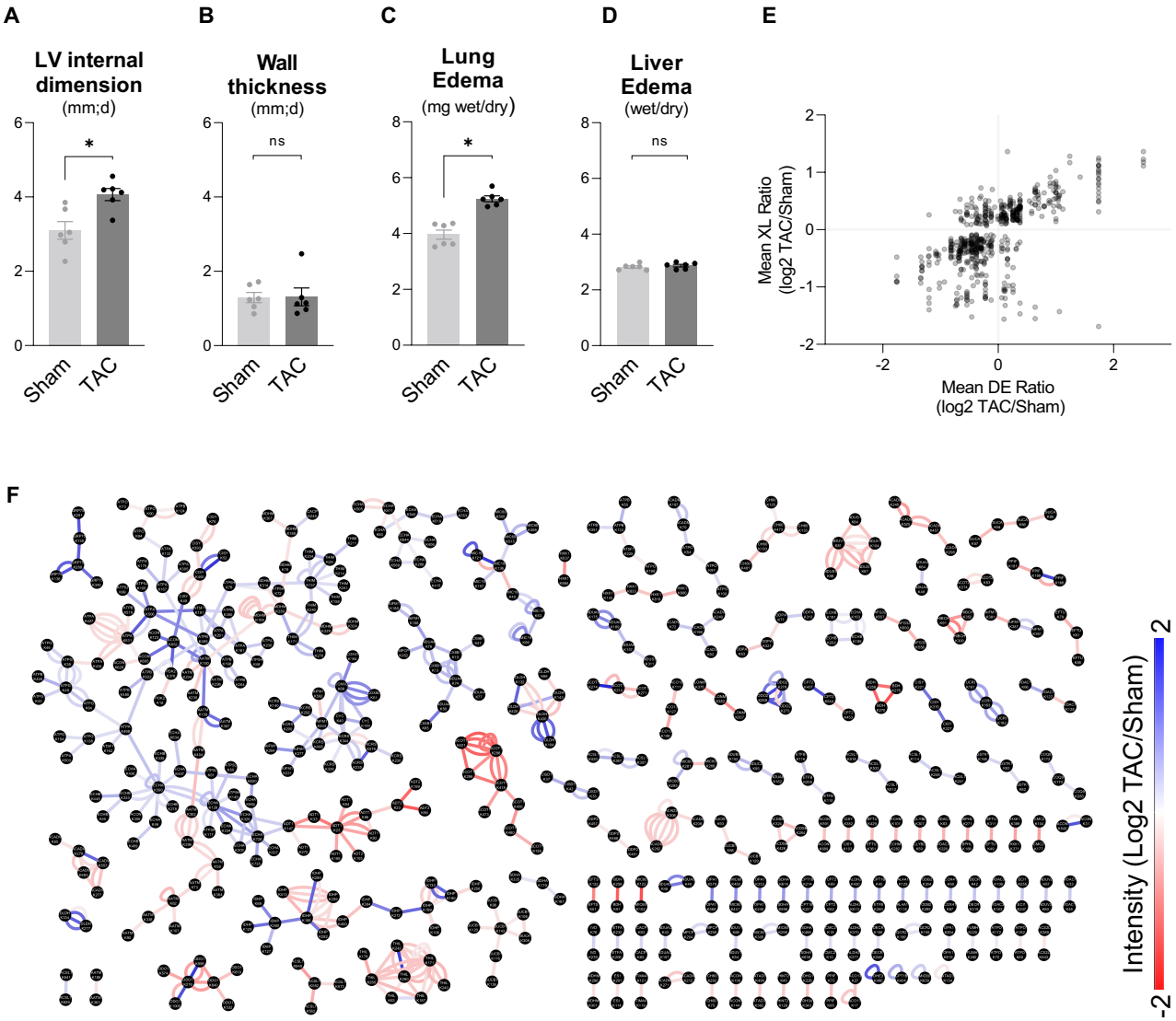

Supplemental Figure 1

(A-B) Left ventricle internal dimension and wall thickness in TAC and Sham groups determined by echocardiography four weeks post-surgery.

(C-D) Lung and liver edema (wet weight/dry weight in mg) measured at tissue harvest.

(E) Quantitation of mean cross-link (XL) ratio vs mean dead-end (DE) ratio for each cross-linked peptide pair statistically changed in TAC in at least 4/6 biological pairs (Log2 TAC/Sham). Sum of Mean DE ratio for Protein A and Protein B is shown to account for cross-links between two different proteins.

(F) Interaction network of lysine residues (black nodes) connected by observed cross-links (edges). Edges are colored according to increasing (red) and decreasing (blue) quantitation of statistically significant subset of cross-links (Log2 TAC/Sham) shown by color scale.

For (A-D), all data are n=6, AVG+/-SEM, * denotes $p<0.05$ by Student's t test.

Supplemental Figure 2

A

Cross-linked peptide pair			Log2 ratio (TAC/Sham)							
Protein	LysA	LysB	3702RH XL	3707RH XL	3713RH XL	3705SH XL	3712SH XL	3752SH XL	**Mean XL**	Mean DE
SCOT1	296	421	1.36	1.44	1.17	1.26	1.23	1.04	**1.25**	0.87
SCOT1	286	418	1.08	1.46	0.98	1.04	0.87	0.87	**1.02**	0.87
SCOT1	296	418	0.76	1.52	0.95	0.88	1.03	1.07	**0.99**	0.87
SCOT1	286	421	1.31	1.6	1.09	0.89	1.26	1.01	**1.12**	0.87
SCOT1	296	296		1.13	1.08	0.86	1.03		**1.05**	0.87
SCOT1	214	274		-1.84		-1.12	-1	-1.57	**-1.69**	0.87
THIL	260	242		-1.42		-1.59	-0.69	-1.55	**-1.47**	0.19

B

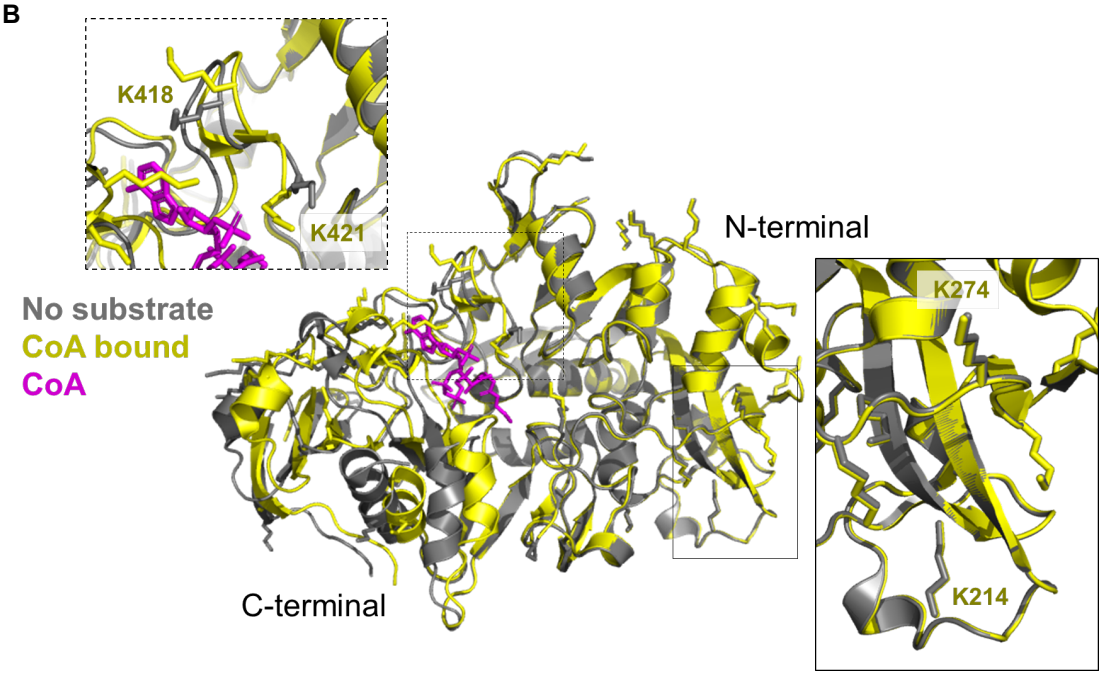

C

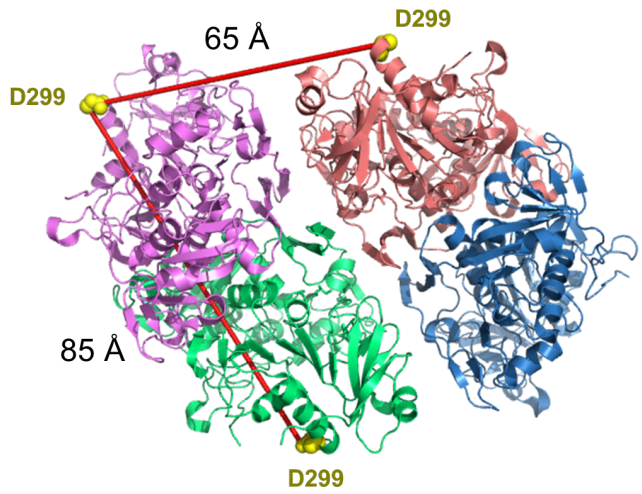

Supplemental Figure 2

(A) Table summarizing the mean cross-linking ratio and DE ratio for cross-linked peptide pairs including values obtained across biological replicates for ketone oxidation proteins.

(B) Alignment of apo (grey, PDB: 3OXO chain A) and substrate-bound (yellow, PDB: 3OXO chain E) monomers of porcine SCOT1. CoA is colored in magenta and bound to the active site. Lysine sidechains are shown in stick representation. Alignment depicts the structural differences between the dynamic C-terminal domain and the static N-terminal domain during substrate-binding. Close up view specifies cross-linked lysines (K214, K274, K418, and K421).

(C) Human SCOT1 tetrameric structure (PDB: 3DLX) illustrating the observed K296-K296 homodimer cross-link that increases in TAC. Molecular interaction distance constraint is exceeded when mapped onto the tetrameric structure. Each monomer is depicted in a different color. K296 is not present in electron density of solved structures, closest resolved residue present in each monomer is shown (D299).

Supplemental Figure 3

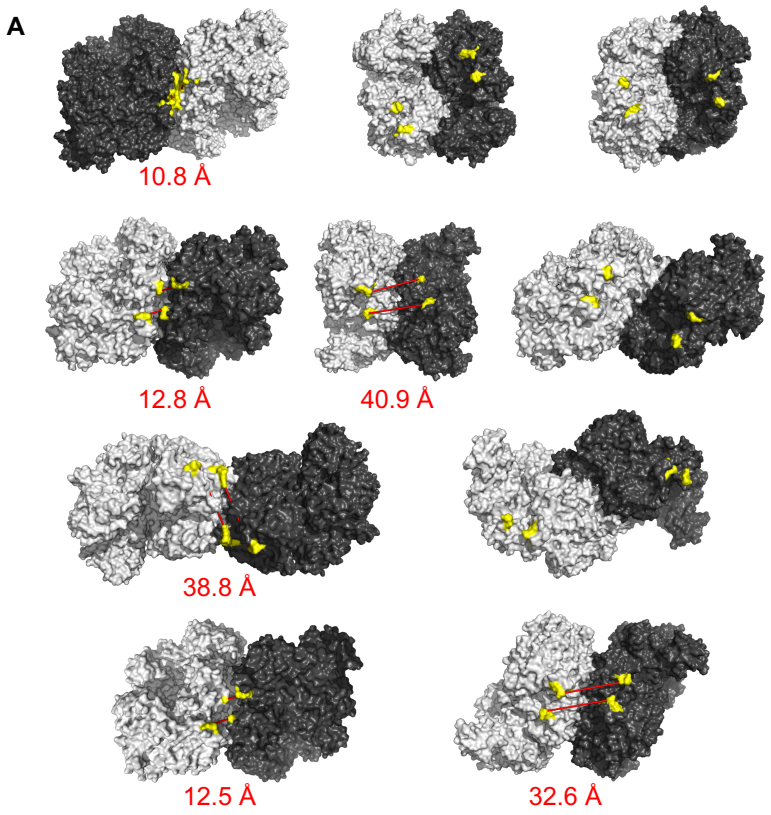

Supplemental Figure 3

(A) Top 10 solutions from molecular docking of two human SCOT1 tetramers (PDB: 3DLX) using Symmdock (31). Approximate location of K296-K296 was examined in each solution. Due to the missing density around K296, residues 284-302 were highlighted (yellow). In 6 of the top 10 solutions, proximity between two tetramers is consistent with molecular distance constraint of cross-linker (listed below structure).

(B) Three (of top ten) docking solutions where residues K214 or K274 are buried at the interface between two SCOT1 tetramers (PDB: 3DLX). Decreasing cross-link between K214 (green) and K274 (magenta) is shown as a blue edge.

(C) Human THIL (PDB: 2IBW) tetrameric structure highlighting the salt bridge formed between K260 (yellow stick representation) and 3' phosphate moiety of CoA (2.9 Å), which may make K260 inaccessible for cross-linking with an adjacent K242/Q245 (yellow sphere) (intra-link distance 28.9 Å) or K242/KQ245 on the opposing monomer (inter-link distance 12.9 Å).

Supplemental Figure 4

A

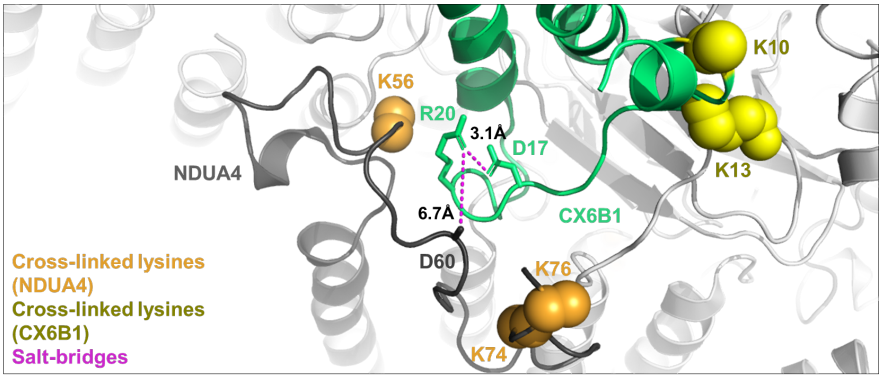

B

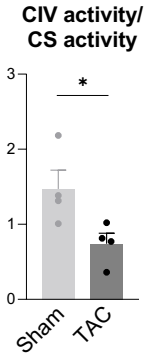

C

Cross-linked peptide pair			Log2 ratio (TAC/Sham)								C-state		M-state	
Protein	LysA	LysB	3702RH XL	3707RH XL	3713RH XL	3705SH XL	3712SH XL	3752SH XL	**Mean XL**	Mean DE	Euclidean distance	Jwalk SASD	Euclidean distance	Jwalk SASD
ADT1	92	23	0.82	0.34	0.91	0.48	1.13	0.65	**0.74**	0.5	22.6	23.78	20.08	99
ADT1	94	23	0.96	0.4	0.3	0.21	1.05	0.35	**0.55**	0.5	28.13	31.94	24.1	61.38
ADT1	96	23	0.71	0.35	1.06	0.49	1.15	0.69	**0.79**	0.5	27.32	29.61	25.47	99
ADT1	199	23	1.14	0.39	1.05	0.41	1.07	0.92	**0.65**	0.5	27.96	32.09	22.62	99
ADT1	33	23		0.82	1.04	1.09	1.39		**1.03**	0.5	13.52	16.64	14.41	17.78
ADT1	147	23		0.86	0.54	0.73	1		**0.65**	0.5	23.53	66.86	27.25	30.92
ADT1	147	33	1.14	0.39	1.05	0.41	1.07	0.92	**0.65**	0.5	19.12	99	24.51	31.65

D

Cross-linked peptide pair				Log2 ratio (TAC/Sham)								
ProteinA	ProteinB	LysA	LysB	3702RH XL	3707RH XL	3713RH XL	3705SH XL	3712SH XL	3752SH XL	**Mean XL**	Mean DE A	Mean DE B
ADT1	ADT2	96	23	1.08	0.22	0.3	0.65	1.16	0.71	**0.36**	0.5	0.62
ADT2	ADT2	96	23		0.81	1.51	0.82	1.78		1.28	0.62	0.62
ADT2	ADT2	199	23		1.16	1.25		2.64	0.89	1.17	0.62	0.62

E

TtAac M-state

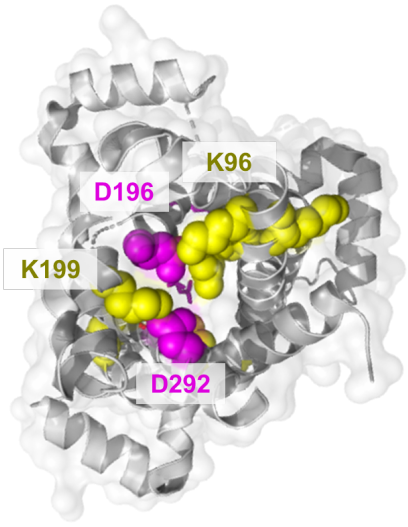

F

Bovine C-state

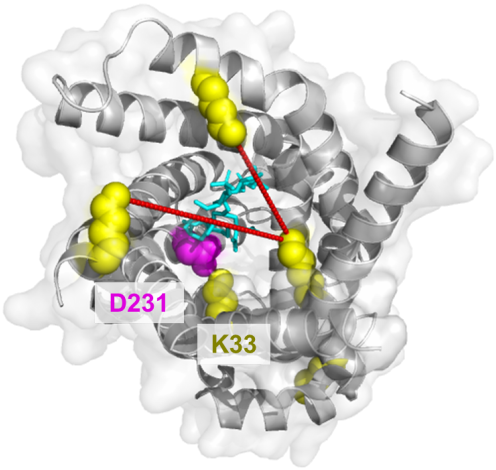

Supplemental Figure 4

(A) Structural insight into CX6B1 R20 forming salt-bridges at NDUA4-CX6B1 interface. R20 sidechain (green) forms a salt-bridge with CX6B1 D16 (green) and NDUA4 D60 (black), which pinpoints an interface necessary for stability of CIV. Side-chains of R20, D16, and NDUA4 D60 (partially resolved) are depicted in stick representation. Cross-linked lysine sidechains are shown as yellow (CX6B1) or orange (NDUA4) spheres.

(B) Cytochrome C oxidase enzymatic activity assay in tissue homogenates from TAC and Sham hearts, normalized to Citrate Synthase activity. N=4, AVG+/-SEM, *denotes $p<0.05$ by Student's t test.

(C) Table summarizing the mean cross-linking ratio and DE ratio for cross-linked peptide pairs including values obtained across biological replicates for ADT1.

(D) Table summarizing the mean cross-linking ratio and DE ratio for cross-linked peptide pairs including values obtained across biological replicates for cross-links in ADT isoforms.

(E) Cross-linked peptide pairs (yellow lysine side chains) mapped onto the M-state conformation of ADT1 (TtAac PDB: 6GCI). Salt-bridges between K96-D196 and K199-D292 contribute to the gating mechanism which closes the M-state to the IMS (41), and would make lysines unavailable for cross-linking. Aspartic acid sidechains are shown in magenta.

(F) Cross-linked peptide pairs (yellow lysine side chains) mapped onto the C-state conformation of bovine ADT1 (PDB: 1OKC). K33 and D231 are known to form a salt-bridge which stabilizes the C-state (40) and would make K33 unavailable for cross-linking. Aspartic acid sidechains are shown in magenta.

Supplemental Table 1: Cross-linked peptide pairs with statistically significant changes in TAC

Protein Pair	Peptide Pair	Log2 ratio 3702RH	Log2 ratio 3707RH	Log2 ratio 3713RH	Log2 ratio 3705SH	Log2 ratio 3712SH	Log2 ratio 3752SH	mean Log2 XL ratio	P value	mean Log2 ratio Protein A	P value Protein A	mean Log2 ratio DE Protein B	P value Protein B
SCOT1_214_SCOT1_274	AWKADR_2_LIKGEKYEKR_5		-1.84		-1.12	-1	-1.57	-1.69	0	0.87	6.27E-28	0.87	6.27E-28
CISY_52_CISY_450	TFKQQHGK_2_ALGFPLERPKSMSTDGLM[147.04]K_9		-1.55		0.33	0.75	-1.5	-1.56	1.80E-40	0.05	0.0703	0.05	0.0703
ODO1_276_ODO1_999	KWSSEKR_5_AKPVWYAGRDPAAAPATGNKK_19		-1.67		-1.55	-1.24	-2.06	-1.55	0	0.32	0.000036	0.32	0.000036
MIC19_121_MIC19_136	AKHLAR_1_KQDAFYKEQLAR_0		-1.66		-1.89	-0.63	-1.63	-1.52	0	-0.23	0.000928	-0.23	0.000928
THIL_260_THIL_242	RVDFSKVPK_5_GKPDVVVKEDEEYKR_1		-1.42		-1.59	-0.69	-1.55	-1.47	0	0.19	1.55E-10	0.19	1.55E-10
PPIF_189_PPIF_166	KIESFGSKSGK_7_TDWLDGKHVVFGHVK_6		-1.33		-1.76	-1.17	-1.67	-1.43	0	0.53	0.000000391	0.53	0.000000391
ODO2_268_ODO2_278	HKDAFLK[170.11]K_1_HNLKLGFMSAFVK_3		-1.56		-1.22	-1.18	-1.59	-1.4	0	-0.6	0.0000161	-0.6	0.0000161
ODO1_276_ODO1_1000	KWSSEKR_5_KTHLTELQR_0		-1.53		-1.35	-1.2	-1.59	-1.35	0	0.32	0.000036	0.32	0.000036
CPT2_457_CPT2_544	GGKEFLKK_6_YHGQLTKEAAMGQGFDR_6		-1.22	0.7		0.77	-1.32	-1.33	0	-0.37	0.000727	-0.37	0.000727
ACON_31_ACON_549	AKVAMSHFEPSEYIR_1_FKLEAPDADELPRSDFDPGQDTYQHPPKDSSGQR_27		-1.3	0.12	0.25		-1.25	-1.32	0	0.06	0.0151	0.06	0.0151
DLDH_430_DLDH_104	AKTNADTDGM[147.04]VK_1_ALLNNSHYYHMAHGKDFASR_14		-1.33		-0.98	-1.25	-1.39	-1.31	0	-0.27	0.000558	-0.27	0.000558
GRP75_291_GRP75_135	HIVKEFKR_6_RYDDPEVQKDTK_8		-1.49		-1.1	-0.9	-1.39	-1.31	1.02E-38	-0.36	0.00106	-0.36	0.00106
GRP75_288_GRP75_138	HIVKEFK_3_RYDDPEVQKDTKNVPFK_11		-1.86		-1.12	-1.02	-1.59	-1.3	7.84E-38	-0.36	0.00106	-0.36	0.00106
DHE3_480_DHE3_480	FGKHGGTIPVVPTAEFQDR_2_FGKHGGTIPVVPTAEFQDR_2		-1.42		-1.56	-0.99	-1.44	-1.28	0	0.19	0.00101	0.19	0.00101
ODO2_273_ODO2_268	DAFLKK_4_HKDAFLKK_1		-1.49		-1.32	-0.93	-1.25	-1.28	6.43E-37	-0.6	0.0000161	-0.6	0.0000161

MIC19_121_MIC19_121	AKHLAR_1_AKHLAR_1		-1.64		-1.7	-0.53	-1.51	-1.25	5.36E-13	-0.23	0.000928	-0.23	0.000928
GRP75_288_GRP75_135	HIVKEFKR_3_RYDDPEVQKDTK_8		-1.43		-1.37	-0.89	-1.15	-1.24	3.12E-29	-0.36	0.00106	-0.36	0.00106
DLDH_430_DLDH_104	AKTNADTDGM[147.04]VK_1_ALLNNSHYYHM[147.04]AHGKDFASR_14		-1.17		-0.56	-1.36	-1.19	-1.23	2.10E-36	-0.27	0.000558	-0.27	0.000558
DLDH_277_DLDH_334	FKLNTKVTGATK_5_RPFTQNLGLEELGIELDPKGR_18		-1.4		-0.86	-0.85	-1.08	-1.23	0	-0.27	0.000558	-0.27	0.000558
ATPA_531_ATPA_506	SDGKISEQSDAK_3_GYLDKLEPSKITKFENAFLSHVISQHQSLLGNIR_12		-1.4		-1.01	-0.64	-1.3	-1.23	1.61E-09	-0.06	0.083	-0.06	0.083
GRP75_288_GRP75_138	HIVKEFKR_3_YDDPEVQKDTKNVPFK_10		-1.7		-1.15	-1.08	-1.25	-1.22	0	-0.36	0.00106	-0.36	0.00106
IDHP_166_IDHP_280	LVPGWTKPITIGR_6_TDFDKNKIWYEHR_4		-1.38		-0.84	-1.19	-1.23	-1.2	4.89E-41	-0.11	0.00705	-0.11	0.00705
IDHP_133_IDHP_180	M[147.04]WKSPNGTIR_2_HAHGDQYKATDFVVDR_7		-1.35		-0.92	-1.05	-1.26	-1.2	2.66E-38	-0.11	0.00705	-0.11	0.00705
ACON_652_PDK2_376	KHGIR_0_LPVYNKSAWR_5		-1.43		-1.01	-1.23	-1.21	-1.2	0	0.06	0.0151	0.06	0.0692
DLDH_420_DLDH_132	IGKFPFAANSR_2_HSAVKALTGGIAHLFK_4		-1.35		-1.12	-0.97	-1.36	-1.19	0	-0.27	0.000558	-0.27	0.000558
ACADV_279_ACADV_557	EKITAFVVER_1_HKKGIVNEQFLLQR_2		-1.11		-1.73	-0.4	-1.26	-1.19	0	0.03	0.244	0.03	0.244
KCRS_335_KCRS_276	IPKLSKDPR_2_VISMEKGGNMKR_5		-1.15		-1.12	-0.37	-1.14	-1.19	0	-0.32	1.46E-10	-0.32	1.46E-10
ODO2_268_ODO2_278	HKDAFLK_1_HNLKLGFM[147.04]SAFVK_3		-1.32		-1.03	-0.96	-1.15	-1.19	3.26E-19	-0.6	0.0000161	-0.6	0.0000161
DLDH_277_DLDH_334	LNTKVTGATKK_3_RPFTQNLGLEELGIELDPKGRIPVNNR_18		-1.25		-0.81	-0.67	-1.12	-1.17	8.16E-24	-0.27	0.000558	-0.27	0.000558
IDHP_199_IDHP_272	LVFTPKDGSSAK_5_FKDIFQEIFDKHYK_10		-1.3		-0.61	-0.64	-0.99	-1.17	0	-0.11	0.00705	-0.11	0.00705
IDHP_133_IDHP_180	MWKSPNGTIR_2_HAHGDQYKATDFVVDR_7		-1.35		-0.97	-1.07	-1.21	-1.17	0	-0.11	0.00705	-0.11	0.00705
DLDH_430_DLDH_104	AKTNADTDGMVK_1_ALLNNSHYYHM[147.04]AHGKDFASR_14		-1.23		-0.98	-1.08	-1.11	-1.14	0	-0.27	0.000558	-0.27	0.000558

DLDH_430_DLDH_104	AKTNADTDGMVK_1_ALLNNSHYYHMAHGKDFASR_14		-1.39	0	-0.95	-1.03	-1.31	-1.11	0	-0.27	0.000558	-0.27	0.000558
GRP75_288_GRP75_345	HIVKEFK_3_HLNMKLTR_4		-1.65		-1.05	-1	-1.3	-1.11	6.10E-43	-0.36	0.00106	-0.36	0.00106
IDHP_129_IDHP_360	VEEFKLKK_6_EHQKGRPTSTNPIASIFAWTR_3		-1.35		-0.73	-0.92	-1.17	-1.11	3.42E-26	-0.11	0.00705	-0.11	0.00705
AATM_159_AATM_387	DVFLPKPSWGNHTPIFR_5_EGSSHNWQHITDQIGM[147.04]FCFTGLKPEQVER_22		-1.28		-0.82	-1.07	-1.24	-1.09	5.61E-45	0.13	8.18E-08	0.13	8.18E-08
DLDH_277_DLDH_334	FKLNTKVTGATK_5_RPFTQNLGLEELGIELDPKGRIPVNNR_18		-1.34		-0.69	-0.93	-1.15	-1.08	0	-0.27	0.000558	-0.27	0.000558
ACON_652_ACON_605	KHGIR_0_CTTDHISAAGPWLKFR_13		-1.26		-1.12	-0.91	-1.12	-1.07	0	0.06	0.0151	0.06	0.0151
CISY_370_CISY_321	HLPKDPMFK_3_EVGKDVSDEKLRDYIWNTLNSGR_3		-1.45		-0.78	-0.76	-1.14	-1.07	0	0.05	0.0703	0.05	0.0703
CISY_370_CISY_327	HLPKDPMFK_3_EVGKDVSDEKLRDYIWNTLNSGR_9		-1.45		-0.91	-0.86	-1.3	-1.05	1.04E-24	0.05	0.0703	0.05	0.0703
AATM_159_AATM_387	DVFLPKPSWGNHTPIFR_5_EGSSHNWQHITDQIGMFCFTGLKPEQVER_22		-1.25		-0.87	-1.02	-1.16	-1.04	0	0.13	8.18E-08	0.13	8.18E-08
IDHP_166_IDHP_282	LVPGWTKPITIGR_6_TDFDKNKIWYEHR_6		-1.23		-0.74	-0.98	-1.13	-1.04	0	-0.11	0.00705	-0.11	0.00705
ACON_652_ACON_723	KHGIR_0_IHPVDKLTIQGLK_5		-1.37		-0.49	-0.87	-0.92	-1.04	7.32E-34	0.06	0.0151	0.06	0.0151
ODO2_268_ODO2_278	HKDAFLK_1_HNLKLGFMSAFVK_3		-1.41		-1.05	-0.92	-0.98	-1.04	0	-0.6	0.0000161	-0.6	0.0000161
NDUA5_40_NDUA5_46	HFPKHAAYR_3_KYTEQITNEKLDMVK_0		-1.31		-0.64	-0.79	-0.95	-1.02	2.16E-43	-0.51	0.00293	-0.51	0.00293
CISY_52_CISY_450	TFKQQHGK_2_ALGFPLERPKSMSTDGLMK_9		-1.42		0.54	0.42	-1.53	-1.02	2.37E-29	0.05	0.0703	0.05	0.0703
CX6B1_85_NDUA4_56	IAEGTFPGKI_8_NNPEPWNKLGPNEQYK_7		-1.06	-0.62	-0.72	-1.4		-1.01	0.000000065	-0.41	0.000633	-0.27	0.00000126
ACON_652_AATM_150	KHGIR_0_FFKFSR_2		-1.36		-0.64	-0.78	-1.05	-0.98	2.32E-39	0.06	0.0151	0.13	8.18E-08
AT5F1_191_ATPA_506	AYKEVK_2_ITKFENAFLSHVISQHQSLLGNIR_2		-1.33		-0.22	-0.8	-0.7	-0.98	1.18E-42	-0.37	0.128	-0.06	0.083
AATM_150_AATM_159	FFKFSR_2_DVFLPKPSWGNHTPIFR_5		-1.49	-0.15	-0.72	-0.72	-1.04	-0.97	0	0.13	8.18E-08	0.13	8.18E-08

IDHP_384_IDHP_272	GKLDGNQDLIR_1_FKDIFQEIFDKHYK_10		-1.37		-0.48	-0.82	-0.88	-0.96	0	-0.11	0.00705	-0.11	0.00705
IDHP_166_IDHP_360	LVPGWTKPITIGR_6_EHQKGRPTSTNPIASIFAWTR_3		-1.1		-0.64	-1.03	-0.86	-0.96	1.67E-30	-0.11	0.00705	-0.11	0.00705
ACON_652_CISY_49	KHGIR_0_IKTFK_1		-0.74		-0.84	-0.6	-0.97	-0.93	6.91E-08	0.06	0.0151	0.05	0.0703
NDUA5_40_NDUA5_46	HFPKHAAYR_3_KYTEQITNEK_0		-1.38		-0.61	-0.76	-1.01	-0.93	0	-0.51	0.00293	-0.51	0.00293
NDUA9_189_NDUA9_175	SKAVGEKEVR_6_FIHVSHLNASMKSSSK_11		-1.26		-0.57	-0.63	-0.86	-0.93	7.96E-29	-0.67	0.000367	-0.67	0.000367
COX6C_68_COX41_164	KAGIFQSAK_0_WDYDKNEWKK_4	-0.48	-0.92	-0.97	-0.66	-1.09		-0.91	0	-0.88	2.41E-08	-0.05	0.314
IDHP_69_IDHP_360	EKLILPHVDVQLK_1_EHQKGRPTSTNPIASIFAWTR_3		0		-0.73	-0.82	-1.11	-0.91	9.3E-14	-0.11	0.00705	-0.11	0.00705
OPA1_568_OPA1_579	ESVEQQADSFKATR_10_FNLETEWKNNYPR_7	-0.59	-1.08	-1.11	-0.74	-1.41	-0.73	-0.91	0	-0.18	0.0626	-0.18	0.0626
COX6C_68_COX6C_61	KAGIFQSAK_0_NYDSMKDFEEM[147.04]R_5	-0.52	-0.84	-0.98	-0.67	-1.35	-0.83	-0.91	0	-0.88	2.41E-08	-0.88	2.41E-08
COX6C_68_COX6C_61	KAGIFQSAK_0_NYDSM[147.04]KDFEEMR_5	-0.46	-0.87	-1	-0.64	-1.26	-0.89	-0.91	0	-0.88	2.41E-08	-0.88	2.41E-08
COX6C_68_COX6C_61	KAGIFQSAK_0_NYDSMKDFEEMR_5	-0.45	-0.89	-0.99	-0.72	-1.16	-0.86	-0.9	0	-0.88	2.41E-08	-0.88	2.41E-08
NDUA9_189_NDUA9_175	AVGEKEVR_4_FIHVSHLNASM[147.04]KSSSK_11		-1.28		-0.53	-0.7	-0.88	-0.85	0	-0.67	0.000367	-0.67	0.000367
MIC19_86_MIC19_86	LKQAR_1_RLKQAR_2		-1		-0.68	-0.32	-0.91	-0.84	0	-0.23	0.000928	-0.23	0.000928
NDUA9_189_NDUA9_175	AVGEKEVR_4_FIHVSHLNASMKSSSK_11		-1.3		-0.51	-0.74	-0.99	-0.84	0	-0.67	0.000367	-0.67	0.000367
MIC60_441_MIC60_450	LEEKR_3_TFDSAVAKALEHHR_7		-0.97		-0.68	-0.37	-0.97	-0.82	0	0.08	0.0825	0.08	0.0825
COX6C_68_COX6C_61	KAGIFQSAK_0_NYDSM[147.04]KDFEEM[147.04]R_5	-0.34	-0.77	-1.01	-0.59	-1.19	-0.82	-0.81	0	-0.88	2.41E-08	-0.88	2.41E-08
ATPB_485_ATPA_506	LVPLKETIK_4_ITKFENAFLSHVISQHQSLLGNIR_2		-1.19	-0.13	-0.06	-0.57	-0.81	-0.8	0	-0.23	3.91E-11	-0.06	0.083
OPA1_245_OPA1_253	KLVLQK_0_DDKGIHHR_2		-1.02		-1.06	-0.42	-0.84	-0.8	4.13E-28	-0.18	0.0626	-0.18	0.0626
ATP5J_105_ATPA_506	FDDPKFEVIDKPQS_10_ITKFENAFLSHVISQHQSLLGNIR_2		-1.12	-0.87	0.2	-0.69	-0.98	-0.8	2.38E-25	-0.15	0.0191	-0.06	0.083

ECHA_129_ECHA_326	MFEKLEK_3_AGLEQGSDAGYLAESQKFGELALTK_16	-0.42		-0.86	-0.63	-0.83		-0.78	1.1E-15	-0.19	1.53E-17	-0.19	1.53E-17
AIFM1_294_AIFM1_277	ALEKISR_3_AGAEVKSR_5	-0.31	-0.88		-0.66	-0.73	-0.69	-0.78	1.80E-19	-0.33	0.0000303	-0.33	0.0000303
SDHA_598_SDHA_616	EDYKVR_3_KPFGEHWR_0		-1.23	-0.39	-0.11	-0.41	-0.99	-0.77	8.98E-20	-0.14	0.0000112	-0.14	0.0000112
UCRI_163_UCRI_181	LSDIPEGKNMAFK_7_TKKEIDQEAAVEVSQLR_1		-0.64	-0.59	-0.54	-0.86		-0.72	1.32E-17	-0.66	6.77E-12	-0.66	6.77E-12
UCRI_163_UCRI_182	LSDIPEGKNMAFK_7_TKKEIDQEAAVEVSQLR_2		-0.9	-0.72	-0.48	-0.79		-0.72	0	-0.66	6.77E-12	-0.66	6.77E-12
AIFM1_108_NDUA4_76	VMGLGLSPEEKQR_10_FYSVNVDYSKLKK_11	-0.32	-0.8	-0.39	-0.57			-0.7	3.91E-15	-0.33	0.0000303	-0.27	0.00000126
KCRS_292_KCRS_200	GLKEVER_2_EVENVAITALEGLKGDLAGR_13			-0.72	-0.47	-0.9	-0.67	-0.7	0	-0.32	1.46E-10	-0.32	1.46E-10
KCRS_292_KCRS_140	GLKEVER_2_VMKHPTDLDASK_2	-0.09	-0.84	-0.75	-0.54	-0.67		-0.69	2.61E-25	-0.32	1.46E-10	-0.32	1.46E-10
ECHA_129_ECHA_728	MFEKLEK_3_FVDLYGAQKVVDR_8	-0.63	-0.74	-0.75	-0.5	-0.81	-0.52	-0.69	0	-0.19	1.53E-17	-0.19	1.53E-17
ECHA_129_ECHA_334	MFEKLEK_3_FGELALTKESK_7	-0.53	-0.57	-0.84	-0.45	-0.81	-0.66	-0.67	0	-0.19	1.53E-17	-0.19	1.53E-17
AATM_150_AATM_150	FFKFSR_2_FFKFSR_2	0.13	-1.46	-0.46	0.09	-0.24	-0.9	-0.66	1.47E-29	0.13	8.18E-08	0.13	8.18E-08
UCRI_163_UCRI_181	LSDIPEGKNM[147.04]AFK_7_TKKEIDQEAAVEVSQLR_1		-0.46	-0.56	-0.47	-0.87		-0.66	2.80E-25	-0.66	6.77E-12	-0.66	6.77E-12
MIC19_63_MIC19_63	YSSVYGASVSDEDLKR_14_YSSVYGASVSDEDLKRR_14	-0.27	-0.81	-0.76	-0.52	-0.77	-0.69	-0.65	4.24E-29	-0.23	0.000928	-0.23	0.000928
VDAC1_122_VDAC1_66	LTFDSSFSPNTGKK_12_TKSENGLEFTSSGSANTETTKVNGSLETK_20	-0.45	-0.73	-0.36	-0.43	-0.31	-0.61	-0.64	0	-0.2	0.0611	-0.2	0.0611
UCRI_163_UCRI_182	LSDIPEGKNMAFK_7_KEIDQEAAVEVSQLR_0		-0.61	-0.63	-0.54	-0.88	-0.6	-0.64	8.77E-43	-0.66	6.77E-12	-0.66	6.77E-12
UCRI_163_UCRI_181	LSDIPEGKNMAFK_7_TKKEIDQEAAVEVSQLRDPQHDLDR_1	-0.36	-0.39	-0.66	-0.84	-1.16	-0.29	-0.64	1.44E-11	-0.66	6.77E-12	-0.66	6.77E-12
ODO2_273_ODO2_278	HKDAFLKK_6_HNLKLGFMSAFVK_3		0.05	-2.02	-0.15	0.38		-0.62	4.40E-35	-0.6	0.0000161	-0.6	0.0000161
MIC60_498_MIC60_515	DVLKVQEQELK_3_YEFEQGLSEKLSEQELEFR_9		-0.65	-0.75	-0.47	-0.74	-0.44	-0.61	9.62E-39	0.08	0.0825	0.08	0.0825
ECHA_620_ECHA_664	FGGGSVELLKQMVSK_9_LPAKPEVSSDEDVQYR_3	-0.42	0.03	-1.53	0.64	-2.11	-0.31	-0.6	2.31E-20	-0.19	1.53E-17	-0.19	1.53E-17

CPT1B_221_CPT1B_214	LQKYLVLK_2_EFQDKTAPR_4	-0.23	-0.79	-0.53	-0.6	-0.49	-0.66	-0.6	0	-0.12	0.192	-0.12	0.192
CPT2_62_CPT2_69	LEDTMKR_5_YLSAQKPLLNDSQFR_5	-0.43	0.53	-0.69	-0.19	-0.98		-0.59	4.26E-13	-0.37	0.000727	-0.37	0.000727
ECHA_728_ECHA_735	FVDLYGAQKVVDR_8_KYESAYGTQFTPCQLLLDHANNSSK_0	-0.13			-0.22	-0.71	-0.09	-0.59	3.51E-08	-0.19	1.53E-17	-0.19	1.53E-17
DLDH_420_DLDH_143	IGKFPFAANSR_2_ALTGGIAHLFKQNK_10		-1.42	0.02	0.55	0.29	-1.45	-0.58	2.66E-10	-0.27	0.000558	-0.27	0.000558
CYC_100_CYC_40	ADLIAYLKK_7_KTGQAAGFSYTDANK_0	-0.29	-0.55	-0.72	-0.47	-0.78	-0.42	-0.58	0	-0.2	0.0475	-0.2	0.0475
CISD1_37_CISD1_42	FYAKENR_3_TKAMVNLQIQK_1	-0.48	-0.62	-0.23	-0.53	-0.45	-0.7	-0.58	4.08E-15	-0.53	0.0000402	-0.53	0.0000402
CPT1B_404_CPT1B_404	QTFFSSGKNK_7_QTFFSSGKNK_7	-0.63	-0.62	-0.11	-0.86	-0.24	-0.78	-0.58	4.3E-15	-0.12	0.192	-0.12	0.192
ATPG_49_ATPB_426	SMKMVAAAK_2_GVQKILQDYK_3	-0.01	0.32	-0.89	-0.25	-0.73	-0.44	-0.57	1.39E-22	-0.29	4.81E-11	-0.23	3.91E-11
MDHM_239_THIM_171	IQEAGTEVVKAK_9_LPMGMTAENLAAKYNISR_12	-0.54		-1.02	-0.55		-0.39	-0.56	1.78E-08	0.16	3.47E-10	-0.41	8.46E-28
UCRI_163_UCRI_182	LSDIPEGKNMAFK_7_TKKEIDQEAAVEVSQLRDPQHDLDR_2	-0.39	-0.86	-0.57	-0.56	-0.86	-0.5	-0.56	6.47E-10	-0.66	6.77E-12	-0.66	6.77E-12
ODO2_278_ODO2_278	HNLKLGFMSAFVK_3_HNLKLGFMSAFVK_3	-1.42	-0.58		-0.6	-0.84	-0.11	-0.56	7.82E-13	-0.6	0.0000161	-0.6	0.0000161
ACSL1_387_ACSL1_420	IFGQANTSLKR_9_NNSLWDKLIFHKIQSSLGGK_11		-0.68		-0.95	-0.23	-1.02	-0.55	4.25E-24	-0.15	0.0033	-0.15	0.0033
ALDH2_513_ALDH2_430	TVTVKVPQK_4_FKTIEEVVGR_1	-0.38		-0.49	-0.3	-0.71		-0.55	4.09E-09	-0.15	0.012	-0.15	0.012
CX6B1_10_NDUA4_74	IKNYK_1_FYSVNVDYSKLK_9	-0.06	-0.64	-0.49	-0.52	-0.58	-0.44	-0.55	0	-0.41	0.000633	-0.27	0.00000126
ETFB_250_CPT1B_40	LKEVGRI_1_HIYLSGINSWKK_10		-0.43	-0.95	-0.28	-0.78		-0.55	0.000000822	-0.23	0.0000101	-0.12	0.192
ECHB_333_ECHB_448	ALAMGYKPK_6_KDGGQYALVAACAAGGQGHAMIVEAYPK_0	-0.23		-0.94	-0.02	-0.69		-0.55	1.51E-08	-0.27	2.01E-11	-0.27	2.01E-11
MPCP_352_NDUA4_76	KLGLTE_0_FYSVNVDYSKLKK_11	-0.26	-0.45	-0.55	-0.42	-1.12	-0.47	-0.54	6.08E-14	-0.4	0.00544	-0.27	0.00000126
AT5F1_191_ATPA_261	AYKEVK_2_STVAQLVKR_7	-0.32	0.27	-0.74	-0.24	-0.61	0.04	-0.52	1.51E-34	-0.37	0.128	-0.06	0.083
MIC60_281_MIC60_285	TVEGALKER_6_KAVDEAADALLK_0	-0.26	-0.64	-0.51	-0.43	-0.47	-0.36	-0.52	8.10E-37	0.08	0.0825	0.08	0.0825

ATPB_133_ATPB_55	VLDSGAPIKIPVGPETLGR_8_AAPAGVHPARDYAAQASAAPKAGTATGR_20	0.56		-0.77	-0.36	-0.74	0.05	-0.51	3.95E-10	-0.23	3.91E-11	-0.23	3.91E-11
ATP5J_99_ATPA_506	FDDPKFEVIDKPQS_4_ITKFENAFLSHVISQHQSLLGNIR_2		-1.22	-0.56	0.11	-0.62		-0.51	2.84E-19	-0.15	0.0191	-0.06	0.083
MIC60_505_MIC60_515	VQEQELKYEFEQGLSEK_6_YEFEQGLSEKLSEQELEFR_9		-0.43	1.79	-0.52	-0.4		-0.51	6.87E-08	0.08	0.0825	0.08	0.0825
NDUB5_152_NDUC2_95	LKEQEVR_1_DHDMFGYIKLHPEDFPEKEK_8		-0.76	-0.41	-0.47	-0.56		-0.51	1.95E-21	-0.66	0.0212	-0.37	0.0032
IDHP_127_IDHP_360	VEEFKLK_4_EHQKGRPTSTNPIASIFAWTR_3		-1.31	-0.37	0.33	-0.29	-0.85	-0.5	4.17E-36	-0.11	0.00705	-0.11	0.00705
CX6B1_10_NDUA4_74	IKNYK_1_FYSVNVDYSKLKK_9	-0.07	-0.61	-0.4	-0.54	-0.46	-0.43	-0.5	0	-0.41	0.000633	-0.27	0.00000126
ATPB_522_ATPB_480	ADKLAEEHGS_2_FLSQPFQVAEVFTGHMGKLVPLKETIK_17	-0.33		-0.73	0.09	-0.64	0.22	-0.5	5.06E-15	-0.23	3.91E-11	-0.23	3.91E-11
THIM_25_THIM_234	TPFGAYGGLLKDFSATDLTEFAAR_10_QTMQVDEHARPQTTLEQLQKLPSVFK_19	0.56	-0.04	-0.63	0.4	-0.43	-1.08	-0.5	0.000000109	-0.41	8.46E-28	-0.41	8.46E-28
MIC60_498_MIC60_515	DVLKVQEQELK_3_VQEQELKYEFEQGLSEKLSEQELEFR_16	-0.18	-0.61	-1.76		-0.29	-0.34	-0.5	4.2E-09	0.08	0.0825	0.08	0.0825
CX6B1_10_NDUA4_76	IKNYK_1_FYSVNVDYSKLKK_11	-0.19	-0.65	-0.33	-0.53	-0.48	-0.36	-0.49	0	-0.41	0.000633	-0.27	0.00000126
CX6B1_13_NDUA4_74	NYKTAPFDSR_2_FYSVNVDYSKLK_9	-0.15	-0.59	-0.41	-0.39	-0.56	-0.29	-0.49	0	-0.41	0.000633	-0.27	0.00000126
ECHA_728_ECHA_337	FVDLYGAQKVVDR_8_ESKALMGLYNGQVLCK_2	-0.38		-0.66	-0.34	-0.57	0.08	-0.49	4.12E-10	-0.19	1.53E-17	-0.19	1.53E-17
THIM_270_THIM_171	KHNFTPLAR_0_LPM[147.04]GMTAENLAAKYNISR_12	-0.26	-0.09	-0.58	-0.22	-0.67		-0.48	2.49E-43	-0.41	8.46E-28	-0.41	8.46E-28
AL4A1_118_AL4A1_129	KEWDLKPMADR_5_AQVFLKAADMLSGPR_5	-0.35		-0.54	-0.13	-0.7		-0.48	3.12E-13	-0.38	0.0000104	-0.38	0.0000104
COX6C_68_COX6C_68	KAGIFQSAK_0_KAGIFQSAK_0		-0.68		-0.54	-0.29	-0.32	-0.48	0.000000162	-0.88	2.41E-08	-0.88	2.41E-08
NDUA9_189_NDUA9_157	AVGEKEVR_4_AIAQASKEAGVER_6	-0.41	0.16	-0.63		-0.52	0.19	-0.48	1.2E-09	-0.67	0.000367	-0.67	0.000367
ECHA_129_ECHA_129	MFEKLEK_3_MFEKLEK_3	-0.32	-0.4	-0.5	-0.38	-0.53	-0.45	-0.47	0	-0.19	1.53E-17	-0.19	1.53E-17

THIM_270_THIM_171	KHNFTPLAR_0_LPMGMTAENLAAKYNISR_12	-0.28	-0.16	-0.63	-0.27	-0.73	-0.18	-0.47	0	-0.41	8.46E-28	-0.41	8.46E-28
COX6C_68_AIFM1_243	KAGIFQSAK_0_GNMVKLNDGSQITFEK_4	-0.41	-0.44	-0.28		-0.54	-0.45	-0.47	0.00000126	-0.88	2.41E-08	-0.33	0.0000303
AIFM1_108_AIFM1_188	VM[147.04]GLGLSPEEKQR_10_ELWFSDDPNVTKTLQFR_11		-0.67	-0.3	-0.2	-0.4		-0.47	5.02E-15	-0.33	0.0000303	-0.33	0.0000303
ODO2_268_ODO2_278	HKDAFLKK_1_HNLKLGFMSAFVK_3		0.09	-1.97	-0.93	0.55		-0.46	2.87E-19	-0.6	0.0000161	-0.6	0.0000161
CX6B1_13_NDUA4_74	NYKTAPFDSR_2_FYSVNVDYSKLKK_9	-0.02	-0.47	-0.36	-0.39	-0.56	-0.4	-0.45	0	-0.41	0.000633	-0.27	0.00000126
COX6C_68_CYC_100	KAGIFQSAK_0_ADLIAYLKK_7	-0.27	-0.53	-0.29	-0.5	-0.46	-0.3	-0.45	7.84E-38	-0.88	2.41E-08	-0.2	0.0475
ATPA_167_ATPA_175	GPIGSKTR_5_VGLKAPGIIPR_3	-0.16	-0.02	-0.55	-0.24	-0.56		-0.45	4.44E-29	-0.06	0.083	-0.06	0.083
CISD1_33_CISD1_42	KFYAK_0_TKAMVNLQIQK_1	-0.49	-0.52	-0.13	-0.27	-0.39	-0.49	-0.45	1.09E-10	-0.53	0.0000402	-0.53	0.0000402
MIC19_86_MIC19_63	LKQAR_1_YSSVYGASVSDEDLKR_14	0.05	-0.49		-0.49	-0.3	-0.48	-0.45	8.21E-13	-0.23	0.000928	-0.23	0.000928
CX6B1_13_NDUA4_76	NYKTAPFDSR_2_FYSVNVDYSKLKK_11	-0.11	-0.52	-0.45	-0.41	-0.53	-0.28	-0.44	2.39E-37	-0.41	0.000633	-0.27	0.00000126
ECHA_390_ECHA_390	TLLKDTTVTGLGR_3_TLLKDTTVTGLGR_3	-0.25	-0.3	-0.48	-0.46	-0.47	-0.46	-0.44	0	-0.19	1.53E-17	-0.19	1.53E-17
NDUB5_152_NDUC2_95	LKEQEVR_1_DHDMFGYIKLHPEDFPEK_8	-0.25	-0.39	-0.4	-0.47	-0.35		-0.44	2.16E-28	-0.66	0.0212	-0.37	0.0032
ATPA_498_ECHA_390	GYLDKLEPSK_4_TLLKDTTVTGLGR_3	-0.39	-0.43	-0.42	-0.13	-0.67	-0.3	-0.43	1.01E-17	-0.06	0.083	-0.19	1.53E-17
ODB2_295_ODB2_304	LREELKPVALAR_5_GIKLSFMPFFLK_2		-1.14	-0.6	0.12	-0.48		-0.42	1.34E-20	-0.54	0.0000431	-0.54	0.0000431
CX6B1_13_NDUA4_74	IKNYKTAPFDSR_4_FYSVNVDYSKLKK_9		-0.44	-0.25	-0.46	-0.41	-0.21	-0.42	2.03E-26	-0.41	0.000633	-0.27	0.00000126
ECHA_457_ECHA_620	HKVLK_1_FGGGSVELLKQMVSK_9	-0.04		-0.64	-0.09	-0.62	-0.23	-0.42	1.43E-27	-0.19	1.53E-17	-0.19	1.53E-17
THIM_137_THIM_25	FGTKFGLDLK_3_RTPFGAYGGLLKDFSATDLTEFAAR_11	-0.22	-0.43	-0.37	-0.32	-0.49	-0.64	-0.42	2.70E-24	-0.41	8.46E-28	-0.41	8.46E-28
CISD1_33_CISD1_42	KFYAK_0_TKAM[147.04]VNLQIQK_1	-0.24	-0.67		-0.29	-0.19	-0.49	-0.42	0.000000252	-0.53	0.0000402	-0.53	0.0000402
AIFM1_277_AIFM1_243	AGAEVKSR_5_GNM[147.04]VKLNDGSQITFEK_4		-0.67	-0.28	-0.07	-0.46	-0.37	-0.42	0.000000541	-0.33	0.0000303	-0.33	0.0000303

COX41_67_COX41_60	EKADWSSLSR_1_DYPLPDVAHVTM[147.04]LSASQKALK_17		0.51	-0.79	0.27	-0.67		-0.41	2.53E-09	-0.05	0.314	-0.05	0.314
ATPG_64_ATPG_49	ELKPAR_2_SM[147.04]KM[147.04]VAAAK_2	-0.04	0.38	-0.66	-0.25	-0.57	-0.08	-0.41	1.94E-08	-0.29	4.81E-11	-0.29	4.81E-11
DECR_319_DECR_42	VTKEEWDIIEGLIR_2_DAPQSKFFQPVLKPMLPPDAFQGK_5	-0.37	-0.39	-0.48	-0.03	-0.43		-0.41	2.57E-08	-0.31	7.67E-11	-0.31	7.67E-11
ACADM_79_ACADM_197	SGEYPFPLIKR_9_M[147.04]WITNGGKANWYFLLAR_7	-0.25	0.28	-0.57	0.03	-0.53	0.01	-0.4	8.38E-43	-0.23	0.0000215	-0.23	0.0000215
AT5F1_191_ATPA_161	AYKEVK_2_VVDALGNAIDGKGPIGSK_11		0.15	-0.65	-0.06	-0.59		-0.4	7.65E-14	-0.37	0.128	-0.06	0.083
NDUA4_77_NDUA4_74	KEGPDF_0_FYSVNVDYSKLK_9	-0.2	-0.54	-0.28	-0.41	-0.3	-0.29	-0.4	4.3E-15	-0.27	0.00000126	-0.27	0.00000126
ECHA_728_ECHA_326	FVDLYGAQKVVDR_8_AGLEQGSDAGYLAESQKFGELALTK_16	-0.13	0.16	-0.71	-0.08	-0.6	0	-0.4	1.72E-35	-0.19	1.53E-17	-0.19	1.53E-17
ECHA_728_ECHA_664	FVDLYGAQKVVDR_8_LPAKPEVSSDEDVQYR_3	-0.41	0.02	-0.98	-0.05	-0.88	-0.02	-0.4	2.88E-13	-0.19	1.53E-17	-0.19	1.53E-17
ECHA_303_ECHA_326	GLYPAPLKIIDAVK_7_AGLEQGSDAGYLAESQKFGELALTK_16	-0.31	0.06	-0.75	-0.16	-0.74	-0.03	-0.4	0	-0.19	1.53E-17	-0.19	1.53E-17
ACADM_79_ACADM_197	SGEYPFPLIKR_9_MWITNGGKANWYFLLAR_7		0.22	-0.51	-0.06	-0.4	-0.01	-0.39	3.39E-41	-0.23	0.0000215	-0.23	0.0000215
ATP5L_55_ECHA_129	KIIQSAK_0_MFEKLEK_3	-0.44	-0.11	-0.66	-0.16	-0.51		-0.39	3.39E-08	0.02	0.385	-0.19	1.53E-17
AIFM1_108_AIFM1_188	VMGLGLSPEEKQR_10_ELWFSDDPNVTKTLQFR_11	-0.12	-0.52	-0.26	-0.37	-0.36		-0.39	3.85E-26	-0.33	0.0000303	-0.33	0.0000303
ACADV_196_ACADV_72	GILLYGTKAQR_7_AESKSFAVGMFK_3	-0.29		-0.53	-0.23	-0.4	-0.1	-0.38	5.67E-20	0.03	0.244	0.03	0.244
KCRS_344_CYC_40	FSKILENLR_2_KTGQAAGFSYTDANK_0	-0.13	-0.4	-0.41	-0.22	-0.57	-0.22	-0.38	1.93E-24	-0.32	1.46E-10	-0.2	0.0475
COX6C_68_CYC_40	KAGIFQSAK_0_KTGQAAGFSYTDANK_0	-0.44	-0.27	-0.33	-0.11	-0.67	-0.19	-0.38	1.14E-10	-0.88	2.41E-08	-0.2	0.0475
VDAC3_163_VDAC3_109	SKLSQNNFALGYK_1_LTLDTIFVPNTGKK_12		-0.67	-0.19	-0.4	0.05		-0.38	4.95E-09	-0.16	0.0945	-0.16	0.0945
NDUA4_74_NDUA4_56	FYSVNVDYSKLK_9_NNPEPWNKLGPNEQYK_7	-0.04	-0.47	-0.23	-0.46	-0.31	-0.27	-0.38	1.51E-34	-0.27	0.00000126	-0.27	0.00000126
AIFM1_277_AIFM1_231	AGAEVKSR_5_KVVHLDVR_0	-0.01	-0.6	-0.15	-0.33			-0.38	2.28E-13	-0.33	0.0000303	-0.33	0.0000303

ECI1_247_ECI1_255	KATADNLIK_0_ATADNLIKQR_7	-0.32	0.23	-0.74	-0.09	-0.78	-0.07	-0.37	2.84E-08	-0.32	0.00116	-0.32	0.00116
CX6B1_13_NDUA4_74	IKNYKTAPFDSR_4_FYSVNVDYSKLK_9	-0.02	-0.5	-0.29	-0.4	-0.46	-0.26	-0.37	2.80E-45	-0.41	0.000633	-0.27	0.00000126
CX6B1_13_NDUA4_76	IKNYKTAPFDSR_4_FYSVNVDYSKLKK_11	-0.09	-0.59	-0.33	-0.45	-0.38	-0.27	-0.37	0	-0.41	0.000633	-0.27	0.00000126
ATPB_198_ATPB_264	VVDLLAPYAKGGK_9_DATSKVALVYGQMNEPPGAR_4	-0.13	0.36	-0.73	-0.12	-0.71	0.25	-0.37	8.07E-23	-0.23	3.91E-11	-0.23	3.91E-11
ECHA_457_ECHA_634	HKVLK_1_KSGKGFYIYQEGSK_3	-0.14	-0.18	-0.48	-0.25	-0.71		-0.37	6.48E-08	-0.19	1.53E-17	-0.19	1.53E-17
THIM_211_THIM_25	AANEAGYFNEEMAPIEVKTKK_19_TPFGAYGGLLKDFSATDLTEFAAR_10		-0.66	1.15	-0.23	0.03	-0.26	-0.37	0.000000656	-0.41	8.46E-28	-0.41	8.46E-28
THIM_240_THIM_171	LPSVFKK_5_LPM[147.04]GMTAENLAAKYNISR_12	-0.32	-0.27	-0.29	0.03	-0.72		-0.37	1.23E-12	-0.41	8.46E-28	-0.41	8.46E-28
ETFB_205_ETFB_116	KIEVVK_0_EKVDLLFLGK_1	-0.33		-0.67	-0.07	-0.55		-0.37	0.00000104	-0.23	0.0000101	-0.23	0.0000101
AIFM1_361_AIFM1_387	EGVKVMPNAIVQSVGVSGGR_3_KVETDHIVTAVGLEPNVELAK_0	0.03	-0.5	-0.33	-0.33	-0.4	-0.29	-0.37	2.92E-25	-0.33	0.0000303	-0.33	0.0000303
ATPB_522_ATPA_498	ADKLAEEHGS_2_GYLDKLEPSK_4	-0.15		-0.51	-0.02	-0.53		-0.36	1.78E-11	-0.23	3.91E-11	-0.06	0.083
ATPA_230_ATPA_161	TSIAIDTIINQKR_11_VVDALGNAIDGKGPIGSK_11	-0.34	0.5	-0.73	-0.22	-0.61	0.07	-0.36	7.37E-15	-0.06	0.083	-0.06	0.083
KCRS_292_KCRS_344	GLKEVER_2_FSKILENLR_2	-0.36	-0.57	-0.26	-0.16	-0.27		-0.36	1.68E-21	-0.32	1.46E-10	-0.32	1.46E-10
MIC60_281_MIC60_281	TVEGALKER_6_TVEGALKER_6	0.24	-0.71	-0.19	-0.31		-0.11	-0.36	0.000000503	0.08	0.0825	0.08	0.0825
NDUV2_60_NDUV2_67	DTPENNPDTPFDFTPENYKR_18_IEAIVKNYPEGHQAAAVLPVLDLAQR_5	-0.02	0.76	-0.75	-0.03	-0.75	0.03	-0.36	1.02E-11	-0.39	0.014	-0.39	0.014
VDAC1_45_VDAC1_33	IDLKTK_3_DVFTKGYGFGLIK_4	-0.32	-0.47	0.04	-0.11	0.25	-0.42	-0.35	2.52E-21	-0.2	0.0611	-0.2	0.0611
ECHB_409_ECHA_46	TKVGSPPLEK_1_THINYGVKGDVAVIR_7	-0.18		-0.46	-0.34	-0.39		-0.35	7.17E-09	-0.27	2.01E-11	-0.19	1.53E-17
THIM_240_THIM_171	LPSVFKK_5_LPMGMTAENLAAKYNISR_12	-0.12	-0.16	-0.35	-0.24	-0.49	-0.24	-0.35	0	-0.41	8.46E-28	-0.41	8.46E-28
MIC19_136_MIC19_157	KQDAFYK_0_SSEFYKVTTEEYQK_5	-0.34	-0.52	-0.2	-0.38	-0.16		-0.35	2.74E-16	-0.23	0.000928	-0.23	0.000928
MIC19_86_MIC19_86	LKQAR_1_LKQAR_1	-0.15	-0.63	-0.29	-0.42	-0.34		-0.35	1.66E-10	-0.23	0.000928	-0.23	0.000928

AIFM1_277_AIFM1_243	AGAEVKSR_5_GNMVKLNDGSQITFEK_4	-0.02	-0.43	-1.66	-0.31	-0.45	-0.31	-0.35	7.17E-09	-0.33	0.0000303	-0.33	0.0000303
ADT1_147_ECHA_728	LAADVGKGSSQR_6_FVDLYGAQKVVDR_8	-0.32		-0.57		-0.55	-0.02	-0.34	7.64E-08	0.5	0.000000399	-0.19	1.53E-17
ATPB_350_ATPA_261	ITTTKK_4_STVAQLVKR_7	-0.41	0.37	-0.62	-0.12	-0.84	0.23	-0.34	1.19E-19	-0.23	3.91E-11	-0.06	0.083
KCRS_335_KCRS_344	IPKLSK_2_FSKILENLR_2	-0.17	-0.53	-0.27	-0.21	-0.33	-0.24	-0.34	0	-0.32	1.46E-10	-0.32	1.46E-10
ECHA_334_ECHA_728	FGELALTKESK_7_FVDLYGAQKVVDR_8	-0.24	0.06	-0.59	-0.19	-0.55	0.02	-0.34	0	-0.19	1.53E-17	-0.19	1.53E-17
NDUC2_95_NDUA8_162	DHDMFGYIKLHPEDFPEK_8_ARPEPNPVIEGDLKPAKHGTR_16		0.01	-0.91	-0.01	0.13		-0.34	1.16E-15	-0.37	0.0032	-0.56	0.0212
ODPA_313_ODPA_77	SKSDPIMLLK_1_MELKADQLYK_3	0.3	-0.26	-0.37	-0.57	-0.46	-0.14	-0.33	7.65E-14	0.04	0.214	0.04	0.214
ACSL1_518_ACSL1_533	GANVFKGYLKDPAR_5_TAEALDKDGWLHTGDIGK_6		-0.46	-0.22	-0.39	-0.07		-0.33	3.44E-27	-0.15	0.0033	-0.15	0.0033
ADT1_147_ECHA_326	LAADVGKGSSQR_6_AGLEQGSDAGYLAESQKFGELALTK_16			-0.47	-0.1	-0.44	-0.24	-0.33	1.78E-08	0.5	0.000000399	-0.19	1.53E-17
ATPB_485_ATPB_198	LVPLKETIK_4_VVDLLAPYAKGGK_9	-0.18	0.3	-0.77	-0.17	-0.68	0.08	-0.33	2.47E-37	-0.23	3.91E-11	-0.23	3.91E-11
ATPB_485_ATP5H_78	LVPLKETIK_4_YNALKIPVPEDK_4	-0.32		-0.42	-0.1	-0.29		-0.33	7.74E-09	-0.23	3.91E-11	-0.06	0.00312
NDUA4_48_NDUA4_64	KNNPEPWNK_0_LGPNEQYKFYSVNVDYSK_7	-0.26	-0.54	-0.13	-0.11	-0.16	-0.2	-0.33	0.00000191	-0.27	0.00000126	-0.27	0.00000126
KCRS_335_KCRS_344	IPKLSKDPR_2_FSKILENLR_2	-0.13	-0.47	-0.3	-0.21	-0.29	-0.28	-0.33	0	-0.32	1.46E-10	-0.32	1.46E-10
COX6C_68_KCRS_344	KAGIFQSAK_0_FSKILENLR_2	-0.2	-0.45	-0.22	-0.12	-0.41	-0.45	-0.33	2.34E-17	-0.88	2.41E-08	-0.32	1.46E-10
ECHA_390_ECHA_46	TLLKDTTVTGLGR_3_THINYGVKGDVAVIR_7	0.18	-0.16	-0.41	-0.57	-0.28		-0.33	4.97E-11	-0.19	1.53E-17	-0.19	1.53E-17
ECHA_519_ECHA_540	TSKDTTASAVAVGLR_2_VIIVVKDGPGFYTTR_5	-0.31	0.04	-0.63	-0.3	-0.68	-0.01	-0.33	5.24E-15	-0.19	1.53E-17	-0.19	1.53E-17
ATP5H_149_ECHA_326	KYPYWPHQPIENL_0_AGLEQGSDAGYLAESQKFGELALTK_16	-0.04	0.28	-0.6	0.02	-0.56	-0.18	-0.33	1.50E-16	-0.06	0.00312	-0.19	1.53E-17
THIM_137_THIM_25	FGTKFGLDLK_3_TPFGAYGGLLKDFSATDLTEFAAR_10	-0.27	-0.21	-0.27	-0.28	-0.43	-0.31	-0.33	1.03E-29	-0.41	8.46E-28	-0.41	8.46E-28
MIC60_639_MIC60_639	FYAVQKLAR_5_FYAVQKLAR_5	-0.39	-0.57	-0.25	-0.24	-0.08	-0.47	-0.33	2.16E-28	0.08	0.0825	0.08	0.0825

ACSL1_208_ACSL1_114	AKLLLEGVENK_1_KPNQPYEWISYK_0	-0.02	-0.6	-0.2	-0.43	-0.11	-0.13	-0.32	8.29E-27	-0.15	0.0033	-0.15	0.0033
ACSL1_387_ACSL1_357	IFGQANTSLKR_9_LLMDDLKVLQPTIFPVVPR_6	-0.74	-0.73	-0.23	-0.3	0	-0.34	-0.32	1.17E-13	-0.15	0.0033	-0.15	0.0033
ACSL1_387_ACSL1_357	IFGQANTSLKR_9_LLM[147.04]DDLKVLQPTIFPVVPR_6		-0.91	-0.12	-0.39	0.32		-0.32	0.000000223	-0.15	0.0033	-0.15	0.0033
ACADV_196_ACADV_52	GILLYGTKAQR_7_EATQAVLDKPETLSSDASTR_8	-0.35	0.5	-0.58	-0.27	-0.71	0.05	-0.32	2.12E-18	0.03	0.244	0.03	0.244
ECHA_129_ECHA_390	MFEKLEK_3_TLLKDTTVTGLGR_3	-0.31	-0.27	-0.38	-0.27	-0.23	-0.32	-0.32	9.81E-45	-0.19	1.53E-17	-0.19	1.53E-17
ATPO_54_ACADM_79	KLDQVEK_0_SGEYPFPLIKR_9	-0.35		-0.88	-0.28	-1		-0.31	0.000000555	-0.1	0.000153	-0.23	0.0000215
ATPA_261_ATPB_485	STVAQLVKR_7_LVPLKETIK_4	-0.2	0.37	-0.8	-0.14	-0.7	0.07	-0.31	4.10E-18	-0.06	0.083	-0.23	3.91E-11
ATPA_261_ATPA_161	STVAQLVKR_7_VVDALGNAIDGKGPIGSK_11	-0.34	0.25	-0.6	-0.07	-0.76	0.16	-0.31	7.75E-14	-0.06	0.083	-0.06	0.083
THIM_137_THIM_158	FGTKFGLDLK_3_LEDTLWAGLTDQHVKLPMGMTAENLAAK_14	-0.47	-0.44	-0.18	-0.32	-0.25	-0.11	-0.31	8.12E-24	-0.41	8.46E-28	-0.41	8.46E-28
AIFM1_361_AIFM1_387	EGVKVM[147.04]PNAIVQSVGVSGGR_3_KVETDHIVTAVGLEPNVELAK_0	0.02	-0.29	-0.97	-0.18	-0.33	-0.4	-0.31	0.00000139	-0.33	0.0000303	-0.33	0.0000303
ACSL1_512_ACSL1_533	GEGEVCVKGANVFK_7_TAEALDKDGWLHTGDIGK_6	0.08	-0.58	-0.21	-0.5	-0.13	-0.26	-0.3	4.93E-25	-0.15	0.0033	-0.15	0.0033
ACSL1_629_ACSL1_641	NKDINK_1_AILDDLLKLGK_7	0.09	-0.6	-0.11	-0.45	0.01	0.02	-0.3	7.87E-16	-0.15	0.0033	-0.15	0.0033
ECHA_303_ECHA_728	GLYPAPLKIIDAVK_7_FVDLYGAQKVVDR_8	-0.25	0.13	-0.63	-0.13	-0.57	-0.03	-0.3	0	-0.19	1.53E-17	-0.19	1.53E-17
THIM_137_THIM_137	FGTKFGLDLK_3_FGTKFGLDLK_3	-0.2	-0.3	-0.25	-0.12	-0.33	-0.07	-0.3	0.00000199	-0.41	8.46E-28	-0.41	8.46E-28
ATPG_43_ATPG_49	NIQKITK_3_SMKMVAAAK_2	-0.67	0.2	-0.6	-0.21	-0.62	0.26	-0.3	2.03E-08	-0.29	4.81E-11	-0.29	4.81E-11
MIC19_45_MIC19_63	ESSPSGSKSQR_7_YSSVYGASVSDEDLKR_14		-0.6	-0.08	-0.44	-0.09	-0.11	-0.3	1.07E-35	-0.23	0.000928	-0.23	0.000928
IVD_239_IVD_76	GMPGFSTSKK_8_AQEIDQTNDFKNLR_10	-0.21	0.35	-0.73	-0.05	-0.71	0.04	-0.3	1.19E-19	-0.18	0.00534	-0.18	0.00534
ATPB_350_AT5F1_191	ITTTKK_4_AYKEVK_2	-0.28	0.29	-0.74	-0.14	-0.66	0.09	-0.29	1.65E-15	-0.23	3.91E-11	-0.37	0.128
ATPA_132_ATPA_167	EGDVVKR_5_GPIGSKTR_5	-0.09	0.37	-0.54	-0.03	-0.48	0.07	-0.29	6.07E-15	-0.06	0.083	-0.06	0.083

KCRS_276_KCRS_230	VISMEKGGNMK_5_LIDDHFLFDKPVSPLLTCAGMAR_9		-0.48	-0.26	-0.22	-0.19		-0.29	0.000000236	-0.32	1.46E-10	-0.32	1.46E-10
ECHA_129_ECHA_390	M[147.04]FEKLEK_3_TLLKDTTVTGLGR_3	-0.29	-0.31	-0.34	-0.27	-0.15	-0.47	-0.29	4.9E-14	-0.19	1.53E-17	-0.19	1.53E-17
ECHA_129_ATP5L_61	MFEKLEK_3_IIQSAKTGSFK_5	-0.09	-0.01	-0.38	-0.27	-0.44	-0.22	-0.29	5.26E-22	-0.19	1.53E-17	0.02	0.385
THIM_240_THIM_137	LPSVFKK_5_FGTKFGLDLK_3	-0.22	-0.37	-0.01	-0.39	-0.25	-0.22	-0.29	0	-0.41	8.46E-28	-0.41	8.46E-28
ATPG_46_ATPG_39	ITKSM[147.04]K_2_SIKNIQK_2	-0.13	0.66	-0.77	0.06	-0.64	0.1	-0.29	0.00000141	-0.29	4.81E-11	-0.29	4.81E-11
ECHB_333_ECHB_45	ALAMGYKPK_6_KTLAKPNMK_0	-0.28	-0.04	-0.59	0.07	-0.74		-0.29	0.000000283	-0.27	2.01E-11	-0.27	2.01E-11
ETFA_206_ETFA_232	LTKSDRPELTGAK_2_SGENFKLLYDLADQLHAAVGASR_5	-0.3	0.45	-0.6	-0.09	-0.69	-0.11	-0.29	4.54E-08	-0.21	0.0000464	-0.21	0.0000464
ACADV_196_ACADV_240	GILLYGTKAQR_7_SSAIPSPCGKYYTLNGSK_9	-0.02		-0.56	-0.12	-0.72	0.09	-0.28	0.000001866	0.03	0.244	0.03	0.244
ATPA_167_ATPA_305	GPIGSKTR_5_DNGKHALIIYDDLSK_3	-0.19	0.14	-0.61	-0.04	-0.53	0.21	-0.28	1.51E-15	-0.06	0.083	-0.06	0.083
ATPA_230_ATP5H_48	TSIAIDTIINQKR_11_LASLSEKPPAIDWAYYR_6	-0.03		-0.59	-0.13	-0.42	0.07	-0.28	3.93E-11	-0.06	0.083	-0.06	0.00312
ATPG_64_ATPG_49	ELKPAR_2_SMKMVAAAK_2	-0.35	0.37	-0.56	-0.06	-0.54	0.01	-0.28	9.89E-12	-0.29	4.81E-11	-0.29	4.81E-11
GSTK1_165_GSTK1_93	ISTQQVKNK_6_DFFGETVKK_7	-0.47	-0.15	-0.17	-0.42	-0.26	-0.17	-0.28	3.56E-31	-0.36	0.0000111	-0.36	0.0000111
MDHM_185_CACP_245	ANTFVAELKGLDPAR_8_IWNSSLQSNKEPVGILTSNHR_9	-0.24	0.43	-0.4	-0.17	-0.38	0.05	-0.27	1.46E-09	0.16	3.47E-10	-0.32	4.23E-13
ATPB_485_ATPB_522	LVPLKETIK_4_ADKLAEEHGS_2	-0.11	0.34	-0.59	-0.08	-0.61	0.14	-0.27	2.74E-08	-0.23	3.91E-11	-0.23	3.91E-11
ECHA_334_ECHA_303	FGELALTKESK_7_GLYPAPLKIIDAVK_7	-0.27	0.12	-0.66	-0.13	-0.54	0.02	-0.27	3.75E-38	-0.19	1.53E-17	-0.19	1.53E-17
ECHA_390_ECHB_335	TLLKDTTVTGLGR_3_ALAMGYKPKAYLR_8	-0.14	0.04	-0.41	-0.08	-0.28		-0.27	1.58E-18	-0.19	1.53E-17	-0.27	2.01E-11
MIC19_136_MIC60_515	KQDAFYK_0_YEFEQGLSEKLSEQELEFR_9	0.08	-0.5	-0.11	-0.3	-0.1		-0.27	2.41E-15	-0.23	0.000928	0.08	0.0825
CACP_85_CACP_93	LQKGLER_2_KMENWLSEWWLK_0	-0.3	0.24	-0.25	-0.17	-0.2		-0.26	0.000000236	-0.32	4.23E-13	-0.32	4.23E-13

ATPB_198_ATPB_264	VVDLLAPYAKGGK_9_DATSKVALVYGQM[147.04]NEPPGAR_4	-0.21	0.33	-0.65	-0.17	-0.74	0.13	-0.26	7.85E-13	-0.23	3.91E-11	-0.23	3.91E-11
ATPB_350_ATPA_161	ITTTKK_4_VVDALGNAIDGKGPIGSK_11	-0.23	0.45	-0.62	-0.18	-0.69	0.13	-0.26	1.35E-11	-0.23	3.91E-11	-0.06	0.083
NDUAC_107_NDUAC_43	KFIWTNHK_0_IGTLVGEDKYGNK_8	-0.15	0.37	-0.5	0.03	-0.53	0.04	-0.26	5.63E-17	-0.32	0.00236	-0.32	0.00236
THIM_137_ATP5H_78	FGTKFGLDLK_3_YNALKIPVPEDKYTALVDQEEKEDVK_4		-1.27	-0.1	-0.25	-0.02	-0.34	-0.26	3.03E-10	-0.41	8.46E-28	-0.06	0.00312
MPCP_290_MPCP_204	EKGSTASQVLQR_1_MYKEEGLNAFYK_2	-0.08	0.64	-0.72	-0.14	-0.79	0.08	-0.26	6.82E-12	-0.4	0.00544	-0.4	0.00544
ATPG_39_ATPG_49	SIKNIQK_2_SMKMVAAAK_2	-0.18	0.34	-0.61	-0.03	-0.49	0	-0.26	2.41E-17	-0.29	4.81E-11	-0.29	4.81E-11
NDUV1_54_NDUV1_66	LKGALR_1_TKEILLK_1	0.02	0.13	-0.52	0.11	-0.38		-0.26	0.000000132	0.17	0.00168	0.17	0.00168
CX6B1_10_CX6B1_47	IKNYK_1_AMTAKGGDVSVCEWYR_4	0.3	-0.4	-0.12	-0.36	-0.1	-0.03	-0.25	1.27E-08	-0.41	0.000633	-0.41	0.000633
AT5F1_162_ATPA_498	AQQALVQKR_7_GYLDKLEPSK_4	-0.17	0.34	-0.48	-0.03	-0.45	0.15	-0.25	1.72E-18	-0.37	0.128	-0.06	0.083
ECHA_353_ECHA_519	NKFGAPQK_1_TSKDTTASAVAVGLR_2	-0.22	-0.02	-0.3	-0.33	-0.24	-0.04	-0.25	1.71E-12	-0.19	1.53E-17	-0.19	1.53E-17
MPCP_290_MPCP_204	EKGSTASQVLQR_1_M[147.04]YKEEGLNAFYK_2	-0.02	0.47	-0.69	-0.15	-0.65	0.15	-0.25	3.59E-09	-0.4	0.00544	-0.4	0.00544
ATPG_64_ATPG_49	ELKPAR_2_SM[147.04]KMVAAAK_2	-0.24	0.16	-0.57	-0.18	-0.55	0.14	-0.25	6.35E-08	-0.29	4.81E-11	-0.29	4.81E-11
ATPG_39_ATPG_49	SIKNIQK_2_SM[147.04]KMVAAAK_2	-0.17	0.33	-0.6	-0.06	-0.47	0.02	-0.25	3.23E-23	-0.29	4.81E-11	-0.29	4.81E-11
ECHB_202_ECHB_189	LSLLSKFR_5_MMLDLNKAK_6	-0.24	0.08	-0.23	-0.14	-0.29		-0.25	1.57E-29	-0.27	2.01E-11	-0.27	2.01E-11
MIC19_45_MIC19_63	ESSPSGSKSQR_7_YSSVYGASVSDEDLKRR_14		-0.29	-0.14	-0.42	-0.09		-0.25	6.06E-10	-0.23	0.000928	-0.23	0.000928
ATPB_133_ATPB_351	VLDSGAPIKIPVGPETLGR_8_KGSITSVQAIYVPADDLTDPAPATTFAHLDATTVLSR_0			-0.25	-0.11	-0.26	-1.85	-0.24	8.12E-08	-0.23	3.91E-11	-0.23	3.91E-11
ECHA_457_ECHA_390	HKVLK_1_TLLKDTTVTGLGR_3	-0.01	-0.02	-0.22	-0.25	-0.26	-0.39	-0.24	0	-0.19	1.53E-17	-0.19	1.53E-17
ACON_305_ECHA_390	KYLSK_0_TLLKDTTVTGLGR_3	-0.29		-0.42	-0.1	-0.24		-0.24	0.000001779	0.06	0.0151	-0.19	1.53E-17
MIC60_298_MIC60_305	AKEELEK_1_M[147.04]KTIIEDAK_1	0	-0.36	-0.29	0.08	-0.22	-0.04	-0.24	5.99E-11	0.08	0.0825	0.08	0.0825

COQ9_172_COQ9_170	KTDQFLR_0_LVQLGQAEKR_8	-0.15		-0.46	0.01	-0.22		-0.24	4.47E-10	-0.25	0.00111	-0.25	0.00111
ATPG_46_ATPG_39	ITKSMK_2_SIKNIQK_2	-0.24	0.42	-0.55	0.02	-0.56	0.18	-0.24	7.37E-12	-0.29	4.81E-11	-0.29	4.81E-11
ACSL1_241_ACSL1_208	KCGVEIISLK_0_AKLLLEGVENK_1	0.32	-0.5	-0.03	-0.49	-0.04	-0.2	-0.23	3E-12	-0.15	0.0033	-0.15	0.0033
AT5F1_191_ATPB_485	AYKEVK_2_LVPLKETIK_4	-0.25	0.32	-0.55	-0.07	-0.57	0.18	-0.23	4.1E-15	-0.37	0.128	-0.23	3.91E-11
ATPG_138_ATPA_503	IKGILYR_1_GYLDKLEPSKITK_9	-0.17	0.48	-0.49	-0.01	-0.6	-0.03	-0.23	2.63E-15	-0.29	4.81E-11	-0.06	0.083
ECHB_333_ECHA_390	ALAM[147.04]GYKPK_6_TLLKDTTVTGLGR_3	-0.12	0.19	-0.41	-0.06	-0.36	-0.02	-0.23	2.47E-37	-0.27	2.01E-11	-0.19	1.53E-17
ATPO_97_ATPO_100	SLNDITKR_6_EKFSPLTANLMNLLAENGR_1	0.04		-0.32	-0.01	-0.22		-0.23	7.88E-13	-0.1	0.000153	-0.1	0.000153
ECHA_60_ECHA_540	INSPNSKVNTLNK_6_VIIVVKDGPGFYTTR_5	-0.19	0.24	-0.54	-0.11	-0.07	-0.27	-0.22	0.00000127	-0.19	1.53E-17	-0.19	1.53E-17
ECHB_333_ECHA_390	ALAMGYKPK_6_TLLKDTTVTGLGR_3	-0.12	0.18	-0.43	-0.07	-0.35	-0.01	-0.22	2.59E-36	-0.27	2.01E-11	-0.19	1.53E-17
ECHA_129_ATP5H_149	MFEKLEK_3_KYPYWPHQPIENL_0	-0.36	0.24	-0.36	-0.1	-0.25	-0.15	-0.22	3.51E-09	-0.19	1.53E-17	-0.06	0.00312
THIL_187_THIL_63	DGLTDVYNKIHMGNCAENTAK_8_TPIGSFLGSLASQPATKLGTAAIQGAIEK_16	-0.21		-0.18	-0.18	-0.3	0.02	-0.22	0.000000239	0.19	1.55E-10	0.19	1.55E-10
NDUA9_157_NDUS1_311	AIAQASKEAGVER_6_NEKGLLTYTSWEDALSR_2	-0.11	0.46	-0.69	-0.08	-0.54	0.07	-0.22	1.27E-09	-0.67	0.000367	0.04	0.386
GSTK1_62_GSTK1_93	KGQYIFK_0_DFFGETVKK_7	-0.33	-0.31	0.01	-0.58	-0.07		-0.22	3.76E-13	-0.36	0.0000111	-0.36	0.0000111
ATPA_531_ATPA_506	SDGKISEQSDAK_3_ITKFENAFLSHVISQHQSLLGNIR_2		0.18	-0.24	-0.06	-0.3	-0.08	-0.21	2.51E-10	-0.06	0.083	-0.06	0.083
ATPG_138_ATPA_498	IKGILYR_1_GYLDKLEPSK_4	-0.16	0.51	-0.45	0.02	-0.41	-0.18	-0.21	2.02E-21	-0.29	4.81E-11	-0.06	0.083
ECHA_390_ECHB_278	TLLKDTTVTGLGR_3_DTVTKDNGIRPSSLEQM[147.04]AK_4	-0.02	0.1	-0.36	-0.09	-0.25	-0.24	-0.21	4.93E-25	-0.19	1.53E-17	-0.27	2.01E-11
ECHA_129_ATP5H_117	M[147.04]FEKLEK_3_IQEYEKQLEK_5	-0.1	0.16	-0.37	-0.22	-0.31	0.11	-0.21	0.000000109	-0.19	1.53E-17	-0.06	0.00312
THIM_137_THIM_234	FGTKFGLDLK_3_QTMQVDEHARPQTTLEQLQKLPSVFK_19	0.72	0.96	-0.68	-0.11	-1.21	-1.06	-0.21	5.12E-15	-0.41	8.46E-28	-0.41	8.46E-28
ATPG_138_ATPG_154	IKGILYR_1_THSDQFLVSFKDVGR_10	-0.13	0.23	-0.45		-0.4	0.14	-0.21	1.17E-16	-0.29	4.81E-11	-0.29	4.81E-11

ATPA_167_AATM_150	GPIGSKTR_5_FFKFSR_2	-0.13		-0.37	-0.02	-0.33	0.26	-0.2	3.32E-09	-0.06	0.083	0.13	8.18E-08
CYC_100_KCRS_344	ADLIAYLKK_7_FSKILENLR_2	-0.1	-0.24	-0.14	-0.11	-0.24	-0.19	-0.2	2.22E-17	-0.2	0.0475	-0.32	1.46E-10
THIM_137_THIM_241	FGTKFGLDLK_3_KDGTVTAGNASGVSDGAGAVIIASEDAVKK_0	-0.11	-0.31	-0.1	-0.17	-0.13	-0.2	-0.2	2.23E-18	-0.41	8.46E-28	-0.41	8.46E-28
SDHA_636_SDHA_498	TGKVTLEYRPVIDK_2_ANAGEESVMNLDKLR_12	-0.02		-0.37	0.32	-0.37	0.13	-0.2	0.000000171	-0.14	0.0000112	-0.14	0.0000112
ATPG_39_ATPG_49	SIKNIQK_2_SMKM[147.04]VAAAK_2	-0.2	0.25	-0.71	-0.13	-0.53	-0.03	-0.2	7.98E-08	-0.29	4.81E-11	-0.29	4.81E-11
ECHB_191_ECHB_202	AKTLGQR_1_LSLLSKFR_5	-0.19	-0.07	-0.24	-0.05	-0.31		-0.2	2.00E-19	-0.27	2.01E-11	-0.27	2.01E-11
ATPG_64_ATPA_498	ELKPAR_2_GYLDKLEPSK_4	-0.29	0.34	-0.57	-0.1	-0.65	0.14	-0.19	7.67E-08	-0.29	4.81E-11	-0.06	0.083
ATPA_161_ATP5H_48	VVDALGNAIDGKGPIGSK_11_LASLSEKPPAIDWAYYR_6	-0.23	0.33	-0.5	-0.02	-0.48	0.08	-0.19	0.000000094	-0.06	0.083	-0.06	0.00312
ECHA_289_ECHA_569	TVEEKVK_4_ILQEGVDPKKLDALTTGFGFPVGAATLADEVGVDVAQHVAEDLGK_8	-0.26	-0.08	-0.22	-0.06	-0.1		-0.19	2.83E-08	-0.19	1.53E-17	-0.19	1.53E-17
ECHA_129_ATP5H_117	MFEKLEK_3_IQEYEKQLEK_5	-0.07	0.12	-0.33	-0.27	-0.2	0.05	-0.19	4.10E-18	-0.19	1.53E-17	-0.06	0.00312
ETFB_205_ETFB_110	KIEVVK_0_VLAKLAEK_3	-0.26	0.35	-0.41	-0.04	-0.46	0.15	-0.19	1.16E-15	-0.23	0.0000101	-0.23	0.0000101
CMC2_10_CMC2_18	VALTKR_4_ADPAELKAIFLK_6		-0.32	-0.14	-0.17	-0.08		-0.19	2.67E-28	-0.05	0.169	-0.05	0.169
ALDH2_377_ALDH2_370	ILGYIKSGQQEGAK_5_TEQGPQVDETQFKK_12	-0.12	0.24	-0.52	-0.2	-0.5	0.18	-0.18	2.02E-23	-0.15	0.012	-0.15	0.012
KCRS_344_KCRS_408	FSKILENLR_2_GQDIKVPPPLPQFGR_4	0.14	-0.42	-0.12	-0.13	-0.18	-0.07	-0.18	8.07E-23	-0.32	1.46E-10	-0.32	1.46E-10
MIC60_298_MIC60_305	AKEELEK_1_MKTIIEDAK_1	0	-0.38	-0.2	-0.17	0.01	-0.22	-0.18	2.16E-11	0.08	0.0825	0.08	0.0825
COQ9_170_COQ9_283	LVQLGQAEKR_8_INDAMNMGHTAKQVK_11		0.39	-0.42	0.05	-0.31		-0.18	1.88E-09	-0.25	0.00111	-0.25	0.00111
DECR_246_DECR_106	TKGAFSR_1_ATAEEISSKTGNK_8	-0.12	0.2	-0.41	-0.08	-0.27	0.15	-0.18	6.12E-11	-0.31	7.67E-11	-0.31	7.67E-11
ECHA_406_ECHA_644	GQQQVFKGLNDK_6_GFYIYQEGSKNK_9	-0.11	-0.03	-0.17	-0.18	-0.08	-0.28	-0.17	3.91E-12	-0.19	1.53E-17	-0.19	1.53E-17
SDHA_179_SDHA_335	AFGGQSLKFGK_7_YAPVAKDLASR_5	0.07	0.6	-0.21	-0.07	-0.34	0.16	-0.17	5.12E-22	-0.14	0.0000112	-0.14	0.0000112

QCR2_159_QCR2_199	SQLKIDK_3_MGKITSEELHYFVQNHFTSAR_2	-0.09	0.33	-0.49	0.06	-0.52	0.12	-0.17	1.19E-19	-0.16	0.0000768	-0.16	0.0000768
QCR2_159_QCR2_199	SQLKIDK_3_M[147.04]GKITSEELHYFVQNHFTSAR_2	-0.25	0.41	-0.45	0.08	-0.53	0.13	-0.17	0.00000017	-0.16	0.0000768	-0.16	0.0000768
ACSL1_387_ACSL1_420	IFGQANTSLKR_9_LIFHKIQSSLGGK_4		-0.73	-0.06	-0.39	0.18		-0.16	1.16E-15	-0.15	0.0033	-0.15	0.0033
ATPA_132_ATPO_84	EGDVVKR_5_VSLAVLNPYIKR_10	-0.05	0.49	-0.48	0.02	-0.4	0.08	-0.16	1.21E-12	-0.06	0.083	-0.1	0.000153
ECHA_390_ECHB_278	TLLKDTTVTGLGR_3_DTVTKDNGIRPSSLEQMAK_4	-0.13	0.08	-0.3	-0.06	-0.23	-0.12	-0.16	1.25E-24	-0.19	1.53E-17	-0.27	2.01E-11
THIM_137_THIM_214	FGTKFGLDLK_3_GKQTMQVDEHARPQTTLEQLQK_1	-0.22	-0.31	0.06	-0.18	-0.05	-0.36	-0.16	0.000000497	-0.41	8.46E-28	-0.41	8.46E-28
SDHA_167_SDHA_179	TEDGKIYQR_4_AFGGQSLKFGK_7	0.03	0.46	-0.23	-0.12	-0.33	0.11	-0.16	8.07E-23	-0.14	0.0000112	-0.14	0.0000112
ATPG_39_ATPG_49	SIKNIQK_2_SM[147.04]KM[147.04]VAAAK_2	-0.04	0.42	-0.62	0.01	-0.48	-0.01	-0.16	3.9E-11	-0.29	4.81E-11	-0.29	4.81E-11
OPA1_819_OPA1_834	KNLESR_0_GVEVDPSLIKDTWHQVYR_9		-0.41	0.04	-0.14	0.11	-0.42	-0.15	0.00000214	-0.18	0.0626	-0.18	0.0626
KCRS_408_KCRS_200	GQDIKVPPPLPQFGR_4_EVENVAITALEGLKGDLAGR_13	-0.08	-0.29	-0.07	0.1	-0.14	-0.12	-0.15	1.21E-33	-0.32	1.46E-10	-0.32	1.46E-10
KCRS_338_KCRS_344	LSKDPR_2_FSKILENLR_2		-0.49	-0.06	-0.15	-0.06	-0.07	-0.15	2.41E-14	-0.32	1.46E-10	-0.32	1.46E-10
ECHA_163_ECHB_191	IATKDR_3_AKTLGQR_1	-0.19	0.09	-0.14	-0.11	-0.16	-0.03	-0.15	4.51E-27	-0.19	1.53E-17	-0.27	2.01E-11
ECHA_569_ECHA_644	ILQEGVDPKK_8_GFYIYQEGSKNK_9	-0.19	0.06	0.02	-0.07	-0.16		-0.13	0.00000109	-0.19	1.53E-17	-0.19	1.53E-17
PDK2_376_PDK2_376	LPVYNKSAWR_5_LPVYNKSAWR_5	-0.59	0.26	-0.01	-0.18	-0.17	0.13	-0.12	0.00000019	0.06	0.0692	0.06	0.0692
FUMH_260_FUMH_220	IKAAM[147.04]PR_1_SKEFAQVIK_1	-0.05	0.68	-0.24	0.13	-0.24	0.26	-0.11	1.89E-11	-0.04	0.0484	-0.04	0.0484
ECHA_163_ECHB_189	IATKDR_3_M[147.04]MLDLNKAK_6		-0.08	-0.14	0.07	-0.14		-0.11	1.07E-09	-0.19	1.53E-17	-0.27	2.01E-11
ECHA_390_ECHA_436	TLLKDTTVTGLGR_3_DSIFSNLIGQLDYKGFEK_13	-0.05	0.23	-0.27	-0.1	-0.16	0.01	-0.1	4.56E-09	-0.19	1.53E-17	-0.19	1.53E-17
ECHA_289_ECHA_415	TVEEKVK_4_KALTSFER_0	-0.05	0.01	-0.14	-0.07	-0.05	0.25	-0.1	0.000000921	-0.19	1.53E-17	-0.19	1.53E-17
ECHA_163_ECHB_189	IATKDR_3_MMLDLNKAK_6		0.14	-0.17	0	-0.11		-0.1	3.08E-09	-0.19	1.53E-17	-0.27	2.01E-11

ATPO_70_ATPO_172	VGQLLKDPK_5_SFLSPNQILKLEIK_9	-0.07	0.44	-0.28	0.14	-0.21	0.35	-0.1	0.000000435	-0.1	0.000153	-0.1	0.000153
ECHB_191_ECHA_163	AKTLGQR_1_IATKDRK_3	-0.13	-0.1	0.1	-0.22	-0.01	-0.07	-0.09	6.46E-08	-0.27	2.01E-11	-0.19	1.53E-17
ATP5H_78_ATP5H_72	YNALKIPVPEDK_4_ANVAKPGLVDDFEKK_13	0.09	0.53	-0.31	0.11	-0.25	0.12	-0.09	0.000000245	-0.06	0.00312	-0.06	0.00312
ECHA_289_ECHA_644	TVEEKVK_4_GFYIYQEGSKNK_9	-0.11	-0.19	0.1	-0.3	0.18	-0.07	-0.08	4.56E-09	-0.19	1.53E-17	-0.19	1.53E-17
ATPO_54_ATPO_97	KLDQVEK_0_SLNDITKR_6	0.08	0.4	-0.02	0.04	-0.01	0.32	0.07	0.000001555	-0.1	0.000153	-0.1	0.000153
ATPO_90_ATPO_73	VKSLNDITKR_1_VGQLLKDPKVSLAVLNPYIK_8	0.19	0.49	-0.14	0.29	-0.13	0.24	0.08	0.00000017	-0.1	0.000153	-0.1	0.000153
DLDH_277_DLDH_334	LNTKVTGATK_3_RPFTQNLGLEELGIELDPKGR_18	0.08	-0.21	-0.05	0.18	0.1	-0.34	0.09	1.28E-08	-0.27	0.000558	-0.27	0.000558
ATPO_199_AT5F1_225	YVDM[147.04]SAKSK_6_HVVKSISVQQEK_3	0.23	0.58	-0.11	0.08	-0.17	0.16	0.09	0.000000625	-0.1	0.000153	-0.37	0.128
ATPB_522_ATPA_531	ADKLAEEHGS_2_SDGKISEQSDAK_3	0.25	0.66	-0.08	0.25	0	0.19	0.1	0.000000094	-0.23	3.91E-11	-0.06	0.083
ATPO_90_ATPB_124	VKSLNDITKR_1_GQKVLDSGAPIKIPVGPETLGR_2	0.25	0.46	-0.07	0.15	-0.08	0.27	0.1	0.000000435	-0.1	0.000153	-0.23	3.91E-11
CH60_125_CH60_473	SIAKEGFEK_3_ALKIPAMTIAK_2	0.1	0.36	0.19	0.19	0.06	-0.06	0.1	0.0000010 9	0.03	0.186	0.03	0.186
ACON_31_ACON_549	AKVAMSHFEPSEYIR_1_SDFDPGQDTYQHPPKDSSGQR_14	0.1	0.71	-0.1	0.28	-0.16	0.34	0.1	4.56E-09	0.06	0.0151	0.06	0.0151
IDHP_199_IDHP_180	LVFTPKDGSSAK_5_HAHGDQYKATDFVVDR_7	0.07	0.45	-0.13	0.39	-0.18	0.2	0.11	3.18E-14	-0.11	0.00705	-0.11	0.00705
ECHA_411_ECHA_60	GLNDKVK_4_INSPNSKVNTLNK_6	0.12	-0.06	0.25	-0.02	0.35	0	0.11	1.89E-11	-0.19	1.53E-17	-0.19	1.53E-17
ATPO_60_ATPO_162	KLDQVEKELLR_6_TVLKSFLSPNQILK_3	0.35	0.62	-0.01	0.23	-0.08	0.16	0.11	1.89E-11	-0.1	0.000153	-0.1	0.000153
SUCB1_108_SUCB1_143	GKGTFTSGLK_1_LITKQTGEK_3	0.1	0.53	0.01	0.12	0.1	0.28	0.11	1.89E-11	0.07	0.00579	0.07	0.00579
ODP2_457_ODP2_468	KELNK_0_GKISVNDFIIK_1	0.18	0.79	-0.17	0.29	-0.05	0.52	0.12	5.97E-12	0.07	0.027	0.07	0.027
THIL_171_THIL_171	GATPYGGVKLEDLIVK_8_GATPYGGVKLEDLIVK_8	0.18	0.4	0.07	0.08	-0.06	0.09	0.12	1.29E-22	0.19	1.55E-10	0.19	1.55E-10
ATAD3_134_ATAD3_134	AQYQDKLAR_5_AQYQDKLAR_5	0.21	-0.13	0.42	-0.06	0.44	0.07	0.12	0.00000021	-0.19	0.0221	-0.19	0.0221
ECHA_411_ECHA_644	GLNDKVK_4_GFYIYQEGSKNK_9	0.08	-0.43	0.6	-0.31	0.61	-0.08	0.13	2.39E-08	-0.19	1.53E-17	-0.19	1.53E-17

THIL_171_THIL_171	GATPYGGVKLEDLIVK_8_GATPYGGVKLEDLIVKDGLTDVYNK_8	0.23	0.4	0.15	0.13	0.09	0.11	0.13	1.72E-18	0.19	1.55E-10	0.19	1.55E-10
ADT1_147_ADT1_272	LAADVGKGSSQR_6_DEGANAFFKGAWSNVLR_8	0.18	0.32	-0.16	0.36	0.21	0.2	0.14	8.68E-09	0.5	0.000000399	0.5	0.000000399
ATPB_133_AT5F1_225	VLDSGAPIKIPVGPETLGR_8_HVVKSISVQQEKETIAK_3	0.35	0.52	-0.04	0.35	-0.11	0.21	0.14	0.000000625	-0.23	3.91E-11	-0.37	0.128
CH60_473_CH60_133	ALKIPAMTIAK_2_ISKGANPVEIR_2	-0.14	0.58	0.02	0.16	0.14	0.29	0.14	1.07E-09	0.03	0.186	0.03	0.186
ATPO_90_ATPO_84	VKSLNDITK_1_VSLAVLNPYIKR_10	0.14	0.42	-0.24	0.06	-0.19	0.25	0.14	0.000000346	-0.1	0.000153	-0.1	0.000153
ATPA_531_ATPB_519	SDGKISEQSDAK_3_GFQQILAGEYDHLPEQAFYM[147.04]VGPIEEAVAKADK_29		0.66	0.02	0.28	0.01		0.15	0.000000415	-0.06	0.083	-0.23	3.91E-11
ATPA_427_ATPA_531	AMKQVAGTMK_2_SDGKISEQSDAK_3	0.34	0.55	0.06	0.09	0.14	0.04	0.15	8.05E-24	-0.06	0.083	-0.06	0.083
ACS2L_643_ACS2L_389	KIITSR_0_LLLKYGDAWVK_3	0.1	0.36	0.2	0.2	0.15	-0.06	0.15	6.48E-18	0.02	0.348	0.02	0.348
SUCB1_143_SUCB1_116	LITKQTGEK_3_GTFTSGLKGGVK_7	0.2	0.68	0.06	0.18	0.01	0.34	0.15	2.05E-16	0.07	0.00579	0.07	0.00579
MDHM_105_AATM_150	KPGMTR_0_FFKFSR_2	0.07	0.69	0.07	0.21	0.15	0.41	0.16	0.0000012	0.16	3.47E-10	0.13	8.18E-08
IDHP_280_IDHP_166	TDFDKNK_4_LVPGWTKPITIGR_6	0.1	0.66	-0.13	0.46	0.1	0.23	0.16	0.000000139	-0.11	0.00705	-0.11	0.00705
KCRS_344_KCRS_276	FSKILENLR_2_VISMEKGGNMK_5	0.19	-0.05	0.26	0.24	0.26	0.17	0.16	4.55E-19	-0.32	1.46E-10	-0.32	1.46E-10
THIL_260_THIL_63	VDFSKVPK_4_TPIGSFLGSLASQPATKLGTAAIQGAIEK_16	0.14	0.3	0.17	0.29	0.28	0.12	0.16	1.76E-09	0.19	1.55E-10	0.19	1.55E-10
NDUV1_104_NDUV1_81	WSFM[147.04]NKPSDGRPK_5_GPDWILGEMKTSGLR_9	0.09	0.37	0.12	0.24	0.17		0.16	5.02E-24	0.17	0.00168	0.17	0.00168
AATM_58_AATM_73	DTNSKK_4_MNLGVGAYRDDNGKPYVLPSVR_13	0.05	0.72	-0.04	0.23	-0.13	0.41	0.17	1.28E-08	0.13	8.18E-08	0.13	8.18E-08
AATM_150_AATM_296	FFKFSR_2_VGAFTVVCKDAEEAKR_8	0.12	0.68	-0.02	0.17	0.1	0.39	0.17	8.07E-23	0.13	8.18E-08	0.13	8.18E-08
AATM_338_AATM_90	KQWLQEVK_0_KAEAQIAAKNLDKEYLPIGGLAEFCK_8	0.14	0.68	0.02	0.46	-0.02	0.16	0.17	5.97E-12	0.13	8.18E-08	0.13	8.18E-08

IDHP_166_IDHP_299	LVPGWTKPITIGR_6_LIDDMVAQVLKSSGGFVWACK_10	0.28	0.54	0.11	0.36	0.08	0.1	0.17	2.16E-11	-0.11	0.00705	-0.11	0.00705
ACADS_306_ACADS_306	NAFGAPLTKLQNIQFK_8_NAFGAPLTKLQNIQFK_8	0.09	0.71	-0.06	0.49	-0.01	0.29	0.17	1.59E-09	0.17	0.000036	0.17	0.000036
ODP2_461_ODP2_468	ELNKMLEGK_3_GKISVNDFIIK_1	0.33	0.8	-0.28	0.3	-0.04	0.56	0.17	0.00000231	0.07	0.027	0.07	0.027
NDUV1_104_NDUV1_81	WSFMNKPSDGRPK_5_GPDWILGEMKTSGLR_9	0.13	0.4	0.19	0.2	0.19	0.09	0.17	0	0.17	0.00168	0.17	0.00168
NDUV1_104_NDUV1_81	WSFMNKPSDGRPK_5_GPDWILGEM[147.04]KTSGLR_9		0.46	0.14	0.27	0.18	0.14	0.17	4.10E-18	0.17	0.00168	0.17	0.00168
ACOT2_83_ACOT2_274	DEKGALFR_2_GPGIGLLGISKGGELGLAMASFLK_10	0.33	0.31	0.22	0.01	0.21	0.15	0.17	2.84E-10	-0.18	0.0741	-0.18	0.0741
AATM_363_AATM_185	TQLVSNLKK_7_YYDPKTCGFDFSGALEDISK_4	-0.01	0.78	0.02	0.29	0.06	0.58	0.18	0.00000033	0.13	8.18E-08	0.13	8.18E-08
MDHM_185_MDHM_78	ANTFVAELKGLDPAR_8_ANVKGYLGPEQLPDCLK_3	0.07	0.74	0.13	0.24	0.06	0.29	0.18	0.000000029	0.16	3.47E-10	0.16	3.47E-10
ACADV_65_ACADV_279	EKPAR_1_EKITAFVVER_1	0.04	-0.21	0.59	-0.14	0.6	0.14	0.18	4.23E-08	0.03	0.244	0.03	0.244
ATPG_39_ATPA_434	SIKNIQK_2_QVAGTMKLELAQYR_6	0.22	0.44	0.06	0.2	0.17	0.16	0.18	2.44E-12	-0.29	4.81E-11	-0.06	0.083
KCRS_344_KCRS_276	FSKILENLR_2_VISMEKGGNMKR_5	0.11	-0.18	0.32	0.12	0.34	0.31	0.18	3.33E-11	-0.32	1.46E-10	-0.32	1.46E-10
SUCB1_143_SUCA_308	LITKQTGEK_3_MGHAGAIIAGGKGGAK_11	0.21	0.63	0.15	0.09	0.3	-0.1	0.18	6.33E-09	0.07	0.00579	-0.08	0.0262
MDHM_301_MDHM_296	GLEKNLGIGK_3_ETECTYFSTPLLLGKK_14	0.15	0.92	0.07	0.25	0.14		0.19	6.12E-11	0.16	3.47E-10	0.16	3.47E-10
MDHM_239_MDHM_314	IQEAGTEVVKAK_9_ITPFEEKMIAEAIPELK_6	0.28	0.76	-0.12	0.2	-0.11	0.36	0.19	2.41E-17	0.16	3.47E-10	0.16	3.47E-10
MDHM_307_MDHM_185	NLGIGKITPFEEK_5_ANTFVAELKGLDPAR_8	0.32	0.68	0	0.24	0.02	0.34	0.19	1.25E-24	0.16	3.47E-10	0.16	3.47E-10
ADT1_96_ADT1_92	YKQIFLGGVDR_1_YFPTQALNFAFKDK_11	-0.04	-0.42	0.33	0.25	0.27	0.11	0.19	1.73E-08	0.5	0.000000399	0.5	0.000000399
THIL_265_THIL_63	LKTVFQK_1_TPIGSFLGSLASQPATKLGTAAIQGAIEK_16	0.39	0.46	0.14	0.22	0.2	0.24	0.19	8.05E-18	0.19	1.55E-10	0.19	1.55E-10
ACON_605_ACON_628	CTTDHISAAGPWLKFR_13_GHLDNISNNLLIGAINIENGKANSVR_20	-0.12	0.07	0.2	0.31	0.23	-0.11	0.19	2.41E-17	0.06	0.0151	0.06	0.0151

ES1_114_ES1_201	GKITSLAQLNAANHDAAIFPGGFGAAK_1_GVEVTVGHEQEEGGKWPYAGTAEAIK_14	0.34	0.8	-0.08	0.19	0.02	0.26	0.19	9.95E-09	0.01	0.422	0.01	0.422
ACOT2_83_ACOT2_274	SALRDEKGALFR_6_GPGIGLLGISKGGELGLAMASFLK_10		0.36	0.15	0.24	0.18	-1.33	0.19	3.20E-22	-0.18	0.0741	-0.18	0.0741
SUCB1_116_SUCB1_139	GTFTSGLKGGVK_7_AVSSQMIGQKLITK_9	0.34	0.76	0.16	-0.06	0.1	0.41	0.19	0.00000088	0.07	0.00579	0.07	0.00579
SUCB1_143_SUCB1_98	LITKQTGEK_3_DVVIKAQVLAGGR_4	0.18	0.69	0.08	0.17	-0.01	0.4	0.19	9.86E-11	0.07	0.00579	0.07	0.00579
SUCB1_143_SUCB1_120	LITKQTGEK_3_GGVKIVFSPEEAK_3	0.24	0.85	0.09	0.1	0.02	0.36	0.19	2.22E-11	0.07	0.00579	0.07	0.00579
AATM_82_AATM_107	KAEAQIAAK_0_NLDKEYLPIGGLAEFCKASAELALGENNEVLK_16	0.12	0.61	0.05	0.21	0.21	0.11	0.2	5.81E-08	0.13	8.18E-08	0.13	8.18E-08
KCRS_344_KCRS_408	FSKILENLR_2_GQDIKVPPPLPQFGRK_4	0.49	-0.04	0.35	0.15	0.35	0.31	0.2	7.25E-27	-0.32	1.46E-10	-0.32	1.46E-10
ODPA_321_ODPA_77	SDPIMLLKDR_7_MELKADQLYK_3	0.24	0.62	-0.13	0.17	-0.11	0.31	0.21	5.63E-17	0.04	0.214	0.04	0.214
ACADV_279_ACADV_557	EKITAFVVER_1_KGIVNEQFLLQR_0	0.11	-0.21	0.67	-0.13	0.76	0.07	0.21	5.63E-17	0.03	0.244	0.03	0.244
CH60_473_CH60_133	ALKIPAM[147.04]TIAK_2_ISKGANPVEIR_2	0.16	0.91	-0.01	0.26	0.2	0.29	0.21	2.26E-15	0.03	0.186	0.03	0.186
ATPA_427_ATPA_531	AM[147.04]KQVAGTMK_2_SDGKISEQSDAK_3	0.4	0.63	0.15	0.13	0.2	0.17	0.21	3.36E-44	-0.06	0.083	-0.06	0.083
ECHA_411_ECHA_505	GLNDKVK_4_VIGMHYFSPVDKMQLLEIITTDK_11	0.12	-0.41	0.6	-0.1	0.56	-0.22	0.21	1.59E-09	-0.19	1.53E-17	-0.19	1.53E-17
CISY_393_CISY_76	IVPNILLEQGKAK_10_GMKGLVYETSVLDPDEGIR_2	0.32	0.67	0.17	0.26	0.2	0.2	0.21	1.25E-24	0.05	0.0703	0.05	0.0703
SUCB1_93_SUCB1_88	LGSKDVVIK_3_SSDEAYAIAKK_9	0.32	0.53	0.27	0.03	0.27	0.16	0.21	3.08E-20	0.07	0.00579	0.07	0.00579
MDHM_239_MDHM_78	IQEAGTEVVKAK_9_ANVKGYLGPEQLPDCLK_3	1.31	0.9	0.05	0.23	0.09	-1.22	0.22	6.59E-13	0.16	3.47E-10	0.16	3.47E-10
IDHP_199_IDHP_106	LVFTPKDGSSAK_5_YFDLGLPNRDQTNDQVTIDSALATQKYSVAVK_25	0.25	0.76	0.1	0.4	0.02	0.24	0.22	1.93E-12	-0.11	0.00705	-0.11	0.00705
ATPA_531_ATPA_531	SDGKISEQSDAK_3_SDGKISEQSDAK_3		0.74	0.14	0.19	0.16	0.25	0.22	3.98E-08	-0.06	0.083	-0.06	0.083

THIL_171_THIL_187	GATPYGGVKLEDLIVK_8_DGLTDVYNKIHMGNCAENTAK_8	0.28	0.31	0.19	0.26	0.29	0.18	0.22	1.10E-27	0.19	1.55E-10	0.19	1.55E-10
TIM44_119_TIM44_121	TSEAIKK_5_KLGELTGTVK_0	0.19	1.02	-0.07	0.17	0.05	0.64	0.23	0.000000688	0.38	0.0314	0.38	0.0314
AATM_404_AATM_159	EFSVYMTKDGR_7_DVFLPKPSWGNHTPIFR_5	0.32	0.77	0.1	0.32	0.11	0.39	0.23	0	0.13	8.18E-08	0.13	8.18E-08
AATM_404_AATM_159	EFSVYM[147.04]TKDGR_7_DVFLPKPSWGNHTPIFR_5	0.26	0.75	0.11	0.34	0.11	0.37	0.23	5.55E-40	0.13	8.18E-08	0.13	8.18E-08
ACSL1_552_ACSL1_573	WLPNGTLKIIDR_7_LAQGEYIAPEKIENIYLR_10		-0.17	0.75	0.09	1.14	0.31	0.23	0.000000778	-0.15	0.0033	-0.15	0.0033
ACADM_212_ACADM_271	SNPDPKVPASK_5_ENVLIGEGAGFKIAMGAFDR_11	0.41	-0.12	0.78	0.07	0.7	0.05	0.23	2.63E-15	-0.23	0.0000215	-0.23	0.0000215
ACADV_483_ACADV_557	GKELTGLGNALK_1_KGIVNEQFLLQR_0	0.19	-0.19	0.55	-0.07	0.66	0.06	0.23	3.96E-10	0.03	0.244	0.03	0.244
IDHP_166_IDHP_299	LVPGWTKPITIGR_6_LIDDM[147.04]VAQVLKSSGGFVWACK_10	0.2	0.75	0.23	0.27	0.22	0.14	0.23	5.71E-18	-0.11	0.00705	-0.11	0.00705
ATPO_90_ATPB_124	VKSLNDITK_1_GQKVLDSGAPIK_2	0.55	0.6	0.05	0.13	0.1	0.54	0.23	4.87E-08	-0.1	0.000153	-0.23	3.91E-11
ATPA_427_ATPA_531	AMKQVAGTM[147.04]K_2_SDGKISEQSDAK_3	0.44	0.66	0.12	0.19	0.2	0.12	0.23	2.07E-32	-0.06	0.083	-0.06	0.083
SUCB1_108_SUCA_308	GKGTFTSGLK_1_MGHAGAIIAGGKGGAK_11	0.06	0.41	0.25	0.16	0.46		0.23	3.55E-10	0.07	0.00579	-0.08	0.0262
AATM_82_AATM_73	KAEAQIAAK_0_DDNGKPYVLPSVR_4	0.28	0.86	0.06	0.27	0.23	0.33	0.24	1.72E-14	0.13	8.18E-08	0.13	8.18E-08
MDHM_329_MDHM_239	KGEDFVK_0_IQEAGTEVVKAK_9	0.4	1.04	0	0.24	0.09	0.56	0.24	5.43E-41	0.16	3.47E-10	0.16	3.47E-10
IDHP_282_IDHP_299	TDFDKNKIWYEHR_6_LIDDMVAQVLKSSGGFVWACK_10	0.39	0.59	0.22	0.52	0.13	0.14	0.24	6.71E-16	-0.11	0.00705	-0.11	0.00705
CH60_75_CH60_292	VTKDGVTVAK_2_LKVGLQVVAVK_1	0.26	0.07	0.52	0.1	0.55	-0.21	0.24	4.54E-08	0.03	0.186	0.03	0.186
ATPA_427_ATPA_531	AM[147.04]KQVAGTM[147.04]K_2_SDGKISEQSDAK_3	0.52	0.75	0.13	0.17	0.17	0.21	0.24	0	-0.06	0.083	-0.06	0.083
ACON_144_ACON_138	AKDINQEVYNFLATAGAK_1_VAVPSTIHCDHLIEAQVGGEKDLR_20	0.36	0.69	0.06	0.31	0.16	0.51	0.24	6.02E-14	0.06	0.0151	0.06	0.0151

DLDH_430_DLDH_132	AKTNADTDGM[147.04]VK_1_HSAVKALTGGIAHLFK_4	0.3	0.61	0.17	0.39	0.15	0.31	0.25	3.78E-30	-0.27	0.000558	-0.27	0.000558
AATM_302_AATM_396	DAEEAKR_5_LTKEFSVYMTK_2	0.19	0.8	0.11	0.29	0.09	0.32	0.25	3.78E-30	0.13	8.18E-08	0.13	8.18E-08
AATM_58_AATM_73	DTNSKK_4_DDNGKPYVLPSVR_4		0.68	-0.09	0.2	0.12	0.39	0.25	6.38E-09	0.13	8.18E-08	0.13	8.18E-08
AATM_58_AATM_396	DTNSKK_4_LTKEFSVYMTK_2	-1.01	-0.81	0.08	-0.99	0.08	1.44	0.25	1.27E-21	0.13	8.18E-08	0.13	8.18E-08
AATM_82_AATM_338	KAEAQIAAK_0_KQWLQEVK_0	0.25	0.77	0.15	0.11	0.15	0.41	0.25	0	0.13	8.18E-08	0.13	8.18E-08
ACADV_279_ACADV_483	EKITAFVVER_1_GKELTGLGNALK_1	0.17	-0.16	0.71	-0.14	0.81	0.13	0.25	5.12E-22	0.03	0.244	0.03	0.244
IDHP_199_IDHP_133	LVFTPKDGSSAK_5_KMWKSPNGTIR_3	0.16	0.71	0.08	0.29	0.32		0.25	1.90E-18	-0.11	0.00705	-0.11	0.00705
IDHP_256_IDHP_180	NTILKAYDGR_4_HAHGDQYKATDFVVDR_7	0.18	0.67	-0.02	0.46	0.19	0.38	0.25	1.76E-09	-0.11	0.00705	-0.11	0.00705
ACADS_306_ACADS_208	NAFGAPLTKLQNIQFK_8_SRQNKGISAFLVPMPTPGLTLGK_4	-0.01	0.62	0.18	0.32	0.25	0.44	0.25	4.57E-20	0.17	0.000036	0.17	0.000036
DLDH_420_DLDH_430	IGKFPFAANSR_2_AKTNADTDGM[147.04]VK_1	0.32	0.77	-0.03	0.53	0.2	0.13	0.26	3.35E-14	-0.27	0.000558	-0.27	0.000558
AATM_58_AATM_396	DTNSKK_4_LTKEFSVYM[147.04]TK_2	0.46	1.05	-0.08	0.4	0.05	0.22	0.26	2.83E-11	0.13	8.18E-08	0.13	8.18E-08
MDHM_105_MDHM_239	KPGMTR_0_IQEAGTEVVKAK_9	0.19	0.88	0.18	0.33	0.19		0.26	5.12E-22	0.16	3.47E-10	0.16	3.47E-10
CH60_130_CH60_473	EGFEKISK_4_ALKIPAM[147.04]TIAK_2		0.82	0.14	0.4	0.32	0.01	0.26	2.67E-28	0.03	0.186	0.03	0.186
ECHA_411_ECHA_505	GLNDKVK_4_VIGM[147.04]HYFSPVDKMQLLEIITTDK_11		-0.47	0.58	-0.26	0.58		0.26	2.31E-09	-0.19	1.53E-17	-0.19	1.53E-17
THIL_171_THIL_187	GATPYGGVKLEDLIVK_8_DGLTDVYNKIHM[147.04]GNCAENTAK_8	0.16	0.55	0.2	0.3	0.32	0.25	0.26	1.25E-24	0.19	1.55E-10	0.19	1.55E-10
CISY_49_CISY_450	IKTFK_1_ALGFPLERPKSMSTDGLM[147.04]K_9	0.16	0.56	0.28	0.31	0.21	0.33	0.26	1.56E-29	0.05	0.0703	0.05	0.0703
CISY_393_CISY_450	IVPNILLEQGKAK_10_ALGFPLERPKSMSTDGLMK_9		0.87	0.22	0.36	0.22		0.26	1.08E-14	0.05	0.0703	0.05	0.0703
ODO2_273_ODO2_278	DAFLKK_4_HNLKLGFMSAFVK_3	0.25	0.89	0.13	0.29	0.14	0.39	0.26	0	-0.6	0.0000161	-0.6	0.0000161

PDK2_376_PDK2_18	LPVYNKSAWR_5_NASLAGAPKYIEHFSK_8	0.06		0.39	-0.16	0.2		0.26	2.58E-08	0.06	0.0692	0.06	0.0692
SUCB1_88_SUCB1_129	SSDEAYAIAKK_9_IVFSPEEAKAVSSQMIGQK_8		0.52	0.26	0.24	0.2	0.25	0.26	4.34E-17	0.07	0.00579	0.07	0.00579
DLDH_66_DLDH_143	SAQLGFKTVCIEK_6_ALTGGIAHLFKQNK_10	0.17	0.85	0.29	0.24	0.41	0.23	0.27	8.63E-19	-0.27	0.000558	-0.27	0.000558
CH60_130_CH60_473	EGFEKISK_4_ALKIPAMTIAK_2	0.03	0.62	0.18	0.28	0.38	0.2	0.27	2.01E-26	0.03	0.186	0.03	0.186
ATPA_531_ATPA_434	SDGKISEQSDAK_3_QVAGTMKLELAQYR_6	0.45	0.34	0.26	0.23	0.36	0.24	0.27	0	-0.06	0.083	-0.06	0.083
AATM_58_AATM_364	DTNSKK_4_KEGSSHNWQHITDQIGMFCFTGLKPEQVER_0	0.26	0.55	0.21	0.34	0.24		0.28	6.64E-13	0.13	8.18E-08	0.13	8.18E-08
MDHM_329_MDHM_324	KGEDFVK_0_MIAEAIPELKASIK_9	0.15	0.82	0	0.18	-0.03	0.45	0.28	1.19E-19	0.16	3.47E-10	0.16	3.47E-10
MDHM_105_MDHM_239	KPGM[147.04]TR_0_IQEAGTEVVKAK_9	0.43	0.86	0.11	0.27	0.26	0.35	0.28	2.19E-40	0.16	3.47E-10	0.16	3.47E-10
ATPA_531_ATPA_434	SDGKISEQSDAK_3_QVAGTM[147.04]KLELAQYR_6	0.54	0.47	0.23	0.23	0.31	0.21	0.28	0	-0.06	0.083	-0.06	0.083
ATAD3_362_ATAD3_490	TLFAKK_4_MYFDKYVLKPATEGK_4	0.54		0.11	0.49	0.47		0.28	9.67E-08	-0.19	0.0221	-0.19	0.0221
ACDSB_324_ACDSB_426	MQFGKR_4_IGTIYEGASNIQLNTIAKHIDAEY_17	0.23	0.47	0.27	0.4	0.34	0.3	0.28	1.52E-11	0.29	0.00000876	0.29	0.00000876
DLDH_430_DLDH_132	AKTNADTDGMVK_1_HSAVKALTGGIAHLFK_4	0.33	0.54	0.2	0.47	0.2	0.2	0.29	0	-0.27	0.000558	-0.27	0.000558
AATM_396_AATM_302	LTKEFSVYM[147.04]TK_2_DAEEAKRVESQLK_5	0.3	0.87	0.02	0.41	0.05	0.31	0.29	1.25E-24	0.13	8.18E-08	0.13	8.18E-08
IDHP_133_IDHP_199	M[147.04]WKSPNGTIR_2_LVFTPKDGSSAK_5	0.42	0.48	0.19	0.39	0.32		0.29	4.08E-25	-0.11	0.00705	-0.11	0.00705
CISY_49_CISY_450	IKTFK_1_ALGFPLERPKSMSTDGLMK_9	0.13	0.68	0.29	0.49	0.14	0.24	0.29	3.11E-33	0.05	0.0703	0.05	0.0703
CISY_49_CISY_450	IKTFK_1_ALGFPLERPKSM[147.04]STDGLMK_9		0.51	0.31	0.32	0.26		0.29	3.31E-16	0.05	0.0703	0.05	0.0703
DLDH_420_DLDH_430	IGKFPFAANSR_2_AKTNADTDGMVK_1	0.2	0.7	0	0.55	0.16	0.32	0.3	8.07E-23	-0.27	0.000558	-0.27	0.000558
AATM_396_AATM_302	LTKEFSVYMTK_2_DAEEAKRVESQLK_5	0.27	0.86	0	0.38	0.11	0.34	0.3	8.05E-24	0.13	8.18E-08	0.13	8.18E-08
CISY_393_CISY_76	IVPNILLEQGKAK_10_GM[147.04]KGLVYETSVLDPDEGIR_2	-1.04	-0.66	1.41	0.36	0.24	1.63	0.3	0	0.05	0.0703	0.05	0.0703
AATM_150_AATM_234	FFKFSR_2_EIASVVKK_6	0.5	0.62	0.13	0.2	0.23	0.56	0.31	1.39E-22	0.13	8.18E-08	0.13	8.18E-08

MDHM_329_MDHM_324	KGEDFVK_0_M[147.04]IAEAIPELKASIK_9		0.93	0.04	0.13		0.4	0.31	1.95E-08	0.16	3.47E-10	0.16	3.47E-10
HXK1_833_HXK1_133	GQISEPLKTR_7_SIPDGSEKGDFIALDLGGSSFR_7	0.7	0.33	0.14	0.82	0.38	-0.18	0.31	0.00000053	0.48	0.0000163	0.48	0.0000163
IDHP_299_IDHP_413	LIDDM[147.04]VAQVLKSSGGFVWACK_10_VCVQTVESGAMTKDLAGCIHGLSNVK_12		0.04	0.71	0.08	0.46	-1.04	0.31	9.55E-09	-0.11	0.00705	-0.11	0.00705
ACADS_306_ACADS_262	NAFGAPLTKLQNIQFK_8_ENLLGEPGMGFKIAM[147.04]QTLDMGR_11		0.56	0.15	0.61	0.28	0.28	0.31	9.13E-29	0.17	0.000036	0.17	0.000036
THIL_242_THIL_260	GKPDVVVK_1_VDFSKVPK_4	0.36	0.18	0.75	0.04	0.61		0.31	1.55E-10	0.19	1.55E-10	0.19	1.55E-10
SCOT1_271_SCOT1_214	LIKGEK_2_AWKADR_2	0.22	1.56	0.21	0.57	0.35		0.31	5.29E-10	0.87	6.27E-28	0.87	6.27E-28
AIFM1_243_AIFM1_592	GNMVKLNDGSQITFEK_4_IIKDGEQHEDLNEVAK_2	0.5	-0.3	0.69	0.06	0.73	0.45	0.31	1.07E-08	-0.33	0.0000303	-0.33	0.0000303
AATM_150_AATM_234	FFKFSR_2_EIASVVKKK_6	0.53	0.73	0.18	0.24	0.22	0.22	0.32	2.47E-37	0.13	8.18E-08	0.13	8.18E-08
CPT2_453_CPT2_544	GGKEFLK_2_YHGQLTKEAAMGQGFDR_6	0.13	0.35	0.38	0.35	0.37		0.32	2.26E-39	-0.37	0.000727	-0.37	0.000727
IDHP_133_IDHP_199	MWKSPNGTIR_2_LVFTPKDGSSAK_5	0.23	0.72	0.13	0.46	0.35	0.31	0.32	0	-0.11	0.00705	-0.11	0.00705
ATPA_531_ATPA_427	SDGKISEQSDAK_3_AMKQVAGTM[147.04]KLELAQYR_2		0.73	0.26	0.29	0.26		0.32	1.72E-11	-0.06	0.083	-0.06	0.083
ACADS_306_ACADS_262	NAFGAPLTKLQNIQFK_8_ENLLGEPGMGFKIAMQTLDM[147.04]GR_11	0.34	0.76	0.28	0.44	0.35	0.17	0.32	0	0.17	0.000036	0.17	0.000036
ACDSB_284_ACDSB_426	IGHGYKYAIGSLNEGR_5_IGTIYEGASNIQLNTIAKHIDAEY_17	0.04	0.33	0.33	0.49	0.43	0.36	0.32	1.73E-21	0.29	0.00000876	0.29	0.00000876
SUCA_90_SUCA_66	LVGGTTPGKGGQK_8_IICQGFTGKQGTFHSQQALEYGTK_8	0.35	0.45	0.63	0.12	0.35	0.22	0.33	0	-0.08	0.0262	-0.08	0.0262
AATM_302_AATM_396	DAEEAKR_5_LTKEFSVYM[147.04]TK_2	0.28	0.78	0.04	0.18	0.1	0.35	0.34	2.23E-18	0.13	8.18E-08	0.13	8.18E-08
AATM_150_AATM_235	FFKFSR_2_EIASVVKKK_7	0.44	0.68	0.33	0.22	0.2	0.57	0.34	5.66E-18	0.13	8.18E-08	0.13	8.18E-08
MDHM_105_MDHM_105	KPGMTR_0_KPGMTR_0	0.32	0.22	0.48	0.17	0.26	0.34	0.34	3.47E-22	0.16	3.47E-10	0.16	3.47E-10

ACADV_277_ACADV_483	DAATGAVKEK_7_GKELTGLGNALK_1	0.23	-0.3	1.06	-0.17	1.06	0.16	0.34	3.9E-11	0.03	0.244	0.03	0.244
MDHM_105_MDHM_105	KPGM[147.04]TR_0_KPGMTR_0	0.45	0.59	0.43	0.18	0.37	0.16	0.35	0	0.16	3.47E-10	0.16	3.47E-10
ACADS_306_ACADS_262	NAFGAPLTKLQNIQFK_8_ENLLGEPGMGFKIAMQTLDMGR_11	0.35	0.64	0.31	0.5	0.35	0.33	0.35	0	0.17	0.000036	0.17	0.000036
ACADS_306_ACADS_262	NAFGAPLTKLQNIQFK_8_ENLLGEPGM[147.04]GFKIAMQTLDMGR_11	0.47	0.68	0.28	0.45	0.35	0.34	0.35	0	0.17	0.000036	0.17	0.000036
THIL_242_THIL_171	GKPDVVVKEDEEYK_1_GATPYGGVKLEDLIVK_8	0.52	0.33	0.48	0.24	0.41	0.32	0.35	1.98E-28	0.19	1.55E-10	0.19	1.55E-10
ADT1_96_ADT2_23	DKYKQIFLGGVDR_3_MTDAAVSFAKDFLAGGVAAAISKTAVAPIER_22	1.08	0.22	1.16	0.3	0.71	0.65	0.36	1.44E-09	0.5	0.000000399	0.62	0.00000137
IDHP_166_IDHP_400	LVPGWTKPITIGR_6_FAQTLEKVCVQTVESGAMTK_6	0.23	0.41	0.18	0.58	0.43	0.19	0.36	1.21E-37	-0.11	0.00705	-0.11	0.00705
ACADS_306_ACADS_262	NAFGAPLTKLQNIQFK_8_ENLLGEPGM[147.04]GFKIAMQTLDM[147.04]GR_11	0.33	0.81	0.27	0.5	0.37	0.36	0.36	0	0.17	0.000036	0.17	0.000036
THIL_265_THIL_260	LKTVFQK_1_VDFSKVPK_4	0.41	0.26	0.63	0.1	0.64	0.31	0.36	0	0.19	1.55E-10	0.19	1.55E-10
NDUS1_87_NDUV1_104	APKVVAACAMPVM[147.04]K_2_WSFMNKPSDGRPK_5		0.57	0.32	0.36	0.48		0.36	4.49E-14	0.04	0.386	0.17	0.00168
HINT2_128_HINT2_45	IAQAQGLKDGYR_7_AQKAAPGGASPTIFSR_2	0.5	0.89	0.22	0.34	-0.02	0.23	0.36	3.08E-14	-0.19	0.198	-0.19	0.198
DLDH_430_DLDH_143	AKTNADTDGMVK_1_ALTGGIAHLFKQNK_10	0.4	-0.02	0.32	0.48	0.34	-0.36	0.37	0	-0.27	0.000558	-0.27	0.000558
ODPA_83_ODPA_321	ADQLYKQK_5_SDPIMLLKDR_7	0.14	0.9	0.16	0.48	0.18	0.45	0.37	7E-12	0.04	0.214	0.04	0.214
ACADV_279_ACADV_483	EKITAFVVER_1_LFVALQGCMDKGKELTGLGNALK_12		-0.09	0.62	-0.05	0.66	0.11	0.37	0.000000862	0.03	0.244	0.03	0.244
ACADS_306_ACADS_262	NAFGAPLTKLQNIQFK_8_IPKENLLGEPGMGFKIAMQTLDMGR_14	0.36	0.53	0.52	0.49	0.45	0.26	0.37	1.71E-12	0.17	0.000036	0.17	0.000036
EFTU_88_EFTU_91	ILAEGGGAKFK_8_KYEEIDNAPEER_0	0.45	0.99	0.06	0.46	0.11	0.45	0.37	2.67E-28	0.35	1.09E-08	0.35	1.09E-08
THIL_260_THIL_171	VDFSKVPK_4_GATPYGGVKLEDLIVKDGLTDVYNK_8	0.33	0.23	0.68	0.13	0.62	0.33	0.37	1.35E-41	0.19	1.55E-10	0.19	1.55E-10

SUCA_94_SUCA_66	GGQKHLGLPVFNTVK_3_IICQGFTGKQGTFHSQQALEYGTK_8	0.54	0.45	0.45	0.28	0.37	0.04	0.37	3.05E-33	-0.08	0.0262	-0.08	0.0262
IDHP_166_IDHP_400	LVPGWTKPITIGR_6_FAQTLEKVCVQTVESGAM[147.04]TK_6	0.27	0.69	0.26	0.53	0.46	0.12	0.38	6.55E-41	-0.11	0.00705	-0.11	0.00705
THIL_171_THIL_242	GATPYGGVKLEDLIVK_8_GKPDVVVKEDEEYKR_1		0.26	0.57	0.19	0.65	0	0.38	4.34E-24	0.19	1.55E-10	0.19	1.55E-10
THIL_242_THIL_171	GKPDVVVK_1_GATPYGGVKLEDLIVK_8	0.5	0.48	0.58	0.14	0.61	0.23	0.38	1.13E-21	0.19	1.55E-10	0.19	1.55E-10
THIL_265_THIL_260	LKTVFQK_1_RVDFSKVPK_5	0.38	0.22	0.68	0.13	0.69	0.24	0.38	1.54E-37	0.19	1.55E-10	0.19	1.55E-10
THIL_260_THIL_171	RVDFSKVPK_5_GATPYGGVKLEDLIVKDGLTDVYNK_8		0.31	0.64	0.21	0.64	0.17	0.38	7.64E-08	0.19	1.55E-10	0.19	1.55E-10
ACADM_212_ACADM_271	SNPDPKVPASK_5_ENVLIGEGAGFKIAM[147.04]GAFDR_11		0.09	0.9	0.17	0.87	0	0.39	2.51E-10	-0.23	0.0000215	-0.23	0.0000215
CH60_130_CH60_481	EGFEKISK_4_IPAMTIAKNAGVEGSLIVEK_7		0.62	0.35	0.32	0.62		0.39	2.41E-12	0.03	0.186	0.03	0.186
IDH3A_343_IDHG1_226	SLTKDLGGNAK_3_ANIMKLGDGLFLQCCR_4	1.33	1.02	0.6	0.43	0.34		0.39	7.18E-10	-0.04	0.252	-0.02	0.167
VDAC1_128_VDAC1_122	IKTGYK_1_LTFDSSFSPNTGKK_12	0.22	-0.1	0.9	0.36	1.16	0.06	0.39	1.74E-12	-0.2	0.0611	-0.2	0.0611
THIL_260_THIL_171	VDFSKVPK_4_GATPYGGVKLEDLIVK_8	0.39	0.39	0.6	0.21	0.59	0.23	0.39	0	0.19	1.55E-10	0.19	1.55E-10
THIL_260_THIL_242	VDFSKVPK_4_GKPDVVVKEDEEYK_1		0.18	0.66	0.12	0.48		0.39	1.09E-13	0.19	1.55E-10	0.19	1.55E-10
MDHM_105_MDHM_105	KPGM[147.04]TR_0_KPGM[147.04]TR_0	0.47	0.6	0.45	0.23	0.46	0.29	0.4	0	0.16	3.47E-10	0.16	3.47E-10
MIC60_269_MIC60_281	KSAQWR_0_TVEGALKER_6	0.38	-0.2	0.83	-0.03	0.91	0.45	0.4	7.54E-26	0.08	0.0825	0.08	0.0825
THIL_242_THIL_265	GKPDVVVK_1_LKTVFQK_1	0.41	0.1	0.92	0.04	0.89	0.28	0.4	7.3E-15	0.19	1.55E-10	0.19	1.55E-10
THIL_260_THIL_187	VDFSKVPK_4_DGLTDVYNKIHMGNCAENTAK_8		0.24	0.51	0.38	0.47		0.4	8.99E-10	0.19	1.55E-10	0.19	1.55E-10
PPIF_85_PPIF_72	ALCTGEKGFGYK_6_ADVVPKTAENFR_5	0.57	0.99	0.16	0.47	0.21	0.55	0.4	2.09E-42	0.53	0.000000391	0.53	0.000000391
ACO13_17_ACO13_17	VMFKVPGFDR_3_VMFKVPGFDR_3	0.09	1.13	0.23	0.51	0.3	0.58	0.4	1.75E-14	0.4	0.00000114	0.4	0.00000114

HXK1_819_HXK1_833	NILIDFTKK_7_GQISEPLKTR_7	0.57	0.3	0.49	0.44	0.55	0.22	0.41	0	0.48	0.0000163	0.48	0.0000163
IDHP_299_IDHP_413	LIDDMVAQVLKSSGGFVWACK_10_VCVQTVESGAM[147.04]TKDLAGCIHGLSNVK_12	0.48	0.81	0.64	0.19	0.6	0.17	0.41	1.19E-15	-0.11	0.00705	-0.11	0.00705
THIL_171_THIL_240	GATPYGGVKLEDLIVK_8_FASEITPITISVKGKPDVVVKEDEEYK_12		0.32	0.54	0.31	0.49		0.41	3.31E-10	0.19	1.55E-10	0.19	1.55E-10
THIL_265_THIL_171	LKTVFQK_1_GATPYGGVKLEDLIVKDGLTDVYNK_8	0.35	0.15	0.59	0.24	0.72	0.3	0.41	2.10E-43	0.19	1.55E-10	0.19	1.55E-10
THIL_260_THIL_242	VDFSKVPK_4_GKPDVVVKEDEEYKR_1	0.96	0.13	0.62	0.26	0.59		0.41	2.62E-09	0.19	1.55E-10	0.19	1.55E-10
NDUV1_81_NDUS1_98	GPDWILGEMKTSGLR_9_VVAACAM[147.04]PVM[147.04]KGWNILTNSEK_10		0.2	0.06	0.56	0.24		0.41	0.000000399	0.17	0.00168	0.04	0.386
NDUS1_84_NDUV1_81	MCLVEIEKAPK_7_GPDWILGEMKTSGLR_9	0.25	0.41	0.48	0.37	0.54	-0.15	0.41	0	0.04	0.386	0.17	0.00168
ACO13_127_ACO13_111	TTGKLIAQGR_3_QGKTLAFASVDLTNK_2	1.02	1.82	0.39	0.36	0.48		0.41	0.000000428	0.4	0.00000114	0.4	0.00000114
ACO13_17_ACO13_27	VMFKVPGFDR_3_VLEKVTLVSAAPEK_3	0.59	0.98	0.17	0.5	0.45	0.43	0.41	1.89E-13	0.4	0.00000114	0.4	0.00000114
ACADV_277_ACADV_557	DAATGAVKEK_7_KGIVNEQFLLQR_0	0.33	-0.34	1.18	-0.11	1.17	0.11	0.42	1.97E-12	0.03	0.244	0.03	0.244
ACAD9_457_ACAD9_298	IKELK_1_VPVENVLGEVGGGFKVAMNILNSGR_14		0.4	1.07	0.55	1.02	0.24	0.42	6.17E-09	0.52	0.00000089	0.52	0.00000089
THIL_265_THIL_171	LKTVFQK_1_GATPYGGVKLEDLIVK_8	0.46	0.39	0.59	0.23	0.65	0.24	0.42	0	0.19	1.55E-10	0.19	1.55E-10
ACON_689_ACON_591	AIITKSFAR_4_GKCTTDHISAAGPWLK_1	0.48	0.56	0.58	0.28	0.58	0.15	0.42	1.25E-39	0.06	0.0151	0.06	0.0151
DLDH_430_DLDH_143	AKTNADTDGM[147.04]VK_1_ALTGGIAHLFKQNK_10	0.54	0.69	0.29	0.52	0.34	0.39	0.43	0	-0.27	0.000558	-0.27	0.000558
ACADV_277_ACADV_557	TPIKDAATGAVKEK_11_KGIVNEQFLLQR_0	0.68	-0.35	0.97	-0.03	1.05		0.43	1.53E-17	0.03	0.244	0.03	0.244
IDHP_384_IDHP_400	GKLDGNQDLIR_1_FAQTLEKVCVQTVESGAMTK_6	0.23	0.82	0.03	0.71	0.28	0.33	0.43	0.000000736	-0.11	0.00705	-0.11	0.00705
ODO1_640_ODO1_532	ILKTR_2_KQKPVLQK_0	0.62	0.78	0.33	0.51	0.34	0.71	0.43	5.14E-26	0.32	0.000036	0.32	0.000036

ODO1_640_ODO1_619	ILKTR_2_SMTCPSTGLEEDVLFHIGKVASSVPVENFTIHGGLSR_18	0.45	0.72	0.36	0.46	0.41	0.58	0.43	0.000000697	0.32	0.000036	0.32	0.000036
NDUS1_84_NDUV1_104	MCLVEIEKAPK_7_WSFMNKPSDGRPK_5	0.12	0.47	0.52	0.26	0.61		0.43	0	0.04	0.386	0.17	0.00168
IDHP_299_IDHP_413	LIDDM[147.04]VAQVLKSSGGFVWACK_10_VCVQTVESGAM[147.04]TKDLAGCIHGLSNVK_12		-0.01	0.66	0.28	0.55		0.44	9.90E-17	-0.11	0.00705	-0.11	0.00705
NDUS1_87_NDUV1_81	APKVVAACAMPVMK_2_GPDWILGEMKTSGLR_9	0.33	0.37	0.62	0.29	0.66	-0.07	0.44	0	0.04	0.386	0.17	0.00168
CISY_103_CISY_382	GYSIPECQKMLPK_8_LVAQLYKIVPNILLEQGK_6	0.17	0.88	-0.08	0.35	0.02	0.23	0.44	0.000000451	0.05	0.0703	0.05	0.0703
AATM_302_AATM_404	DAEEAKR_5_EFSVYMTKDGR_7	0.24	0.9	0.07		0.1	0.41	0.46	1.23E-23	0.13	8.18E-08	0.13	8.18E-08
AFG32_557_AFG32_600	VIGGLEKK_6_GKGLGYAQYLPK_1	0.51	0.94	0.25	0.68	0.33	0.71	0.46	2.34E-17	0.44	0.0116	0.44	0.0116
NDUS1_87_NDUV1_81	APKVVAACAMPVM[147.04]K_2_GPDWILGEMKTSGLR_9		0.96	0.55	0.34	0.62		0.46	0	0.04	0.386	0.17	0.00168
ACDSB_324_ACDSB_284	MQFGKR_4_IGHGYKYAIGSLNEGR_5		0.38	0.51	0.45	0.65	0.22	0.46	0	0.29	0.00000876	0.29	0.00000876
EFTU_361_EFTU_429	VEAQVYILSKEEGGR_9_DGNKTIGTGLVTDVPAMTEEDKNIK_3	0.31	1.03	0.14	0.34	0.22	0.5	0.47	3.79E-17	0.35	1.09E-08	0.35	1.09E-08
MIC19_136_MIC19_45	KQDAFYK_0_ESSPSGSKSQR_7		0.03	1.04	-0.05	1.11		0.47	9.89E-12	-0.23	0.000928	-0.23	0.000928
HIBCH_300_HIBCH_352	VINKMSPTSLK_3_AVLIDKDQTPK_5	0.75	0.46	0.68	0.29	0.3	0.36	0.48	6.74E-11	0.45	0.0000666	0.45	0.0000666
THIL_265_THIL_187	LKTVFQK_1_DGLTDVYNKIHMGNCAENTAK_8		0.63	0.64	0.25	0.66		0.48	2.34E-28	0.19	1.55E-10	0.19	1.55E-10
NDUS1_87_NDUV1_104	APKVVAACAMPVMK_2_WSFMNKPSDGRPK_5	0.27	0.47	0.63	0.37	0.61		0.48	0	0.04	0.386	0.17	0.00168
SCOT1_214_SCOT1_271	AWKADR_2_LIKGEKYEK_2	0.47	1.29	0.32	0.58	0.42	0.67	0.48	1.00E-38	0.87	6.27E-28	0.87	6.27E-28
AATM_82_AATM_82	KAEAQIAAK_0_KAEAQIAAK_0	0.46	0.85	0.23	0.02	0.44	0.69	0.49	1.58E-13	0.13	8.18E-08	0.13	8.18E-08
THIL_171_THIL_240	GATPYGGVKLEDLIVK_8_FASEITPITISVKGKPDVVVKEDEEYKR_12	0.79	0.22	0.67	0.29	0.86	0.14	0.49	3.20E-30	0.19	1.55E-10	0.19	1.55E-10

ECHM_282_ECHM_101	EGMTAFVEKR_8_AFAAGADIKEMQNR_8		0.53	0.46	0.32	0.55		0.5	4.00E-16	0.02	0.423	0.02	0.423
CLYBL_59_CLYBL_307	KIPSLK_0_EHQQLGKGAFTFR_6	0.5	0.6	0.59	0.43	0.49		0.5	7.68E-29	0.27	0.0256	0.27	0.0256
NDUV1_81_NDUS1_98	GPDWILGEMKTSGLR_9_VVAACAM[147.04]PVMKGWNILTNSEK_10		0.48	0.59	0.41	0.64	-0.15	0.5	5.61E-45	0.17	0.00168	0.04	0.386
SCOT1_214_SCOT1_214	AWKADR_2_AWKADR_2	0.37	1.07	0.25	0.57	0.38	0.7	0.5	7.49E-29	0.87	6.27E-28	0.87	6.27E-28
SUCA_57_SUCA_94	NTKIICQGFTGK_2_GGQKHLGLPVFNTVK_3		-0.01	0.71	0.09	0.95		0.5	3.37E-17	-0.08	0.0262	-0.08	0.0262
IDHP_166_IDHP_413	LVPGWTKPITIGR_6_VCVQTVESGAMTKDLAGCIHGLSNVK_12	0.71	0.55	0.49	0.69	0.53	0.23	0.51	0	-0.11	0.00705	-0.11	0.00705
ACAD9_457_ACAD9_525	IKELK_1_FGKNIVEEQLVLK_2	0.3	0.67	0.57	0.48	0.6		0.51	1.87E-11	0.52	0.00000089	0.52	0.00000089
AFG32_558_AFG32_600	KTQVLQPEEK_0_GKGLGYAQYLPK_1	0.61	1.09	0.41	0.57	0.5	0.79	0.51	2.03E-10	0.44	0.0116	0.44	0.0116
THIL_171_THIL_240	GATPYGGVKLEDLIVK_8_FASEITPITISVKGKPDVVVK_12	0.82	0.41	0.72	0.27	0.71	0.31	0.52	0	0.19	1.55E-10	0.19	1.55E-10
THIL_260_THIL_171	RVDFSKVPK_5_GATPYGGVKLEDLIVK_8		0.39	0.71	0.19	0.67		0.52	3.96E-38	0.19	1.55E-10	0.19	1.55E-10
NDUV1_81_NDUS1_98	GPDWILGEMKTSGLR_9_VVAACAMPVMKGWNILTNSEK_10		0.3	0.63	0.29	0.65		0.52	2.46E-19	0.17	0.00168	0.04	0.386
HXK1_819_HXK1_680	NILIDFTKK_7_GFKATDCVGHDVATLLR_2		1.02	0.66	0.51	0.43		0.53	0.00000016	0.48	0.0000163	0.48	0.0000163
AIFM1_381_AIFM1_387	LLIKLK_3_KVETDHIVTAVGLEPNVELAK_0		0.12	0.84	0.28	0.99	0.75	0.53	1.26E-44	-0.33	0.0000303	-0.33	0.0000303
ODO1_276_ODO1_1000	WSSEKR_4_KTHLTELQR_0	0.53	0.92	0.53	0.58	0.55		0.54	0	0.32	0.000036	0.32	0.000036
EFTU_91_EFTU_79	KYEEIDNAPEER_0_TTLTAAITKILAEGGGAK_8	0.66	1.1	0.13	0.58	0.09	0.44	0.54	5.29E-10	0.35	1.09E-08	0.35	1.09E-08
ADT1_94_ADT1_23	YFPTQALNFAFKDKYK_13_DFLAGGIAAAVSKTAVAPIER_12	0.96	0.4	0.3	0.21	1.05	0.35	0.55	2E-13	0.5	0.000000399	0.5	0.000000399
VDAC3_226_VDAC3_63	YKLDCR_1_YKVCNYGLTFTQK_1	0.13	-0.08	1.13	0.6	1.28	-0.02	0.55	6.25E-10	-0.16	0.0945	-0.16	0.0945
ACAD9_457_ACAD9_525	IKELK_1_FGKNIVEEQLVLKR_2	0.52	0.58	0.66	0.44	0.74	0.53	0.55	0	0.52	0.00000089	0.52	0.00000089

MIC19_121_MIC19_136	AKHLAR_1_KQDAFYK_0	0.55	-0.16	1.13	0.02	1.1		0.55	1.46E-09	-0.23	0.000928	-0.23	0.000928
NDUV1_81_NDUS1_87	GPDWILGEMKTSGLR_9_MCLVEIEKAPKVVAACAMPVMK_10	0.47	0.47	0.78	0.22	0.75	0.1	0.56	1.46E-31	0.17	0.00168	0.04	0.386
SCOT1_480_SCOT1_185	GVFDVDKK_6_DGSVAIASKPR_8	0.62	1.08	0.35	0.57	0.51		0.57	4.43E-08	0.87	6.27E-28	0.87	6.27E-28
ACSL1_552_ACSL1_562	WLPNGTLKIIDR_7_HIFKLAQGEYIAPEK_3		-0.02	1.07	0.05	1.43		0.58	6.06E-10	-0.15	0.0033	-0.15	0.0033
ACAD9_525_ACAD9_245	FGKNIVEEQLVLK_2_TEVVDSDGSKTDKMTAFIVER_12		0.46	1.09	0.57	0.86	0.83	0.58	0.000000548	0.52	0.00000089	0.52	0.00000089
BPHL_188_BPHL_271	WSEKAR_3_LHLMPEGKHNLHLR_7		0.52	0.41	0.94	-1.17		0.59	1.34E-42	0.34	0.000115	0.34	0.000115
PPIF_189_PPIF_166	IESFGSKSGK_6_TDWLDGKHVVFGHVK_6	0.71	0.78	0.51	0.43	0.58		0.59	3.19E-29	0.53	0.000000391	0.53	0.000000391
PPIF_181_PPIF_189	EGMDVVKK_6_IESFGSKSGK_6	0.67	0.73	0.76	0.38	0.57	0.28	0.6	1.23E-13	0.53	0.000000391	0.53	0.000000391
EFTU_49_EFTU_311	KTYVR_0_TVVTGIEMFHKSLER_10	0.82	1.63	0.41	0.74	0.45		0.61	5.78E-28	0.35	1.09E-08	0.35	1.09E-08
THIL_265_THIL_178	LKTVFQK_1_LEDLIVKDGLTDVYNK_6		0.76	0.79	0.48	0.72		0.61	0.00000184	0.19	1.55E-10	0.19	1.55E-10
ACO13_127_ACO13_108	TTGKLIAQGR_3_IGEEIVITAHILKQGK_12	0.64	1.09	0.45	0.6	0.59	0.64	0.64	0	0.4	0.00000114	0.4	0.00000114
SCOT1_455_SCOT1_418	IMEKCTLPLTGK_3_YGDLANWMIPGKMVK_11	0.45	1.8	0.49	0.75	0.63		0.64	5.22E-18	0.87	6.27E-28	0.87	6.27E-28
ADT1_199_ADT1_23	AAYFGVYDTAKGM[147.04]LPDPK_10_DFLAGGIAAAVSKTAVAPIER_12	1.14	0.39	1.05	0.41	1.07	0.92	0.65	5.04E-34	0.5	0.000000399	0.5	0.000000399
ADT1_147_ADT1_23	LAADVGKGSSQR_6_DFLAGGIAAAVSKTAVAPIER_12		0.86	0.54	0.73	1		0.65	3.70E-23	0.5	0.000000399	0.5	0.000000399
ADT1_92_ADT1_23	YFPTQALNFAFKDKYK_11_DFLAGGIAAAVSKTAVAPIER_12	0.69	0.36	1.04	0.41	1.2	0.57	0.65	0	0.5	0.000000399	0.5	0.000000399
ODO1_574_ODO1_276	SKDEK_1_WSSEKR_4	0.53	1.15	0.46	0.73	0.49	0.78	0.65	7.07E-41	0.32	0.000036	0.32	0.000036
ODO1_276_ODO1_999	WSSEKR_4_AKPVWYAGRDPAAAPATGNKK_19	0.86	1.03	0.65	0.59	0.59	0.79	0.65	1.53E-38	0.32	0.000036	0.32	0.000036
ADT2_105_ADT1_23	QIFLGGVDKR_8_DFLAGGIAAAVSKTAVAPIER_12		0.33	1.1	0.45	1.2		0.66	1.26E-44	0.62	0.00000137	0.5	0.000000399
ODO1_640_ODO1_999	ILKTR_2_DPAAAPATGNKK_10		0.99	0.64	0.38	0.62	0.41	0.66	2.51E-10	0.32	0.000036	0.32	0.000036

LONM_375_LONM_382	EVEEKIK_4_KYLLQEQLK_0	0.72	1.41	0.37	0.78	0.5	0.65	0.66	4.15E-21	0.34	0.132	0.34	0.132
HXK1_371_HXK1_389	MAKESLLFEGR_2_GKFTTSDVAAIETDKEGVQNAK_1		0.41	0.72	0.66	0.84		0.68	9.73E-21	0.48	0.0000163	0.48	0.0000163
ODO1_276_ODO1_999	WSSEKR_4_DPAAAPATGNKK_10	0.81	1.32	0.66	0.55	0.76	0.55	0.69	0	0.32	0.000036	0.32	0.000036
ODO1_640_ODO1_276	ILKTR_2_KWSSEKR_5	0.56	1.12	0.65	0.69	0.66	0.57	0.7	0	0.32	0.000036	0.32	0.000036
CMC2_177_CMC2_104	TGKVSAIDFR_2_AGKGEVTFEDVK_2	0.83	0.39	0.62	0.5	1.22	1.2	0.7	9.19E-09	-0.05	0.169	-0.05	0.169
SCOT1_473_SCOT1_418	IITEKGVFDVDKK_4_YGDLANWMIPGKMVK_11	0.92	1.13	0.74		0.73	0.8	0.72	7.77E-28	0.87	6.27E-28	0.87	6.27E-28
ACSL1_649_ACSL1_552	EAGLKPFEQVK_4_WLPNGTLKIIDR_7		0.2	1.29	0.14	1.41		0.73	5.11E-12	-0.15	0.0033	-0.15	0.0033
ODO1_640_ODO1_276	ILKTR_2_WSSEKR_4	0.7	1.06	0.73	0.57	0.11	0.57	0.73	0	0.32	0.000036	0.32	0.000036
ADT1_92_ADT1_23	YFPTQALNFAFKDK_11_DFLAGGIAAAVSKTAVAPIER_12	0.82	0.34	0.91	0.48	1.13	0.65	0.74	0	0.5	0.000000399	0.5	0.000000399
ACAD9_525_ACAD9_245	FGKNIVEEQLVLKR_2_TEVVDSDGSKTDKMTAFIVER_12		0.14	1.36	0.45	1.14		0.74	0.000000626	0.52	0.00000089	0.52	0.00000089
ADT1_96_ADT1_23	DKYKQIFLGGVDR_3_DFLAGGIAAAVSKTAVAPIER_12	1.02	0.35	1.15	0.5	1.19	0.68	0.75	0	0.5	0.000000399	0.5	0.000000399
HIBCH_352_HIBCH_91	AVLIDKDQTPK_5_GAGGKAFCAGGDIK_4	0.62	0.78	0.93	0.53	1.01	0.56	0.76	0	0.45	0.0000666	0.45	0.0000666
LONM_357_LONM_382	KEFELSK_0_KYLLQEQLK_0	0.52	1.34	0.14	0.71	0.65	1.2	0.78	4.3E-15	0.34	0.132	0.34	0.132
SCOT1_480_SCOT1_455	GVFDVDKK_6_IMEKCTLPLTGK_3		2.35	0.53	0.87	0.54	1.11	0.78	4.91E-08	0.87	6.27E-28	0.87	6.27E-28
ADT1_96_ADT1_23	YKQIFLGGVDR_1_DFLAGGIAAAVSKTAVAPIER_12	0.71	0.35	1.06	0.49	1.15	0.69	0.79	0	0.5	0.000000399	0.5	0.000000399
HXK1_884_HXK1_537	TVCGVVSKR_7_LSKQALMEVK_2	1.13	0.52	1	0.89	1.03		0.81	1.51E-20	0.48	0.0000163	0.48	0.0000163
HIBCH_300_HIBCH_91	VINKM[147.04]SPTSLK_3_GAGGKAFCAGGDIK_4		0.71	1.11	0.61	1.19		0.81	5.54E-21	0.45	0.0000666	0.45	0.0000666
SCOT1_286_SCOT1_296	KEGDGK_0_SGKPGGDVR_2	0.89	1.49	0.66	0.61	0.77	1.09	0.81	2.62E-17	0.87	6.27E-28	0.87	6.27E-28
ADT1_147_ADT1_33	LAADVGKGSSQR_6_VKLLLQVQHASK_1	0.71	0.73	0.86	0.73	1.21	0.74	0.84	0	0.5	0.000000399	0.5	0.000000399

SCOT1_296_SCOT1_418	SGKPGGDVR_2_YGDLANWMIPGKM[147.04]VK_11	0.39	1.54	0.95	0.74	1.09	1.08	0.88	1.85E-15	0.87	6.27E-28	0.87	6.27E-28
SCOT1_296_SCOT1_418	SGKPGGDVR_2_YGDLANWMIPGKMVK_11	0.82	1.04			0.99	0.82	0.89	5.3E-15	0.87	6.27E-28	0.87	6.27E-28
HIBCH_300_HIBCH_91	VINKMSPTSLK_3_GAGGKAFCAGGDIK_4	1.05	0.7	1.15	0.71	1.23		0.92	0	0.45	0.0000666	0.45	0.0000666
EFTS_51_EFTS_132	ELLMKLR_4_NLKFQQLVQQVALGTMAHCQNLTDR_2	0.67	1.06	0.74	0.95	0.87	1.42	0.92	1.38E-15	0.71	0.000943	0.71	0.000943
SCOT1_296_SCOT1_296	SGKPGGDVR_2_K[170.11]EGDGK[170.11]GKSGKPGGDVR_10		1.32	0.93	1	1.03		0.96	2.13E-13	0.87	6.27E-28	0.87	6.27E-28
SCOT1_296_SCOT1_418	SGKPGGDVR_2_YGDLANWM[147.04]IPGKMVK_11	0.76	1.52	0.95	0.88	1.03	1.07	0.99	4.26E-43	0.87	6.27E-28	0.87	6.27E-28
SCOT1_286_SCOT1_418	KEGDGK_0_YGDLANWMIPGKMVK_11	1.08	1.46	0.98	1.04	0.87	0.87	1.02	6.31E-31	0.87	6.27E-28	0.87	6.27E-28
ADT1_33_ADT1_23	VKLLLQVQHASK_1_DFLAGGIAAAVSKTAVAPIER_12		0.82	1.04	1.09	1.39		1.03	0	0.5	0.000000399	0.5	0.000000399
SCOT1_296_SCOT1_296	SGKPGGDVR_2_K[170.11]EGDGKGK[170.11]SGKPGGDVR_10		1.13	1.08	0.86	1.03		1.05	1.13E-08	0.87	6.27E-28	0.87	6.27E-28
BDH_258_BDH_275	IQAIAKK_5_KYFDEK_0	1.72	2.93	0.85	1.28	0.97		1.11	1.26E-12	1.26	5.87E-11	1.26	5.87E-11
SCOT1_296_SCOT1_421	SGKPGGDVR_2_M[147.04]VKGMGGAMDLVSSSK_2	0.98	1.46	1.63	0.81	1.29	1.07	1.11	3.33E-12	0.87	6.27E-28	0.87	6.27E-28
SCOT1_286_SCOT1_421	KEGDGK_0_MVKGMGGAMDLVSSSK_2	1.31	1.6	1.09	0.89	1.26	1.01	1.12	1.62E-14	0.87	6.27E-28	0.87	6.27E-28
SCOT1_296_SCOT1_421	SGKPGGDVR_2_MVKGMGGAMDLVSSSK_2	0.91	1.77	1.11	0.98	1.21	1.07	1.12	3.62E-43	0.87	6.27E-28	0.87	6.27E-28
ADT2_199_ADT2_23	AAYFGIYDTAKGM[147.04]LPDPK_10_DFLAGGVAAAISKTAVAPIER_12		1.16	1.25		2.64	0.89	1.17	0.000000509	0.62	0.00000137	0.62	0.00000137
BDH_270_BDH_258	KDYGR_0_IQAIAKK_5	1.37	2	0.62	1.46	1.11	1.15	1.18	3.29E-18	1.26	5.87E-11	1.26	5.87E-11
SCOT1_296_SCOT1_421	SGKPGGDVR_2_MVKGM[147.04]GGAMDLVSSSK_2	1.29	1.87	1.26	1.16	1.22	1.11	1.21	2.18E-35	0.87	6.27E-28	0.87	6.27E-28
BDH_91_BDH_259	DKGDAGVK_1_KMWDDLPEVVR_0	1.04	3.12	0.7	1.43	1.06	1.2	1.23	6.58E-30	1.26	5.87E-11	1.26	5.87E-11

SCOT1_296_SCOT1_421	SGKPGGDVR_2_MVKGMGGAM[147.04]DLVSSSK_2	1.36	1.44	1.17	1.26	1.23	1.04	1.25	9.44E-29	0.87	6.27E-28	0.87	6.27E-28
ADT2_96_ADT2_23	YKQIFLGGVDKR_1_DFLAGGVAAAISKTAVAPIER_12		0.81	1.51	0.82	1.78		1.28	2.81E-38	0.62	0.00000137	0.62	0.00000137
BDH_270_BDH_275	KDYGR_0_KYFDEK_0	1.25	2.44	0.84	1.43	1.21	1.42	1.36	0	1.26	5.87E-11	1.26	5.87E-11
MIC60_102_MIC60_122	KPVQSGPLK_0_DSKLPVAQSQK_2		0.71	1.75	0.32	2.02		1.36	1.02E-08	0.08	0.0825	0.08	0.0825

Supplemental Table 2: Correlation of biological replicates

Row name	Column name	Row index	Column index	R squared	Direction
3702RH	3707RH	1	2	0.44	FF
3702RH	3713RH	1	3	0.57	FF
3702RH	3705SH	1	4	0.33	FR
3702RH	3712SH	1	5	0.56	FR
3702RH	3752SH	1	6	0.61	FR
3707RH	3713RH	2	3	0.64	FF
3707RH	3705SH	2	4	0.69	FR
3707RH	3712SH	2	5	0.17	FR
3707RH	3752SH	2	6	0.30	FR
3713RH	3705SH	3	4	0.52	FR
3713RH	3712SH	3	5	0.36	FR
3713RH	3752SH	3	6	0.46	FR
3705SH	3712SH	4	5	0.31	FF
3705SH	3752SH	4	6	0.41	FF
3712SH	3752SH	5	6	0.84	FF

Forward/Reverse	R squared	Forward/Forward	R squared
FR	0.33	FF	0.44
FR	0.56	FF	0.57
FR	0.61	FF	0.64
FR	0.69	FF	0.31
FR	0.17	FF	0.41
FR	0.30	FF	0.84
FR	0.52	**Mean**	**0.54**
FR	0.36		
FR	0.46		
Mean	**0.45**		

Supplemental Table 3: Cross-linked peptide pairs between NDUA4 and CX6B1 subunits of Complex IV

Cross-linked peptide pair				Log2 ratio (TAC/Sham)								
ProteinA	ProteinB	LysA	LysB	3702RH XL	3707RH XL	3713RH XL	3705SH XL	3712SH XL	3752SH XL	**Mean XL**	Mean DE A	Mean DE B
CX6B1	NDUA4	85	56		-1.06	-0.62	-0.72	-1.4		**-1.01**	-0.41	-0.27
CX6B1	NDUA4	10	74	-0.06	-0.64	-0.49	-0.52	-0.58	-0.44	**-0.55**	-0.41	-0.27
CX6B1	NDUA4	10	76	-0.19	-0.65	-0.33	-0.53	-0.48	-0.36	**-0.49**	-0.41	-0.27
CX6B1	NDUA4	13	74	-0.02	-0.47	-0.36	-0.39	-0.56	-0.4	**-0.45**	-0.41	-0.27
CX6B1	NDUA4	13	76	-0.11	-0.52	-0.45	-0.41	-0.53	-0.28	**-0.44**	-0.41	-0.27

Supplemental Video 1

This video can be viewed by anyone with the following link:

https://drive.google.com/file/d/1G8NtkRJylq1xKNzMa4ovpwFlupzenzht/view?usp=sharing

4.6 References

1. S. Rath *et al.*, MitoCarta3.0: an updated mitochondrial proteome now with sub-organelle localization and pathway annotations. *Nucleic Acids Research* **49**, D1541-D1547 (2020).
2. D. J. Pagliarini *et al.*, A Mitochondrial Protein Compendium Elucidates Complex I Disease Biology. *Cell* **134**, 112-123 (2008).
3. L. Qi *et al.*, Cryo-EM structure of the human mitochondrial translocase TIM22 complex. *Cell Research* **31**, 369-372 (2021).
4. H. R. Bridges *et al.*, Structure of inhibitor-bound mammalian complex I. *Nature Communications* **11**, 5261 (2020).
5. J. Gu *et al.*, Cryo-EM structure of the mammalian ATP synthase tetramer bound with inhibitory protein IF1. *Science* **364**, 1068 (2019).
6. T. E. Spikes, M. G. Montgomery, J. E. Walker, Structure of the dimeric ATP synthase from bovine mitochondria. *Proceedings of the National Academy of Sciences* **117**, 23519 (2020).
7. K. Tucker, E. Park, Cryo-EM structure of the mitochondrial protein-import channel TOM complex at near-atomic resolution. *Nature Structural & Molecular Biology* **26**, 1158-1166 (2019).
8. A. Sinz, Cross-linking Mass Spectrometry Goes In-Tissue. *Cell Systems* **6**, 10-12 (2018).

9. X. Tang, G. R. Munske, W. F. Siems, J. E. Bruce, Mass Spectrometry Identifiable Cross-Linking Strategy for Studying Protein−Protein Interactions. *Analytical Chemistry* **77**, 311-318 (2005).

10. D. K. Schweppe *et al.*, Mitochondrial protein interactome elucidated by chemical cross-linking mass spectrometry. *Proceedings of the National Academy of Sciences* **114**, 1732-1737 (2017).

11. J. D. Chavez *et al.*, Cross-linking measurements of the Potato leafroll virus reveal protein interaction topologies required for virion stability, aphid transmission, and virus-plant interactions. *Journal of Proteome Research* **11**, 2968-2981 (2012).

12. C. R. Weisbrod *et al.*, In Vivo Protein Interaction Network Identified with a Novel Real-Time Cross-Linked Peptide Identification Strategy. *Journal of Proteome Research* **12**, 1569-1579 (2013).

13. Juan D. Chavez, Devin K. Schweppe, Jimmy K. Eng, James E. Bruce, In Vivo Conformational Dynamics of Hsp90 and Its Interactors. *Cell Chemical Biology* **23**, 716-726 (2016).

14. J. D. Chavez *et al.*, Chemical Cross-linking Mass Spectrometry Analysis of Protein Conformations and Supercomplexes in Heart Tissue. *Cell Systems* **6**, 136-141.e135 (2018).

15. S.-E. Ong *et al.*, Stable Isotope Labeling by Amino Acids in Cell Culture, SILAC, as a Simple and Accurate Approach to Expression Proteomics. *Molecular & Cellular Proteomics* **1**, 376-386 (2002).

16. J. D. Chavez *et al.*, Quantitative interactome analysis reveals a chemoresistant edgotype. **6**, 7928 (2015).

17. J. D. Chavez, A. Keller, B. Zhou, R. Tian, J. E. Bruce, Cellular Interactome Dynamics during Paclitaxel Treatment. *Cell Reports* **29**, 2371-2383.e2375 (2019).

18. J. D. Chavez, A. Keller, J. P. Mohr, J. E. Bruce, Isobaric Quantitative Protein Interaction Reporter Technology for Comparative Interactome Studies. *Analytical Chemistry* **92**, 14094-14102 (2020).

19. D. A. Brown *et al.*, Mitochondrial function as a therapeutic target in heart failure. *Nature Reviews Cardiology* **14**, 238-250 (2017).

20. E. Barth, G. Stämmler, B. Speiser, J. Schaper, Ultrastructural quantitation of mitochondria and myofilaments in cardiac muscle from 10 different animal species including man. *Journal of Molecular and Cellular Cardiology* **24**, 669-681 (1992).

21. D. K. Schweppe *et al.*, XLinkDB 2.0: integrated, large-scale structural analysis of protein cross-linking data. *Bioinformatics* **32**, 2716-2718 (2016).

22. B. M. Broom *et al.*, A Galaxy Implementation of Next-Generation Clustered Heatmaps for Interactive Exploration of Molecular Profiling Data. *Cancer Research* **77**, e23 (2017).

23. D. Murashige *et al.*, Comprehensive quantification of fuel use by the failing and nonfailing human heart. *Science* **370**, 364 (2020).

24. G. Aubert *et al.*, The Failing Heart Relies on Ketone Bodies as a Fuel. *Circulation* **133**, 698-705 (2016).

25. K. C. Bedi *et al.*, Evidence for Intramyocardial Disruption of Lipid Metabolism and Increased Myocardial Ketone Utilization in Advanced Human Heart Failure. *Circulation* **133**, 706-716 (2016).

26. S. C. Kolwicz, S. Airhart, R. Tian, Ketones Step to the Plate. *Circulation* **133**, 689-691 (2016).

27. S. D. Tammam, J.-C. Rochet, M. E. Fraser, Identification of the Cysteine Residue Exposed by the Conformational Change in Pig Heart Succinyl-CoA:3-Ketoacid Coenzyme A Transferase on Binding Coenzyme A. *Biochemistry* **46**, 10852-10863 (2007).

28. M. E. Fraser, K. Hayakawa, W. D. Brown, Catalytic Role of the Conformational Change in Succinyl-CoA:3-Oxoacid CoA Transferase on Binding CoA. *Biochemistry* **49**, 10319-10328 (2010).

29. S.-F. Coker *et al.*, The high-resolution structure of pig heart succinyl-CoA:3-oxoacid coenzyme A transferase. *Acta Crystallographica Section D* **66**, 797-805 (2010).

30. N. Shafqat *et al.*, A structural mapping of mutations causing succinyl-CoA:3-ketoacid CoA transferase (SCOT) deficiency. *Journal of inherited metabolic disease* **36**, 983-987 (2013).

31. D. Schneidman-Duhovny, Y. Inbar, R. Nussinov, H. J. Wolfson, PatchDock and SymmDock: servers for rigid and symmetric docking. *Nucleic Acids Research* **33**, W363-W367 (2005).

32. A. M. Haapalainen *et al.*, Crystallographic and Kinetic Studies of Human Mitochondrial Acetoacetyl-CoA Thiolase: The Importance of Potassium and Chloride Ions for Its Structure and Function. *Biochemistry* **46**, 4305-4321 (2007).

33. Kristin E. Dittenhafer-Reed *et al.*, SIRT3 Mediates Multi-Tissue Coupling for Metabolic Fuel Switching. *Cell Metabolism* **21**, 637-646 (2015).

34. A. J. Still *et al.*, Quantification of Mitochondrial Acetylation Dynamics Highlights Prominent Sites of Metabolic Regulation. *Journal of Biological Chemistry* **288**, 26209-26219 (2013).

35. S. Zong *et al.*, Structure of the intact 14-subunit human cytochrome c oxidase. *Cell Research* **28**, 1026-1034 (2018).

36. E. Balsa *et al.*, NDUFA4 Is a Subunit of Complex IV of the Mammalian Electron Transport Chain. *Cell Metabolism* **16**, 378-386 (2012).

37. V. Massa *et al.*, Severe infantile encephalomyopathy caused by a mutation in COX6B1, a nucleus-encoded subunit of cytochrome c oxidase. *American Journal of Human Genetics* **82**, 1281-1289 (2008).

38. U. N. Abdulhag *et al.*, Mitochondrial complex IV deficiency, caused by mutated COX6B1, is associated with encephalomyopathy, hydrocephalus and cardiomyopathy. *European Journal of Human Genetics* **23**, 159-164 (2015).

39. M. G. Rosca *et al.*, Cardiac mitochondria in heart failure: decrease in respirasomes and oxidative phosphorylation. *Cardiovascular Research* **80**, 30-39 (2008).

40. E. Pebay-Peyroula *et al.*, Structure of mitochondrial ADP/ATP carrier in complex with carboxyatractyloside. *Nature* **426**, 39-44 (2003).

41. J. J. Ruprecht *et al.*, The Molecular Mechanism of Transport by the Mitochondrial ADP/ATP Carrier. *Cell* **176**, 435-447.e415 (2019).

42. J. Karch *et al.*, Inhibition of mitochondrial permeability transition by deletion of the ANT family and CypD. *Science Advances* **5**, eaaw4597 (2019).

43. M. J. Bround, D. M. Bers, J. D. Molkentin, A 20/20 view of ANT function in mitochondrial biology and necrotic cell death. *Journal of Molecular and Cellular Cardiology* **144**, A3-A13 (2020).

44. A. M. Bertholet *et al.*, H+ transport is an integral function of the mitochondrial ADP/ATP carrier. *Nature* **571**, 515-520 (2019).

45. R. Ramzan, A. Rhiel, P. Weber, B. Kadenbach, S. Vogt, Reversible dimerization of cytochrome c oxidase regulates mitochondrial respiration. *Mitochondrion* **49**, 149-155 (2019).

46. J. E. Kokoszka *et al.*, The ADP/ATP translocator is not essential for the mitochondrial permeability transition pore. *Nature* **427**, 461-465 (2004).

47. J. D. Chavez *et al.*, Mitochondrial protein interaction landscape of SS-31. *Proceedings of the National Academy of Sciences* **117**, 15363 (2020).

48. J. M. A. Bullock, J. Schwab, K. Thalassinos, M. Topf, The Importance of Non-accessible Cross-links and Solvent Accessible Surface Distance in Modeling Proteins with Restraints From Cross-linking Mass Spectrometry. *Molecular & Cellular Proteomics* **15**, 2491-2500 (2016).

49. Y. Perez-Riverol *et al.*, The PRIDE database and related tools and resources in 2019: improving support for quantification data. *Nucleic Acids Research* **47**, D442-D450 (2018).

50. O. Tarnavski *et al.*, Mouse cardiac surgery: comprehensive techniques for the generation of mouse models of human diseases and their application for genomic studies. *Physiological Genomics* **16**, 349-360 (2004).

51. J. Ritterhoff *et al.*, Metabolic Remodeling Promotes Cardiac Hypertrophy by Directing Glucose to Aspartate Biosynthesis. *Circulation Research* **126**, 182-196 (2020).

52. A. Thompson *et al.*, Tandem Mass Tags: A Novel Quantification Strategy for Comparative Analysis of Complex Protein Mixtures by MS/MS. *Analytical Chemistry* **75**, 1895-1904 (2003).

53. P. L. Ross *et al.*, Multiplexed protein quantitation in Saccharomyces cerevisiae using amine-reactive isobaric tagging reagents.

54. J. D. Chavez *et al.*, Systems structural biology measurements by in vivo cross-linking with mass spectrometry. *Nature Protocols* **14**, 2318-2343 (2019).

55. S. Tyanova *et al.*, The Perseus computational platform for comprehensive analysis of (prote)omics data. *Nature Methods* **13**, 731-740 (2016).

56. G. W. Rogers *et al.*, High Throughput Microplate Respiratory Measurements Using Minimal Quantities Of Isolated Mitochondria. *PLOS ONE* **6**, e21746 (2011).

57. M. Spinazzi, A. Casarin, V. Pertegato, L. Salviati, C. Angelini, Assessment of mitochondrial respiratory chain enzymatic activities on tissues and cultured cells. *Nature Protocols* **7**, 1235-1246 (2012).

58. A. Keller, J. Eng, N. Zhang, X.-j. Li, R. Aebersold, A uniform proteomics MS/MS analysis platform utilizing open XML file formats. *Molecular Systems Biology* **1**, 2005.0017 (2005).

59. J. P. Mohr, P. Perumalla, J. D. Chavez, J. K. Eng, J. E. Bruce, Mango: A General Tool for Collision Induced Dissociation-Cleavable Cross-Linked Peptide Identification. *Analytical Chemistry* **90**, 6028-6034 (2018).

60. J. D. Chavez, C. R. Weisbrod, C. Zheng, J. K. Eng, J. E. Bruce, Protein Interactions, Post-translational Modifications and Topologies in Human Cells. *Molecular & Cellular Proteomics* **12**, 1451-1467 (2013).

61. S. E. Calvo, K. R. Clauser, V. K. Mootha, MitoCarta2.0: an updated inventory of mammalian mitochondrial proteins. *Nucleic Acids Research* **44**, D1251-D1257 (2015).

62. A. Keller, J. D. Chavez, J. E. Bruce, Increased sensitivity with automated validation of XL-MS cleavable peptide cross-links. *Bioinformatics* **35**, 895-897 (2018).

63. A. Keller, A. I. Nesvizhskii, E. Kolker, R. Aebersold, Empirical Statistical Model To Estimate the Accuracy of Peptide Identifications Made by MS/MS and Database Search. *Analytical Chemistry* **74**, 5383-5392 (2002).

Chapter 5: Other techniques and strategies used to study mitochondrial function

Other projects that contributed to my thesis work include a wide range of techniques, metabolic and animal models. We examined cardiac metabolism and heart failure in obesity, primary mitochondrial disease, and across genders. This work can be found in the following publications:

Targeting NAD+ metabolism as interventions for mitochondrial disease.

Lee, CF., **Caudal, A**., Abell, L, Nagana Gowda GA., Tian, R. Scientific Reports. 2019 PMID: 30816177.

Increasing Fatty Acid Oxidation Prevents High Fat Diet Induced Cardiomyopathy through Regulating Parkin Mediated Mitophagy

Shao, D., Kolwicz, SC., Wang, P., Roe, N., Villet, O., Nishi, K., Hsu, Y., Flint, G.V., **Caudal, A**., Wang, W., Regnier, M., Tian, R. 2020. Circulation. 2020 PMID: 32597196.

A Novel Approach to Measure Mitochondrial Respiration in Previously Frozen Biological Samples

Acin-Perez, R., Benador, IY., Petcherski, A., Veliova, M., Lagarrigue, S., **Caudal, A**., Vergnes, L., Murphy, A., Karamanlidis, G., Tian, R., Reue, K., Wanagat, J., Sacks, H., Amati, F., Darley-Usmar, VM., Liesa, M., Divakaruni, AS., Stiles, L., Shirihai, O. EMBO J. 2020 PMID: 32432379.

Increasing fatty acid oxidation elicits a sex-dependent response in failing mouse hearts.

Ritterhoff, J., McMillen, T.S., Villet, O., Young, S., Kolwicz, SC., Senn, T., **Caudal, A**., Tian, R. Journal of Molecular and Cellular Cardiology. 2021 PMID: 33989657.

Chapter 6: Conclusions and Future Directions

The studies in this dissertation resolved large-scale, protein-protein interaction networks using qualitative XL-MS in isolated mitochondria and in-tact cardiac tissue, and quantitative XL-MS for comparative analysis of healthy and failing murine hearts.

In isolated mitochondria, we provided a proof-of-principle method that it was possible to resolve known protein interactions from the native physiological condition. The mitochondrial interactome provides evidence for protein interactions and complex interfaces of high value for the community in general (e.g., MICOS/MIB site interactions). The interactome also provides evidence for the presence and orientation of OXPHOS supercomplexes from and in-tact system. In heart tissue, XL-MS cross-links provide structural information on key protein systems including the sarcomere and OXPHOS complexes and paved way for comparative studies.

The final chapter describes application of iqPIR technology in the first quantitative comparison between mitochondria isolated from healthy and diseased hearts. iqPIR technology achieved one of the highest levels of cross-linking complexity resolved from tissue thus far, yielding quantitative changes in 98 mitochondrial proteins, providing a system's view of protein structure remodeling in heart failure. Among the 602 cross-linked peptide pairs that showed statistically significant level differences in TAC vs. Sham hearts, enrichment of active ketone oxidation enzymes, altered interactions among Complex IV subunits and novel conformational enrichment of the ADP/ATP transporter were revealed in TAC hearts.

The strength of the work described above is the generation of new perspective to preexisting problems and cardiac models, and this unique viewpoint has the potential to extend beyond the context of heart failure. XL-MS technology is a bridge for comparative disease studies in conditions not easily replicated in a dish, such as neurodegeneration, tumor

microenvironments, and aging. Along these lines, tissue-specific responses to drugs, such as chemotherapy-induced heart failure, could shed molecular insight on common off-target effects of drugs in clinical trials. On the other hand, tissue-specific responses to whole-body stimulus such as diet and exercise could be incredibly impactful for understanding physiology.